ISSN VOLUME 1 • NO. 1 (2023)

GLOBAL SUSTAINABILITY CHALLENGES

Publisher
Faculty of Ecology and Environmental Protection, University "Union-Nikola Tesla", Belgrade, Serbia

GLOBAL SUSTAINABILITY CHALLENGES

ГЛОБАЛНИ ИЗАЗОВИ ОДРЖИВОСТИ

Издавач: Универзитет „Унион-Никола Тесла“

Ко-издавач: Универзитет Exeter, Stocker Rd, Exeter EX4 4PY, UK
https://www.exeter.ac.uk/

Адреса: Цара Душана 62-64, 11158 Београд

Телефон: 011 2180-271

E-mail: vladanka.gsc@unionnikolatesla.edu.rs

info@unionnikolatesla.edu.rs

Веб-сајт: https://www.unionnikolatesla.edu.rs/sr

ISSN: 2956-1051 (Online), Број 1/2023, vol. 1, година I

Часопис излази једном годишње електронски и радови се објављују на енглеском језику

CONTENTS

САДРЖАЈ

Global Sustainability Challenges
2023; Vol. 1(1): 1-8
https://gsc.unionnikolatesla.edu.rs/index.php/gsc/index
UDC: 628.34:674
ISSN: 2956-1051 (Online)

Application of waste iron in ferrate(VI) synthesis and phenol removal as confirmation of efficiency

Ljiljana Nikolić Bujanović[1,*], Milan Čekerevac[2], Miloš Simičić[2], Milena Tomić[2]

[1]Faculty of Ecology and Environmental Protection, University Union-Nikola Tesla, Belgrade, Serbia
[2]IHIS Techno-experts, Research and Development Center, Batajnički put 23, Belgrade, Serbia

[*]**Corresponding author:** ljnikolicbujanovic@unionnikolatesla.edu.rs, bujanovic08@gmail.com

To cite this article:
Nikolić-Bujanović, Lj., Čekerevac, M., Simičić, M. and Tomić, M. (2023). Application of waste iron in ferrate(VI) synthesis and phenol removal as confirmation of efficiency. *Global sustainability challenges, 1*(1), pp. 1-8

Received: July 28, 2022; **Revised**: Dec 02, 2022; **Accepted**: Dec 21, 2022

Abstract: Ferrate (VI) is a strong oxidizing, coagulating and flocculating agent. Due to its characteristics, it is suitable for treatment of waters of different origins. In these processes, resulting is an environmentally friendly and non-toxic product, $Fe(OH)_3$, which according to the results of this paper can be recycled and re-synthesized to ferrate(VI). This paper presents a method for the synthesis of ferrate salts by oxidation process from steel pickling wastewater containing $FeCl_2$ and $FeCl_3$ salts. The method for synthesis involves the process of oxidation of ferrous and ferric ions by means of $Ca(ClO)_2$ in solid state and in the presence of KOH in solid state. The recording of the x-ray diffractometer demonstrates a significant presence of K_2FeO_4, while analysis revealed a yield of 15%.
The application of ferrate synthesized from waste iron is shown in the process of treating waste water from the wood industry. The example given of this paper is treatment of samples of WW from the wood industry, from the thermal dryer and steam chamber, using the Jar procedure. The initial concentration of phenol in the sample from the thermal dryer was 27 mg/l and in the sample from the steam chamber 30 mg/l. This wastewater also has a high content of natural organic matter (COD of the sample from the thermal dryer was 3233.1 mgO2/l and COD of the sample from the steam chamber was 4692.1 mgO2/l). The efficiency of removal of phenol by ferrate(VI) was 74.85% and 72.67% for samples from the thermal dryer and the steam chamber, respectively.

Keywords: potassium ferrate, ferrous chloride, ferric chloride, phenol, x-ray

1. Introduction

Ferrate(VI) salts have a wide range of potential applications due to their high efficient oxidation performance. In the area of environmental application ferrate has been considered for water and wastewater treatment because of its environmentally friendly properties without hazardous compounds forming, such as chlorine or bromine, carcinogenic organic pollutants (Audette et al., 1971; J. Q. Jiang & Lloyd, 2002; Yunho et al., 2004). Due to the fact that Fe(III), generated during oxidation by ferrate, exhibits valuable coagulating properties makes an additional contribution to water treatment processes.

Research works performed by Fremy(Fremy, 1841, 1842)are frequently cited in literature as the first to scientifically reveal the existence of iron in a hexavalent state and to effectively achieve ferrates synthesis. Since then, the preparation methods, developed mostly on a laboratory scale, have made little progress, and can be classified into three groups:

- The high temperature route consisting of heating and/or melting various iron oxides bearing materials under high concentration of alkali substances and oxygen flow (Kiselev et al., 1989). These synthesis methods, performed at temperatures as high as 800°C, seem to be mostly ineffective since Fe(VI) is not stable at temperatures higher than 200°C. Most probably, Fe(VI) resulted from the dismutation of synthetized Fe(IV) and/or Fe(V) during manipulation of the synthesis product.
- The wet/humid oxidation of Fe(III) salts bearing solutions, under strong alkaline conditions, using hypochlorite or chlorine as an oxidant. This method is the most used since the 1950s (Ockerman & Schreyer, 1951; Schreyer et al., 1953). One of the drawbacks is that the wet

method used pure chemicals and required many operations for Fe(VI) preparation and separation, making it very costly. Moreover, the water reacts with ferrate leading to its reduction into Fe(III).

- The electrochemical method (Licht et al., 2002; Mácová et al., 2009; L. N. Nikolić-Bujanović et al., 2012), by anodic dissolution of iron or its alloys in a strong alkaline solution (pH > 10) in the transpassive region. Ferrate obtained by electrochemical synthesis has many advantages compared to chemically synthesized ferrate (Mácová et al., 2009), such as: simplicity, lower consumption of chemicals, non-toxic products and exceptional purity of obtained ferrate. However, the decomposition of Fe(VI) by water, low current efficiency and anode passivation are some of the concerns for this route.

Ferrate(VI) salt is a potent oxidant. Under acidic and alkaline conditions, its respective reduction potentials are 2.20 and 0.700 V, being a potential for replacing traditional oxidants, such as ozone, hypochlorite, permanganate, and others(Audette et al., 1971); their respective half-cell reduction potentials in acidic conditions are 2.08, 1.48, and 1.69 V, respectively (Yunho et al., 2004), all less than Fe(VI). Potassium ferrate, other than acting as a powerful oxidant, can be an inorganic coagulant when chemically reduced to $Fe(OH)_3$; it can effectively remove suspended solids, heavy metals, and a variety of contaminants from water (J. Q. Jiang & Lloyd, 2002). Further, using traditional oxidants to treat pollutants/contaminants usually can result in a noteworthy toxic byproduct problem, such as tri-halo-methane and bromates (Gombos et al., 2012). In contrast, potassium ferrate, as a water treatment agent, is reduced to environment friendly $Fe(OH)_3$ (J. Q. Jiang & Lloyd, 2002). Prior to the chlorination process for drinking water, using Fe(VI) as a pre-treatment agent can effectively reduce the formation of hazardous by-products (Yang et al., 2013).

Despite the advantages Fe(VI) can provide, it is expensive for using it to treat pollutants and contaminants. There is also the problem of removing the resulting $Fe(OH)_3$ precipitate which also contains the removed pollutants. The paper presents the possibility of recycling $Fe(OH)_3$ from which Fe(VI) is recovered by a chemical process. For example, synthesizing Fe(VI) by using spent steel pickling liquid as an iron source can achieve a dual-win benefit by not only reducing the cost of Fe - raw chemicals source for Fe(VI) synthesis but also recycling spent steel pickling liquid for environmental sustainability.

Spent pickling liquid is unwantedly produced by the steel industry. Products like steel plates, pipes, and coils always require cleaning with acid to remove their surface impurities before being subjected to further processing. The impurities include black surfaces, iron oxides, and other contaminants. Hydrochloric acid is usually used as the pickling acid for carbon steel products due to its relatively lower price, lower acid consumption rate, and providing a faster pickling process, despite its shortcomings of a higher volatilization rate (Agrawal & Sahu, 2009).

If spent pickling liquid is treated as waste water, toxic metal present in it is generally removed through different approaches, such as the precipitation method, ion exchange, and others. Among them, precipitation as hydroxide is the most often used technology. Although the technology is technically simple, its neutralization step requires a large amount of alkaline or alkaline earth-based chemicals, and it would be much more praised if spent steel pickling liquid could be recycled.

When hydrochloric acid is used as a pickling agent, most iron in spent steel pickling liquid would be present in the form of ferrous chloride through the following chemical reaction (Agrawal & Sahu, 2009)

$$FeO + 2HCl \rightarrow FeCl_2 + H_2O \quad (1)$$

A large amount of attention has recently been focused on the removal of phenol and its derivatives from wastewater (WW) due to their toxicity and high concentration in wastewater. Phenol is a common pollutant in industrial discharges and is also believed to be an intermediate product in the oxidation process of higher molecular weight aromatic hydrocarbons. Their high concentration in the WW of wood industry originates from pentachlorophenol (PCP), which is used for wood conservation (Lee et al., 1991).

The contamination of water system by phenols and their compounds is a major problem because of the toxicity of phenol even at low concentrations. Toxic phenol concentrations are in the range of 10 - 24 mg / l for humans and from 9 - 25 mg / l for aquatic life. Lethal concentration of phenol is around 150mg / 100ml. Phenol and phenolic compounds are designated as priority pollutants by the Environmental Protection Agency in the US, and take 11th place in the list of 126 undesirable chemicals (Environmental Protection Agency). (Environmental Protection Agency (EPA), Manual Report for List of Chemical Priority, USA, (2002)).

Phenol and phenolic compounds are classified as teratogenic and carcinogenic compounds (Iurascu et al., 2009). Phenolic compounds are well known for high salinity, acidity, chemical oxygen demand (COD) and low biodegradability (Turhan & Uzman, 2008). In addition, they have low volatilities and easily form azeotropes and eutectics(López-Montilla et al., 2005). All these properties make them difficult to treat.

Phenol has acute and chronic effects on human health. Inhalation and dermal exposure to phenol is highly irritating to skin, eyes, and mucous. The other acute health effects are headache, dizziness, fatigue, fainting, weakness, nausea, vomiting and lack of appetite at high levels. Effects from chronic exposure (longer than 365 days) include irritation of the gastrointestinal tract. Phenol also can change blood pressure and can cause liver and kidney damage. Nervous system is affected negatively for long time exposures (EPA, 2002). Animal studies have not shown tumors resulting from oral exposure to phenol, while dermal studies have reported that phenol applied to the skin may be a tumor promotor and/or a weak skin carcinogen in mice.

Due to its toxicity to aquatic life and humans, regulations for phenol concentration in WW are very strict. Maximum allowable discharge concentration of phenol varies from country to country, but generally it is about 10 mg / l (Yamada et al., 2005). According to the Ordinance on Hazardous Substances in Water (Official Gazette of SRS, no. 31/82) the maximum content of phenol in the waters of categories I and II is 1 mg / l, while in the waters of categories III and IV the limit is 300 mg / l.

Conventional methods for removing phenolics from wood industry WW include biological degradation, solvent extraction, adsorption and chemical oxidation(Hameed & Rahman, 2008; H. Jiang et al., 2003; Nair et al., 2008).

Biological treatment is economical and environmentally friendly method but at high concentrations of phenol, application of this method is not possible because of the inactivation of microorganisms. Other disadvantages are necessity of large land area and long time for microbial degradation, which makes this process less flexible in design and operation (Pinto et al., 2005; Rengaraj et al., 2002).

In the solvent extraction method the residual phenol concentration in wastewater barely meets the strict US Environmental Protection Agency (EPA) requirements (less than 1 mg/L in the wastewater). What is more, the separation of solute from the solvent is expensive and the loss of solvent requires additional treatment.

The adsorption process is proven to be efficient for the removal of organic contaminants and it is usually used only to treat dilute wastewater (Sharma, 2002; Waite & Gilbert, 1978). The most popular adsorbent is activated carbon due to its excellent adsorption abilities for phenolic compounds (Rengaraj et al., 2002). Drawback of this method is high initial cost; the regeneration of saturated carbons is also costly and results in loss of adsorbents. In addition, this treatment requires complexing agents to improve properties of activated carbon (Ahmaruzzaman, 2008).

One of the possible methods of phenol removal from aqueous environments is chemical oxidation by ferrate(VI), an environmentally friendly oxidant, coagulant and disinfectant (J. Q. Jiang & Lloyd, 2002).

2. Materials and Methods

As a starting material for the synthesis of ferrate from scrap iron, wastewater from the plant for corrosion of carbon steel is used. Other chemicals used are as follows: a solution of $Ca(ClO)_2$, 99%, 85% KOH, 99% NaOH, n-C_5H_{12} 99%, 96% C_2H_5OH, $(C_2H_5)_2O$ 99.5%.

Due to the fact that the concentration of Fe in used wastewater was high, 133 g/L, a drying process at 85°C will produce a precipitate containing mostly hydrated $FeCl_2$ and a smaller proportion of hydrated $FeCl_3$.

K_2FeO_4 was synthesized by using the obtained residue as a raw material. After drying, grinding of the solid residue was performed to obtain a larger reactive surface area. A rotating ball mill was formed in the laboratory, (Fig 1), to which in addition to the resulting ground residue added was $Ca(ClO)_2$ 99% in solid form and KOH 85% in solid form in relation to: solid residue : $Ca(ClO)_2$: KOH, 1 : 2: 3. The mixing is carried out in a ball mill, at a speed of 80 rotations per minute for 3 hours.

Since the reaction is exothermic, if necessary, cooling is performed from the outside of the mill. The resulting mixture was cooled in an ice bath, and then sequentially washed with 0.5 ml of n-pentane, methyl alcohol and ethyl ether for about 2 min. The solids on the filter paper were then dried in a vacuum furnace under pressure <30 mm Hg at room temperature for one hour to give a dry, K_2FeO_4. The resulting K_2FeO_4 is of technical quality, and for a purer ferrate it needs recrystallization i.e. dissolving of NaOH and re-deposition using KOH. The obtained K_2FeO_4 yield was determined by the chromite method (Waite & Gilbert, 1978).

In the second part of the experiment, the possibility of using ferrate synthesized from scrap iron in the treatment of waste water from a wood processing plant was examined.

Figure 1. Appearance of the rotary ball mill, in which the reactions take place.

Two wastewater samples from the wood processing plant were used in the experimental work: a sample from the thermal dryer and a sample from the steam chamber. The initial concentration of phenol in the sample from the thermal dryer was 27 mg / l and in a sample from the steam chamber 30 mg / l. This wastewater is characterized by a high content of natural organic matter. Chemical oxygen demand (COD) of the sample from the thermal dryer was 3233.1 mg O2 / l and of the sample from the steam chamber 4692.1 mg O2 / l. pH value of the sample from the thermal dryer was 4 and pH value of the sample from steam chamber was 5. the samples were treated with the solution of electrochemically synthesized ferrate(VI) concentration of 8 g / l in molar ratio phenol : ferrate(VI) = 1 : 5. The process of electrochemical synthesis of the alkaline solution of ferrate(VI) was based on transpassive anodic dissolution of iron alloys in a 10 M NaOH solution, in accordance with previous studies (Čekerevac et al., 2010; Nikolić-Bujanović et al., 2012) and it was carried out in a laboratory facility for electrochemical synthesis of ferrate(VI). The change in the concentration of phenol and COD value of the samples were determined using standard

methods at MOL Institute, Stara Pazova.

The resulting $Fe(OH)_3$ needs to be annealed at 700°C to remove the pollutants which it precipitated as a coagulant, especially if they are organic compounds. Further procedure is in a ball mill, as previously described.

3. Results and Discussion

As reported in literature (Wei et al., 2015), iron sources for use in the process of dry and wet oxidation for Fe(VI) synthesis are mostly iron chloride and iron nitrate. Among them the iron nitrate is preferred because of the characteristics of fast dissolving and quick chemical reactions with hypochlorite to form Fe(VI). The rate of oxidation of iron chloride using hypochlorite is relatively low, since chloride ions which are released from the iron chloride will slow down the rate of dissociation of hypochlorite, which prolongs the time of Fe(VI) synthesis (Jiang et al., 2012). However, iron chloride will cost much less than iron nitrate.

Using the ratio of the reagent as an example, the ratio between the prices of these iron compounds (per unit of iron) was approximately (iron(III)chloride) : (iron(II)chloride) : (iron(III) nitrate), 1.0: 1.25 : 2.5. However, the goal of the study was to demonstrate the possibility of using wastewater from the steel pickling plant. According to data (Wei et al., 2015), wastewater from pickling steel contains many kinds of heavy metals and their concentrations are significantly higher than the legally permitted for wastewater. Heavy metals include Cr, Bi, Tl, Cd, Co, Cu, Ni, Pb and Zn. Fe and Cl are the most prevalent components, wherein Mn and Ca (respectively 1.386 and 1.551 g/L) are the second most numerous elements. In general, when the Fe content in the solution for pickling steel reaches 70-100 g/L, the solution is not used further in the process of etching of steel (Agrawal & Sahu, 2009).

It is obvious that the solution for pickling is used up to the Fe content of 133 g/L.

As the sum of Fe and Cl, 485 g/L is a third of the solution mass of 1.0 L (i.e., 1.4 kg), only a small amount of heat is required for the evaporation of its liquid components, including water and HCl. The solution is evaporated at a temperature of 85°C. The resulting precipitate was refined by grinding in order to obtain a large reactive surface during the mixing with $Ca(ClO)_2$, and KOH. In the Figure 1 is shown a ball mill with an electric motor in which the reactants were mixed and in which the reactions took place. Mixing was performed at a speed of 80 rotations per minute for 3 h.

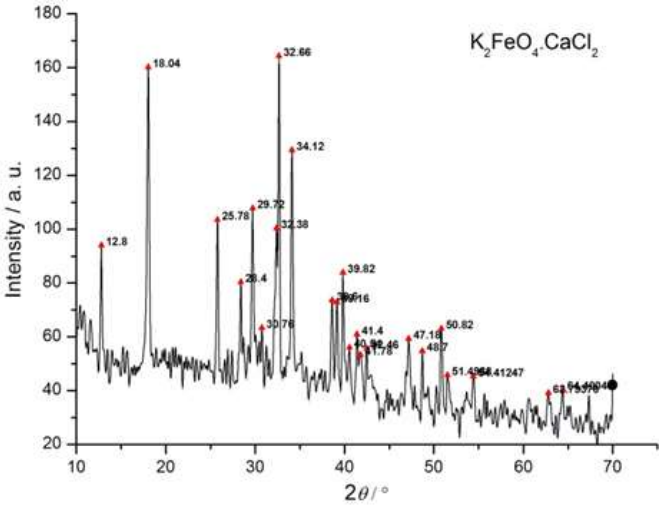

Figure 2. X-ray diffractogram of K_2FeO_4 admixture with $CaCl_2$.

The process that takes place during mixing in the ball mill can be represented by the following chemical reaction:

$$FeCl_2 \text{ x } 4H_2O + Ca(ClO)_2 + 2KOH \rightarrow K_2FeO_4 + CaCl_2 + 2HCl + 4H_2O \quad (2)$$

$$2FeCl_3 \text{ x } 6H_2O + 3Ca(ClO)_2 + 4KOH \rightarrow 2K_2FeO_4 + 3CaCl_2 + 3Cl_2 + 8H_2O \quad (3)$$

$$2FeCl_3 \text{ x } 6H_2O + 3Cl_2 + 8KOH \rightarrow 2K_2FeO_4 + 4KCl + 8HCl + 6H_2O \quad (4)$$

The process is exothermic and cooling is needed from the outside although the released water during the reaction lowers the temperature of the process. After the completion of mixing and cooling the resulting mixture in an ice bath, rinsing in organic solvents is conducted, and then drying in a vacuum dryer at room temperature. The obtained precipitate is dark purple in color proving the presence of Fe(VI), as confirmed by x-ray diffractometer. X-ray diffractogram of potassium ferrate (VI), (Fig. 2), is in good correlation with diffractograms presented in relevant literature (Xu et al., 2007), which has confirmed purity of this reactant.

This method provides K_2FeO_4 of sufficient purity for use in the treatment of wastewaters of different origin. The yield of ferrate salt is calculated from the following equation:

$$yield(mol\%) = \frac{(K_2FeO_4\ product\ weight) \times (product\ purity)\ \times\ (Fe\ atomic\ weight)}{(K_2FeO_4\ molecular\ weight) \times (Fe\ mass\ in\ the\ solid\ derived)} \quad (5)$$

The analysis of the obtained ferrate salt showed a purity of 82 wt. % while the yield was 15 Mol. %, which, given that waste Fe is used, it is more cost-effective than any other method of synthesis of ferrate from iron or its alloys.

The basic idea of this study was the use of $Fe(OH)_3$ as raw material for the synthesis of ferrate. Ferrous hydroxide occurs as a product in the reduction of ferrate in the reaction with the pollutants as their coagulant in wastewater treatment. The formed precipitate could be used for the recovery of ferrate using the process described in this paper according to the given reactions 6 and 7:

$$Fe(OH)_2(s) + 2ClO^- + 2OH^- \rightarrow FeO_4^{2-} + 2Cl^- + 2H_2O \quad (6)$$

$$2FeO(OH)(s) + 3ClO^- + 4OH^- \rightarrow 2\ FeO_4^{2-} + 3Cl^- + 3H_2O \quad (7)$$

Results of phenol removal by ferrate(VI) from the samples of wastewater from the thermal dryer and steam chamber are shown in Table1.

Table 1. Reduction of the phenol concentration in the samples of wastewater from the thermal dryer and steam chamber before and after the treatment.

	Phenol concentration in the untreated sample, mg / l	Phenol concentration in the treated sample, mg / l	Removal efficiency, %
Thermal dryer	27	6,79	74,9
Steam chamber	30	8,20	72,7

The results of the treatment shows high removal efficiency of phenol by ferrate(VI), 74.9% and 72.7%, for wastewater from thermal dryer and steam chamber, respectively, Table 1. Phenol is removed from aqueous solution by flocculation and coagulation with ferrous hydroxide, reactions, Figure 3, which is obtained as a product of ferrate(VI) reduction and has a very developed absorption area(Jiang & Lloyd, 2002). Since ferrous hydroxide has an extremely low solubility in these conditions, presence of residual Fe is not expected.

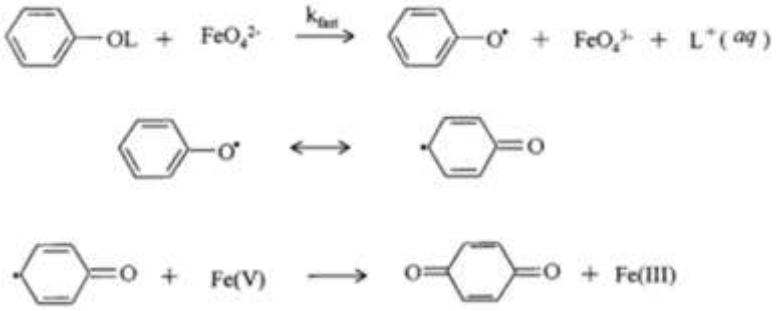

Figure 3. Removal of phenol from water using ferrate(VI).

Possibility of phenol removal using ferrate(VI) was additionally confirmed by determining the value of COD in the samples treated by ferrate(VI), Table 2.

Table 2. Percentage of COD removal during oxidation reaction of phenol by ferrate(VI)

	COD of untreated sample, mgO_2 / l	COD of treated sample, mgO_2 / l	Reduction efficiency of COD, %
Thermal dryer	3233.1	2384	26.3
Steam chamber	4692.1	2594	44.7

After the addition of ferrate(VI) into the solution, Figure 4, showed a COD reduction of4692.1 mgO_2 / l, for thermal dryer WW and steam also characterized by high initial COD values, 3233.1 and 26.3 % for thermal dryer and 44.7 % for steam chamber.

Using higher doses of ferrate(VI) could reach a more efficient reduction of COD values which requires further optimization of the treatment process of WW from wood industry by ferrate(VI)

The resulting precipitate was subjected to treatment according to the described method. After cooling and examination, the precipitate acquired a purple color, which indicates the presence of ferrate. Chromite analysis determined the presence of 70 wt.% K_2FeO_4.

4. Conclusion

This paper presents the recycling of wastewater from the process of pickling steel which in itself besides iron contains a large percentage of other heavy metals. The core of this work was to use the present $FeCl_2$ and $FeCl_3$ as raw materials for getting K_2FeO_4.

Figure 4. Sample of WW from the steam chamber before the treatment and after the second step of the treatment by ferrate (VI).

Using the rotary ball mill the synthesized K_2FeO_4 has a purity of 82 wt. % with a yield of 15 Mol. %.

The resulting reaction product was a dark purple color which indicates the presence of ferrate, and x-ray diffraction confirmed it. Showed was that with this procedure it is possible to round off the process of synthesis and use of

ferrate(VI) because the product formed in the process of wastewater treatment, $Fe(OH)_3$, can be recycled and from it derive ferrate(VI) again.

Acknowledgements

The work was financially supported by The Ministry of Education, Science and Technological Development, Republic of Serbia, within Projects TRp 34025, TRp 31080 2011/2019.

References

Agrawal, A., & Sahu, K. K. (2009). An overview of the recovery of acid from spent acidic solutions from steel and electroplating industries. *Journal of Hazardous Materials*, *171*(1–3), 61–75. https://doi.org/10.1016/J.JHAZMAT.2009.06.099

Ahmaruzzaman, M. (2008). Adsorption of phenolic compounds on low-cost adsorbents: A review. *Advances in Colloid and Interface Science*, *143*(1–2), 48–67. https://doi.org/10.1016/J.CIS.2008.07.002

Audette, R. J., Quail, J. W., & Smith, P. J. (1971). Ferrate (VI) ion, a novel oxidizing agent. *Tetrahedron Letters*, *12*(3), 279–282. https://doi.org/10.1016/S0040-4039(01)96418-4

Čekerevac, M. I., Nikolić-Bujanović, L. N., Mirković, M. B., & Popović, N. H. (2010). Application of electrochemically synthesized ferrate(VI) in the purification of wastewater from coal separation plant. *Hemijska Industrija*, *64*(5), 423–430. https://doi.org/10.2298/HEMIND100325047C

Fremy, E. (1841). Recherches sur l'action des peroxydes alcalins sur les oxydes métalliques:Lettre de M. Ed. Fremy à M. Pelouze. *Comptes Rendus de l'Académie Des Sci. Paris*, *12*, 23–24.

Fremy, E. (1842). Recherches sur les acides métalliques. *Comptes Rendus de l'Académie Des Sci Paris*, *14*, 442–446.

Gombos, E., Felföldi, T., Barkács, K., Vértes, C., Vajna, B., & Záray, G. (2012). Ferrate treatment for inactivation of bacterial community in municipal secondary effluent. *Bioresource Technology*, *107*, 116–121. https://doi.org/10.1016/J.BIORTECH.2011.12.053

Hameed, B. H., & Rahman, A. A. (2008). Removal of phenol from aqueous solutions by adsorption onto activated carbon prepared from biomass material. *Journal of Hazardous Materials*, *160*(2–3), 576–581. https://doi.org/10.1016/J.JHAZMAT.2008.03.028

Iurascu, B., Siminiceanu, I., Vione, D., Vicente, M. A., & Gil, A. (2009). Phenol degradation in water through a heterogeneous photo-Fenton process catalyzed by Fe-treated laponite. *Water Research*, *43*(5), 1313–1322. https://doi.org/10.1016/J.WATRES.2008.12.032

Jiang, H., Fang, Y., Fu, Y., & Guo, Q. X. (2003). Studies on the extraction of phenol in wastewater. *Journal of Hazardous Materials*, *101*(2), 179–190. https://doi.org/10.1016/S0304-3894(03)00176-6

Jiang, J. Q., & Lloyd, B. (2002). Progress in the development and use of ferrate(VI) salt as an oxidant and coagulant for water and wastewater treatment. *Water Research*, *36*(6), 1397–1408. https://doi.org/10.1016/S0043-1354(01)00358-X

Jiang, J. Q., Zhou, Z., & Pahl, O. (2012). Preliminary study of ciprofloxacin (cip) removal by potassium ferrate(VI). *Separation and Purification Technology*, *88*, 95–98. https://doi.org/10.1016/J.SEPPUR.2011.12.021

Kiselev, Yu. M., Kopelev, N. S., Zav'yalova, N. A., Perfil'ev, Yu. D., & Kazin, P. E. (1989). On the preparation of alkali metal ferrates(6). *Zhurnal Neorganicheskoj Khimii*, *34*(9), 2199–2202.

Lee, L. S., Suresh, P., Rao, C., & Brusseau, M. L. (1991). Nonequilibrium Sorption and Transport of Neutral and Ionized Chlorophenols. *Environmental Science and Technology*, *25*(4), 722–729. https://doi.org/10.1021/ES00016A018/ASSET/ES00016A018.FP.PNG_V03

Licht, S., Tel-Vered, R., & Halperin, L. (2002). Direct electrochemical preparation of solid Fe(VI) ferrate, and super-iron battery compounds. *Electrochemistry Communications*, *4*(11), 933–937. https://doi.org/10.1016/S1388-2481(02)00493-9

López-Montilla, J. C., Pandey, S., Shah, D. O., & Crisalle, O. D. (2005). Removal of non-ionic organic pollutants from water via liquid-liquid extraction. *Water Research*, *39*(9), 1907–1913. https://doi.org/10.1016/J.WATRES.2005.02.018

Mácová, Z., Bouzek, K., Híveš, J., Sharma, V. K., Terryn, R. J., & Baum, J. C. (2009). Research progress in the electrochemical synthesis of ferrate(VI). *Electrochimica Acta*, *54*(10), 2673–2683. https://doi.org/10.1016/J.ELECTACTA.2008.11.034

Manual Report for List of Chemical Priority, (2008) Environmental Protection Agency (EPA), USA, 2002

Nair, C. I., Jayachandran, K., & Shashidhar, S. (2008). Biodegradation of phenol. *African Journal of Biotechnology*, *7*(25), 4951–4958. https://doi.org/10.5897/AJB08.087

Nikolić-Bujanović, L., Čekerevac, M., Vojinović-Miloradov, M., Jokić, A., & Simičić, M. Š. (2012). A comparative study of iron-containing anodes and their influence on electrochemical synthesis of ferrate(VI). *Journal of Industrial and Engineering Chemistry*, *18*(6), 1931–1936. https://doi.org/10.1016/J.JIEC.2012.05.007

Nikolić-Bujanović, L. N., Simičić, M. v., & Čekerevac, M. I. (2012). Electrochemical preparation of solid ferrates(VI). *Hemijska Industrija*, *66*(4), 455–460. https://doi.org/10.2298/HEMIND111207004N

Ockerman, L. T., & Schreyer, J. M. (1951). Preparation of Sodium Ferrate(VI). *Journal of the American Chemical Society*, *73*(11), 5478. https://doi.org/10.1021/JA01155A545/ASSET/JA01155A545.FP.PNG_V03

Pinto, R. T. P., Lintomen, L., Luz, L. F. L., & Wolf-Maciel, M. R. (2005). Strategies for recovering phenol from wastewater: thermodynamic evaluation and environmental concerns. *Fluid Phase Equilibria*, *228–229*, 447–457. https://doi.org/10.1016/J.FLUID.2004.09.005

Regulation on hazardous substances in water, *Official Gazette of SRS*, no. 31/82

Rengaraj, S., Moon, S. H., Sivabalan, R., Arabindoo, B., & Murugesan, V. (2002). Removal of phenol from aqueous solution and resin manufacturing industry wastewater using an

agricultural waste: rubber seed coat. *Journal of Hazardous Materials*, *89*(2–3), 185–196. https://doi.org/10.1016/S0304-3894(01)00308-9

Schreyer, J. M., Thompson, G. W., & Ockerman, L. T. (1953). Potassium Ferrate(VI). *Inorganic Syntheses*, *IV*, 164–168.

Sharma, V. K. (2002). Potassium ferrate(VI): an environmentally friendly oxidant. *Advances in Environmental Research*, *6*(2),

143–156. https://doi.org/10.1016/S1093-0191(01)00119-8

Turhan, K., & Uzman, S. (2008). Removal of phenol from water using ozone. *Desalination*, *229*(1–3), 257–263. https://doi.org/10.1016/J.DESAL.2007.09.012

Waite, T. D., & Gilbert, M. (1978). Oxidative Destruction of Phenol and Other Organic Water Residuals by Iron (VI) Ferrate. *Journal (Water Pollution Control Federation)*, *50*(3), 543–551.

Wei, Y. L., Wang, Y. S., & Liu, C. H. (2015). Preparation of Potassium Ferrate from Spent Steel Pickling Liquid. *Metals 2015, Vol. 5, Pages 1770-1787*, *5*(4), 1770–1787. https://doi.org/10.3390/MET5041770

Xu, Z., Wang, J., Shao, H., Tang, Z., & Zhang, J. (2007). Preliminary investigation on the physicochemical properties of calcium ferrate(VI). *Electrochemistry Communications*, *9*(3), 371–377. https://doi.org/10.1016/J.ELECOM.2006.09.015

Yamada, K., Akiba, Y., Shibuya, T., Kashiwada, A., Matsuda, K., & Hirata, M. (2005). Water purification through bioconversion of phenol compounds by tyrosinase and chemical adsorption by chitosan beads. *Biotechnology Progress*, *21*(3), 823–829. https://doi.org/10.1021/BP0495668

Yang, X., Guo, W., Zhang, X., Chen, F., Ye, T., & Liu, W. (2013). Formation of disinfection by-products after pre-oxidation with chlorine dioxide or ferrate. *Water Research*, *47*(15), 5856–5864. https://doi.org/10.1016/J.WATRES.2013.07.010

Yunho, L., Cho, M., Kim, J. Y., & Yoon, J. (2004). Chemistry of Ferrate (Fe(VI)) in Aqueous Solution and its Applications as a Green Chemical. *J. Ind. Eng. Chem.*, *10*, 161–171.

Primena otpadnog gvožđa u sintezi ferata(VI) i uklanjanje fenola kao potvrda efikasnosti

Ljiljana Nikolić Bujanović[1,*], Milan Čekerevac, Miloš Simičić, Milena Tomić[2]

[1]Fakultet za ekologiju i zaštitu životne sredine, Univerzitet Union-Nikola Tesla, Beograd, Srbija
[2]IHIS Techno-experts, Istraživački i razvojni centar, Batajnički put 23, Beograd, Srbija

*Autor za korespondenciju: ljnikolicbujanovic@unionnikolatesla.edu.rs, bujanovic08@gmail.com

Abstrakt: Ferat (VI) je jako oksidaciono, koagulaciono i flokulaciono sredstvo. Zbog svojih karakteristika pogodan je za tretman voda različitog porekla. U ovim procesima nastaje ekološki i netoksičan proizvod, $Fe(OH)_3$, koji se prema rezultatima ovog rada može reciklirati i ponovo sintetizovati u ferat(VI). U ovom radu je prikazana metoda za sintezu feratnih soli postupkom oksidacije iz otpadnih voda od nagrizanja čelika koje sadrže soli $FeCl_2$ i $FeCl_3$.
Metoda za sintezu podrazumeva proces oksidacije fero i feri jona pomoću $Ca(ClO)_2$ u prisustvu KOH u čvrstom stanju. Snimak rendgenskog difraktometra pokazuje značajno prisustvo K_2FeO_4, dok je analiza pokazala prinos od 15%.traž
Prikazana je primena ferata sintetizovanog iz otpadnog gvožđa u procesu prečišćavanja otpadnih voda iz drvne industrije. Primer koji je dat u ovom radu je tretman uzoraka WW iz drvne industrije, iz termo sušare i parne komore, primenom Jar testa. Početna koncentracija fenola u uzorku iz termičke sušare iznosila je 27 mg/l, a u uzorku iz parne komore 30 mg/l. Ova otpadna voda takođe ima visok sadržaj prirodne organske materije (HPK uzorka iz termo sušare je 3233,1 mgO_2/l i HPK uzorka iz parne komore 4692,1 mgO_2/l). Efikasnost uklanjanja fenola feratom(VI) iznosila je 74,85% i 72,67% za uzorke iz termičke sušare i parne komore, respektivno.

Ključne reči: kalijimferat, ferohlorid, ferihlorid, fenol, x-rey

Global Sustainability Challenges
2023; Vol. 1(1): 9-22
https://gsc.unionnikolatesla.edu.rs/index.php/gsc/index
UDC: 502.132:620.197.3
620.193:669.715
ISSN: 2956-1051 (Online)

A review on cerium-based conversion coatings on aluminium surfaces

Samira Naghdi[1], Vesna Mišković Stanković[2,*]

[1] Physikalisch-Technische Bundesanstalt, Abbestr. 2-12, 10587 Berlin, Germany
[2] Faculty of Ecology and Environmental Protection, University Union-Nikola Tesla, Belgrade, Serbia

[*]**Corresponding author:** vesna.miskovicstankovic@gmail.com

To cite this article:
Naghdi, S. and Mišković-Stanković, V. (2023). A review on cerium-based conversion coatings on aluminium surfaces. *Global sustainability challenges, 1*(1), pp. 9-22

Received: July 21, 2022;: **Revised:** Dec 12, 2022; **Accepted:** Dec 17, 2022

Abstract: Conversion coatings containing hexavalent chromium (chromate) have been widely used for decades as part of corrosion protection systems on aluminium alloys. However, chromates are prohibited in many fields due to their toxicity and should be replaced by "green" environmentally friendly alternatives. Cerium-based conversion coatings (CeCCs) are among the most prospective alternatives because of their anticorrosion efficiency, environmentally friendly characteristics, and low cost. This review is focused on the protective properties of CeCCs on aluminium as a sole protecting coating or as a conversion one in combination with top organic coating.

Keywords: cerium; corrosion; electrodeposition; EIS; polarization measurements

1. Introduction

For years, different coating deposition techniques, i.e., electrophoretic deposition, chemical vapour deposition, sol-gel, dip coating, spray coating, and various materials, carbon-based nanomaterials, organic coatings (or paints), etc., were investigated and recommended for protecting metal substrates from corrosion (Naghdi, Jevremović, et al., 2016; Naghdi & Miskovic-Stankovic, 2022; Naghdi et al., 2018; Naghdi et al., 2020; Naghdi et al., 2017). Using an organic coating is the most common way to protect metals (Mg alloys, aluminium alloys, steel, etc.) against corrosion. The effectiveness of such coatings is to ensure the best possible adhesion to the base material and prevent the coating adhesion loss under the environmental influence.

Among the various protective coating, chemical conversion coatings are presented as the most effective pre-treatments, with the facile operation and low-cost coating technique. The reaction of an active solution with a metal substrate provides the ions needed to form a conversion coating that improves the adhesion of organic coatings and enhances the corrosion protection of the underlying metal. Immersion of metals in a bath containing chromate ions was the most effective and popular procedure for producing a chromate conversion coating (CCC) as the protective layer on the metal surface. Due to its outstanding corrosion resistance, favourable adhesion with top organic coatings, and simplicity in production, this coating was the most conventional industrial surface treatment of metal materials(Hagans & Haas, 1994). The self-repairing effect of CCC is one of the reasons for its superior corrosion resistance than other coatings. When CCC covers the metal substrate, it releases chromate, which can migrate and repair corrosion (Zhao et al., 2001). CCC presented an excellent corrosion protection ability of pure aluminium, aluminium alloys, zinc alloys, Mg alloys, etc., that widely used in automotive, aerospace, and electronics industries for many years (Gigandet et al., 1997; Ilevbare & Scully, 2001; Lunder et al., 2005; Piao et al., 2019).

However, over the last decades, the high toxicity of the hexavalent chromium compounds in CCC was recognized and imposed restrictions on their use in industry and food applications. Therefore, due to the environmental and health hazard in their use and disposal, a great deal of research efforts has been done to develop a new environmentally friendly alternative for CCC. Among the numerous materials, which presented a good anti-corrosion behaviour, a high benefit/cost relation, and mainly, low environmental impacts,

the conversion coatings based on phosphate, cerium, zirconium, titanium salts, titanium zirconium salt, cobalt salts, molybdate, etc. have been developed and widely studied.

2. Conversion coating

As an alternative to CCC, phosphate conversion coating (PCC) could replace CCC as surface pre-treatment in various industrial applications, such as the automotive and appliance industries. Moreover, due to their low toxicity and high chemical stability, PCC received extensive attention in the field of medical metal surface modification. Cost-effectiveness, low coating formation time, simple operation, suitability for irregular surfaces, and low impact on the mechanical properties of metal substrates are some of the unique advantages of PCC. Various factors can impact the anti-corrosion performance of PCC, i.e., pH, phosphating temperature, bath ingredient, and the surface characters of the metal substrate, including compositions, microstructure, and its electrochemical activity. Altering the surface morphology of the metal substrate using laser surface texturing (LST) was presented as an effective strategy to improve the corrosion resistance of magnesium alloy (H. Liu et al., 2021). The high specific area and surface roughness produced by LST accelerated the deposition of PCC, increased the adhesion of the coating, and enhanced the adhesion of the coating to the substrate. The electrochemical tests presented a better long-term corrosion resistance of PCC coating on the metal substrate modified by LST. Using PCC as a coating on titanium (Ti) implants is also presented as an effective method for simultaneously regulating the elemental compositions and crystallographic morphological of Ti implant surfaces (Zhao et al., 2021). The PCC-coated Ti implants showed good biocompatibility that can prevent a prolonged healing period and even implantation failure. Furthermore, doping PCC coating with Zinc (Zn) that has strong antibacterial properties showed inhibition of biofilm formation on the PCC-coated Ti implant after continuous incubation up to 24 h (Zuo et al., 2022). Application of PCC on sand-cast and die-cast Mg alloys showed the effect of the production method of the substrate on the characteristics of the coating (Zhou et al., 2021). The PCC was more compact on the die-cast substrate, exhibited lower electrical contact resistance (ECR), and had better corrosion resistance (due to the intensified micro-galvanic effect through the grain refinement of the die-cast alloy) compared to the PCC on sand cast Mg alloy.

Zr-based conversion coating is another type of chromate-free pre-treatments technique that, due to its potential to lower operational cost in the area of energy, maintenance, and reducing the environmental impacts, has gained acceptance. During Zr-based conversion coating, the bath may contain various additives, i.e., organic polymers, metal ions, etc., to improve corrosion protection and adhesion properties and establish a base for subsequent painting. Liu et al. showed that adding Cu^{2+} and PAMAM positively impacted on the kinetics of the coating growth and enhanced the adhesion of the subsequent organic coating (X. Liu et al., 2021). The combination of Zr and Ti as a conversion coating (Zr-Ti conversion coating) as an alternative for toxic CCC has been studied in the automobile industry (Kolesnikova et al.). The studies showed that the application of Zr-Ti conversion coating on aluminium alloy 5556 enhanced its corrosion resistance to pitting corrosion. Adding Mo to the Zr-Ti conversion coating was investigated to further improve the corrosion resistance of LY12 aluminium alloy (Qian et al., 2021). The electrochemical tests showed that the continuous dense Mo-Zr-Ti conversion coating significantly reduced the I_{corr}, increased the film resistance R_f in the temperature range from 0 to 60 ºC, and reduced the corrosion rate. Hoang et al. investigated the impact of adding (3-aminopropyl)triethoxysilane (APTES) to Zr conversion coating on steel (Hoang et al., 2022). The results showed that Zr conversion coating containing APTES improved the corrosion protection of the bare steel and reduced the adhesion loss.

As a viable alternative to CCC, Ti conversion coating (TiCC) presented a proper anti-corrosion performance on different substrates such as Mg alloys, Al alloys, steel, and galvanized steel (Wang & Xu, 2021). Combination of such coating with cerium (Ti-CeCC) and cobalt (Ti-CoCC) was investigated as anti-corrosion resistance coatings for enhancing the adhesion property of the organic coating applied on Al-2024 substrate (Roshan & Sarabi, 2021). Results suggest that Ce and Co additives changed the morphology of the TiCC and increased the surface energy of the coating, and compared to the bare sample, Ti-CeCC and Ti-CoCC improved the anti-corrosion resistance of the sample.

Another promising candidate for replacing CCC is Ce-based chemical conversion coatings (CeCC). To obtain the best results from CeCC, pre-treatment methods, i.e., cleaning or etching to remove inorganic contamination or eliminate the native oxide layer, are required (Deng et al., 2021; Sainis & Zanella, 2022; Sun et al., 2021). Using solutions containing $CeCl_3$ and H_2O_2 was studied as a pre-treatment method for depositing CeCC on AA2024-T3 and AA7075-T6 substrates (Alba-Galvín et al., 2021). The results showed that the formation of CeCC over AA7075 was faster than over AA2024. CeCC in all samples offered cathodic protection, and the anti-corrosion properties of CeCC coating were enhanced due to the pre-treatment technique. Moreover, HF pre-treatment of Zn–5% Al alloy was revealed an increased growth rate of CeCC, and CeCC was preferentially deposited on the surface of the Al-rich phase. Furthermore, due to the uniform and thick coating formation, the HF pre-treatment exhibited a positive effect on the corrosion resistance of the coated samples (Sun et al., 2021).

The impact of bath temperature and the heating process on the formation of the CeCC on Fe50Mn30Co10Cr10 (at.%) dual-phase high-entropy alloy (DP-HEA) was investigated by Chen et al.(Chen et al., 2021). The electrochemical tests showed a decrease in both anodic current densities and

corrosion current densities of the CeCC coated specimens compared to the untreated DP-HEA. Furthermore, the bath-heating process was introduced to increase the coating thickness and the superior anti-corrosion properties of the coating. In addition to the pre-treatment techniques and the coating condition, additives, i.e., Cu and manganese (Mn), were reported as a positive factor in improving the corrosion resistance of CeCC coated galvanized steel in 3.5 wt% NaCl solution (Khast et al., 2021). Kamde et al. reported deposition of a few microns' thick CeCC on the surface of Mg-4 wt%Y(Kamde et al., 2021). Increasing the deposition duration from 30 to 1800 s negatively affected the coating. Due to hydrogen bubble formation on the substrate surface, the CeCC delaminated at a few places. Moreover, due to dehydration while drying, the CeCC was deposited at a short duration (30 s, 60 s), cracks formed all over the coating. Altogether, the presence of the CeCC on Mg-4 wt%Y exhibited a better corrosion resistance than the bare substrate. The impact of Mo additive on the CeCC on Al alloy 6063 (AA6063) was investigated by Lu et al. (Lu et al., 2020). CeCC and Ce-Mo conversion coating (CeMCC) were deposited on AA6063 by immersion in alkaline conversion baths. CeMCC presented a more uniform and smoother structure than CeCC. Both coatings presented a better corrosion resistance than bare AA6063, while the CeMCC had lower corrosion current density and higher corrosion resistance than CeCC in a 3.5 wt% NaCl solution.

In addition to the conversion coatings named above, there are other types of conversion coatings, i.e., boehmite and silica conversion coatings (Braga et al., 2020), molybdate conversion coating (MCC) (Yang et al., 2021), rare earth elements (lanthanum, neodymium and yttrium) (Shih & Mansfeld, 1992), that was introduced as an alternative for replacing CCC.

3. Cerium-based conversion coatings deposition

Investigations on cerium-based conversion coatings focus on appropriate processes of their depositions. The coatings can be applied by spraying, immersion processes (M. Bethencourt et al., 1998; Fedel et al., 2014; Jegdić et al., 2013; Johansen et al., 2012; Mansfeld et al., 1991; Mansfeld et al., 1992; Onofre-Bustamante et al., 2009; Živković et al., 2013), or electrodeposition (Exbrayat et al., 2014; Stoychev, 2013; Živković et al., 2015; Živković et al., 2014). The most used method is immersing aluminium or its alloys into hot aqueous cerium solutions for a long time. The applied ceria coating has caused a multifold increase in corrosion resistance of Al. In order to reduce the deposition time of oxide/hydroxide film onto aluminium and improve the corrosion resistance, hydrogen peroxide is usually added to the solution of cerium ions (Dabala et al., 2001; Hughes et al., 1995; Yu et al., 2001; Živković et al., 2015). Besides the time of immersion, the parameters such as the temperature, pH of the conversion solution, the concentration of cerium ions, time, and potential of electrodeposition, etc., were also examined (Dabala et al., 2004; Živković et al., 2015; Živković et al., 2014). Since it was found that ceria coating morphology has the main role in corrosion protection of aluminium (Živković et al., 2014), either as a sole protecting coating or as a conversion one in combination with protectors based on metals (Exbrayat et al., 2014; Nemes et al., 2013) and organic (Živković et al., 2015; Živković et al., 2013) or silane(Zand et al., 2013) compounds, it is essential to obtain the coating with uniform fine-grained structure. This structure is expected to dry rapidly with a low tendency to crack. The sol-gel process is now well accepted as a technology for preparing such thin films and coatings (Hamdy, 2006; Schem et al., 2009), with a promising impact on corrosion protection of aluminium and its alloys (Hollamby et al., 2012; Zuo et al., 2015).

3.1. Sol-gel method

The ceria sol is obtained by forced hydrolysis according to the following procedure (Gulicovski et al., 2014; Gulicovski et al., 2009). The appropriate amount of $Ce(NO_3)_4$ solution in 0.2 M HNO_3 is added drop-wise to the boiling HNO_3 solution being vigorously stirred by a mechanic stirrer. During the ageing for 20 h, the oxide solid-phase nucleates and grows continuously, creating particles of defined shape and size. The CeO_2 coatings are formed onto aluminium panels by the dripping method. Upon application of CeO_2 coating, a smooth surface appears, with the in-place generation of narrow cracks around the pits on Al substrate beneath (Fig. 1b, d and f) (Gulicovski et al., 2016), which is the usual appearance of sol-gel-prepared ceria coatings on Al-based materials (Zuo et al., 2015). It is important to note that the size of islands between the cracks is similar to the size of the pits of the Al surface beneath the ceria coating (Fig. 1a, c and e). EIS data showed greater corrosion resistance of CeO_2-coated aluminium in comparison to bare Al during a long exposure time (Fig. 2) due to the formation of a uniform protective CeO_2 coating/Al interphase, cross-linked by AlO(OH) fibre-like structures (Gulicovski et al., 2016).

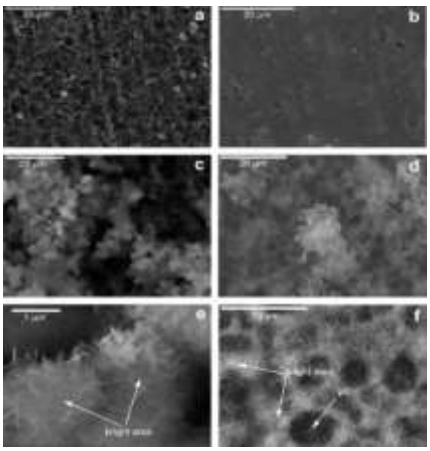

Figure 1. Surface morphology of aluminium (a) and cerium oxide coating before (b) and after exposure to 3 wt.% NaCl solution (c and e - Al after 384 h of exposure; d and f - Al/CeO_2 after 552 h of exposure) (Reprinted from (Gulicovski et al., 2016) with permission from Springer, Copyright 2016).

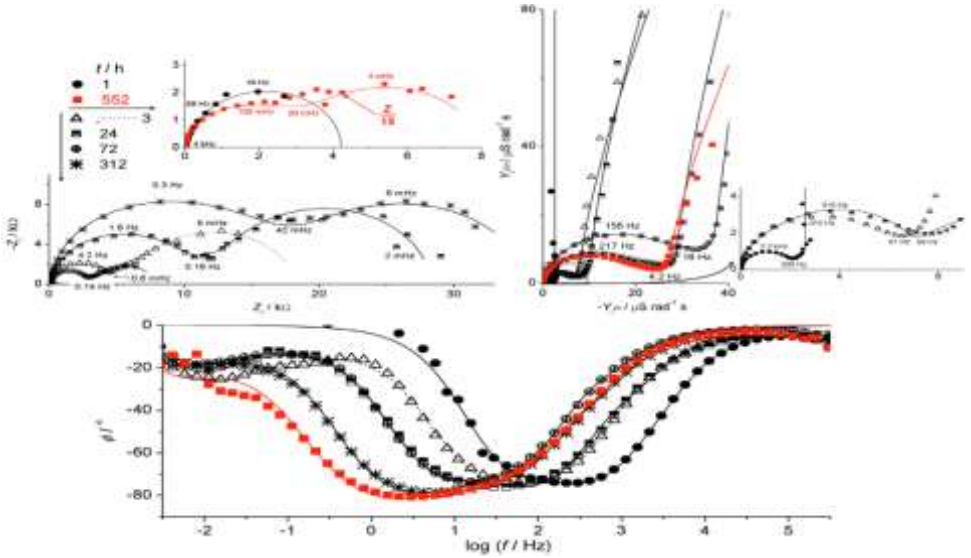

Figure 2. Experimental (symbols) and fitting (lines) data of Al/CeO_2 registered at open circuit potential after different times of exposure to NaCl solution presented as impedance and capacitance complex plane spectra and Bode phase angle plots (Reprinted from (Gulicovski et al., 2016) with permission from Springer, Copyright 2016).

3.2. Dip inmersion method

The deposition mechanism involves both anodic oxidation of Al, Eq. (1) and cathodic reduction of soluble oxygen and/or H_2O_2 added, Eqs. (2) and (3), respectively (Creus et al., 2006; Decroly & Petitjean, 2005; Pinc et al., 2009; Stoffer et al., 2006; Tang et al., 2011) as follows:

$$Al \rightarrow Al^{3+} + 3e^- \quad (1)$$

$$2H_2O + O_2 + 4e^- \rightarrow 4OH^- \quad (2)$$

$$H_2O_2 + 2e^- \rightarrow 2OH^- \quad (3)$$

$$Ce^{3+} + 3OH^- \rightarrow Ce(OH)_3 \quad (4)$$

The generation of hydroxide ions at cathodicsites leads to a strong local increase in pH near the alloy surface, which promotes the formation of $Ce(OH)_3$ precipitate or/and soluble ionic complexes such as $7e(OH)_2^+$. When H_2O_2 is added, the deposition of Ce(IV) is more favourable than Ce(III) (Creus et al., 2006; Tang et al., 2011), Eqs. (4)-(7).

$$2Ce^{3+} + 3OH^- + H_2O_2 \rightarrow 2Ce(OH)_2^+ \quad (5)$$

$$2Ce(OH)_2^+ + 2OH^- \rightarrow Ce(OH)_4 \quad (6)$$

$$Ce(OH)_4 \rightarrow CeO_2 \cdot 2H_2O \quad (7)$$

The inhibition effect is achieved by the insoluble Ce oxide/hydroxide layer formed at cathodic sites, which suppresses the oxygen reduction reaction (Eq. 2), thereby providing a cathodic inhibition (Hill et al., 2011). The number of variables that influence the rate of CeCC deposition is extensive and includes solution chemistry (cerium salt used chloride or nitrate, additives such as gelatine, glycerol to reduce cracking), concentrations of cerium and H_2O_2, pH, temperature, time of immersion, etc. In addition, the surface composition and electrochemical behaviour of the range of alloys, as a function of alloying elements, add to the complexity of the deposition mechanism.

A variety of conversion solutions, heated or at room temperature, has been proposed to prepare CeCCs by dip immersion or spray processes. The most commonly used is the cerium chloride solution (Allachi et al., 2010; Aziz et al., 2011; Campestrini et al., 2004; Conde et al., 2008; Hughes et al., 2009; Stoffer et al., 2006), followed by the cerium nitrate one (Bethencourt et al., 2002, 2004; Bethencourt et al., 2008; Dabala, 2001; De Frutos et al., 2008; Fahrenholtz et al., 2002; Rangel et al., 2008; Zhang & Zuo, 2008), with or without H_2O_2 as an oxidizing agent. Although components, concentration, temperature, or immersion time (number of spray processes) are somewhat different, the processing steps are similar, including substrate pre-treatment (acid or alkaline), (De Frutos et al., 2008; Fahrenholtz et al., 2002; Johnson et al., 2005; Joshi et al., 2011; Pinc et al., 2009; Rangel et al., 2008) deposition and subsequent post-treatment (Heller et al., 2009, 2010; Pinc et al., 2009).

In order to investigate the effect of deposition time and post-treatment (Jegdić et al., 2013), the CeCCs were deposited on aluminium alloy AA6060 by 5 and 20 min immersion into chloride solution, 0.05 M $CeCl_3$ and subsequent post-treated in the 2.5 % Na_3PO_4, pH4.5, at 85 ^oC.EIS results indicated that CeCCs prepared at longer deposition time and post-treated exhibited better corrosion protection than those prepared at short deposition time and without post-treatment (Fig. 3).

Similarly, smaller cathodic currents were measured for CeCCs than bare AA6060 since the CeCCs decreased

cathodic current density of oxygen reduction (Fig. 4a) (Jegdić et al., 2013).

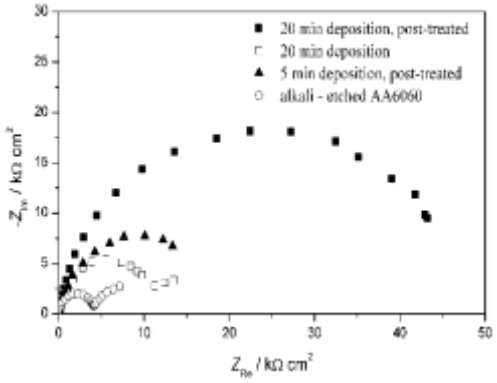

Figure 3. Nyquist plots for CeCCs: 20 min deposition without and with post-treatment, and 5 min deposition from 0.05 M $CeCl_3$ with post-treatment, after 1 h of exposure to 0.5 mol·dm^{-3} NaCl solution (Reprinted from (Jegdić et al., 2013) with permission from Serbian Chemical Society, Copyright 2013).

The CeCC deposited for 20 min reduced the current more than the one deposited for 5 min due to the diminution of cathodic sites (Bethencourt et al., 1998; Pepe et al., 2004). The anodic polarization curves (Fig. 4b) clearly indicated a reduced anodic activity of CeCCs on AA6060, especially pronounced for the sample deposited for 20 min and post-treated.

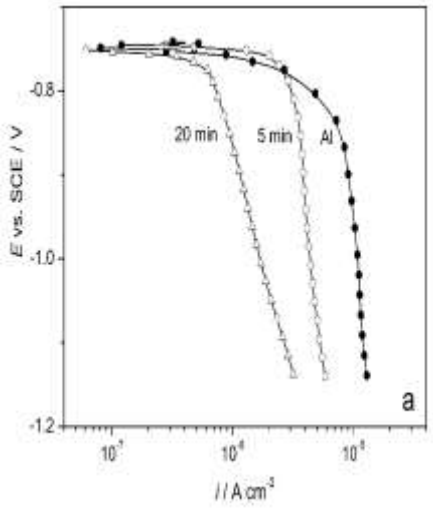

Although the CeCCs increased corrosion resistance of AA6060, slowing down the anodic and cathodic reaction rates with respect to the bare AA6060, the EIS study indicated the low pore resistance values and consequently low corrosion protection in 0.5 mol·dm^{-3} NaCl solution (Fig. 5).

In order to investigate the effect of counter ion, chloride or nitrate anion used as cerium precursor salts, CeCCs have been deposited on AA 6060 by immersion in 0.05 M $CeCl_3$ and 0.05 M $Ce(NO_3)_3$ aqueous solutions (Živković et al., 2013). Nonhomogeneous layers with visible cracks and lower impedance values were deposited from nitrate solution, while CeCCs from the chloride solution were more homogenous and crack-free, with greater impedance (Fig. 6). A subsequent post-treatment in the 2.5 % Na_3PO_4, pH 4.5, at 85 °C improved the quality of coatings in both cases.

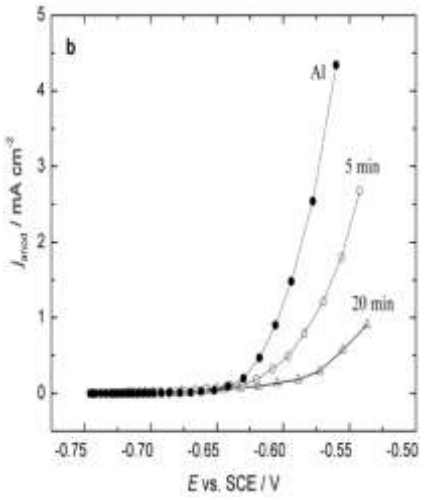

Figure 4. Cathodic (a) and anodic (b) polarization curves for CeCCs deposited for 5 and 20 min from 0.05 M $CeCl_3$ and post-treated, and alkali-etched AA6060 in 0.5 mol·dm^{-3} NaCl solution (Reprinted from (Jegdić et al., 2013) with permission from Serbian Chemical Society, Copyright 2013).

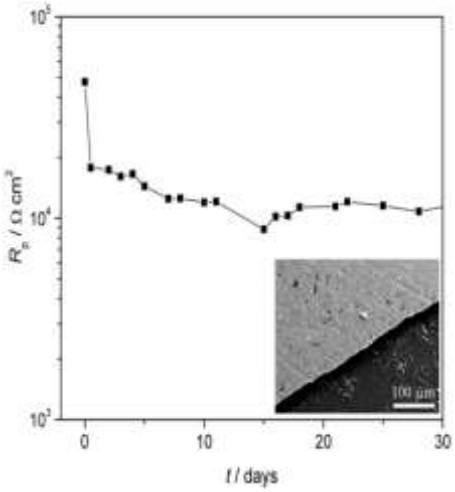

Figure 5. The time dependences of pore resistance, R_p, for CeCC deposited for 20 min from 0.05 M $CeCl_3$ and post-treated, during exposure to 0.5 mol·dm^{-3}NaCl solution (inset shows cross-sectional SEM micrograph of CeCC) (Reprinted from (Jegdić et al., 2013) with permission from Serbian Chemical Society, Copyright 2013).

On the contrary, in combination with a top polyester coating, the protective system with CeCC deposited from nitrate solution exhibited greater pore resistance during exposure to 0.5 mol·dm^{-3} NaCl solution compared to the CeCC from chloride solution (Fig. 7) due to better adhesion as a consequence of greater contact area between the cracked surface of CeCC from nitrate solution and top polyester coating. The similar values of pore resistance with polyester coating on chromate conversion coating proved the successful replacement of toxic chromate coating with "green" CeCC.

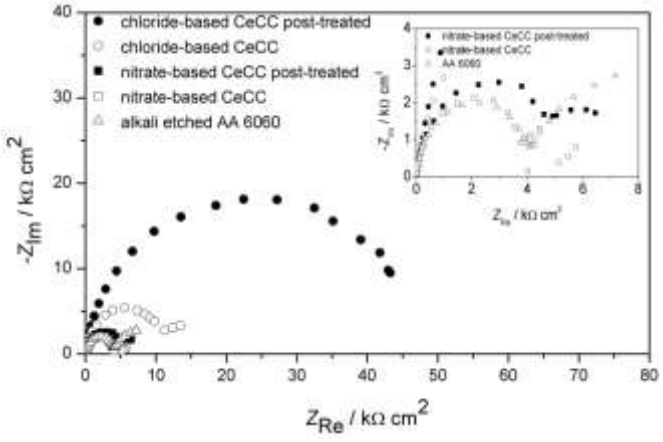

Figure 6. Nyquist plots for bare alkali-etched AA6060 and CeCCs deposited from nitrate and chloride bath for 20 min deposition without and with post-treatment, after 1h of exposure to 0.5 mol·dm^{-3} NaCl solution (Reprinted from (Živković et al., 2013) with permission from Elsevier, Copyright 2013).

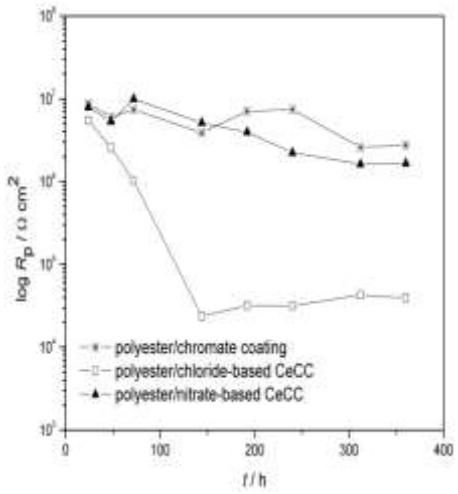

Figure 7. The time dependence of pore resistance for polyester coatings, R_p, on AA6060 with chromate conversion coating and CeCCs deposited from nitrate and chloride bath, during exposure to 0.5 mol dm^{-3}NaCl.

3.3. Electrodeposition

Electrolytic deposition (ELD) represents a powerful and cost-effective route for preparing high-quality thin oxide films on conductive substrates. It offers an easy way to vary the process parameters such as electrolyte properties (acidity level, reactant concentrations, additives), deposition current and time, temperature etc., which enables tuning of deposit characteristics (composition, morphology, thickness) (Naghdi et al., 2015; Naghdi, Jaleh, et al., 2016). Another advantage is rapid film formation. Switzer and Zhou (Zhou & Switzer, 1996) pioneered the electrochemical synthesis of ceria, followed by Zhitomirskyand Petric(Zhitomirsky, 2002; Zhitomirsky & Petric, 1999, 2001) and many other research groups. Even though ceria films have been successfully prepared by anodic deposition (Golden & Wang, 2003; Kulp et al., 2007), most authors have been using a cathodic electrolytic deposition.

The cathodic ELD method is based on reducing oxygen precursors to generate OH^- ions, causing a local increase in pH near the electrode surface. With Ce^{3+} ions in the electrolytic solution, it is generally believed that the electrogenerated base induces the formation of colloidal particles of $Ce(OH)_3$ or hydrous oxide precipitate on the working electrode (Creus et al., 2006; Zhitomirsky, 2002; Zhitomirsky & Petric, 1999, 2001; Zhou & Switzer, 1996) and also the formation of ionic species $Ce(OH)_2^{2+}$, that hydrolyzes into ceria layer. During cathodic electrodeposition of ceria on aluminium, the OH^-ions can be produced from the reduction of dissolved O_2, reduction of NO_3^- ions, as well as from electrochemical evolution of hydrogen (Arurault et al., 2004; Hamlaoui et al., 2009). These processes occur in different ranges of cathodic potentials.

Both electrodeposition time and voltage were identified as important factors in the corrosion stability of CeCCs, along with their microstructure (Živković et al., 2014). The CeCCs were prepared from 0.05 M $Ce(NO_3)_3$ solutions, applying cathodic potentials of -1.1, -1.4 and -1.6 V *vs* SCE for different deposition times (5-20 min). The lowest potential produced thin and crack-free films. Higher potentials and/or longer time promoted cerium deposition leading to thicker layers. However, the highest potential (-1.6 V) led to highly cracked and non-adherent coatings even at the shortest deposition. The CeCCs formed at -1.4 V for 10 and 20 min exhibited the highest corrosion stability, i.e., the highest coating pore resistance, R_p and the smallest constant phase element, CPE (Table 1). It can be seen that all CeCCs deposited at -1.1 and -1.4 V for a different time, show an order of magnitude smaller corrosion current densities, j_{corr} as compared to bare aluminium (Table 2). The smallest corrosion current densities were determined for CeCCs deposited at -1.4 V for 10 and 20 min. The reason for such a finding could be a more homogeneous structure of greater thickness of the coating produced at potential -1.4 V (as compared with CeCC formed at -1.1 V). The corrosion potential, E_{corr}, values of the bare aluminium and the one coated with CeCCs are also presented in Table 2. The difference between E_{corr} and E_{pit} (pitting potential) can be used to evaluate the pitting corrosion resistance of Al ($E_{pit}\approx$ -775 mV). The values of ΔE for the specimens are presented in Table 2. As can be seen, the value of 79 mV was obtained in the case of AA6060 coated with CeCC deposited at -1.1 V and over 200 mV for CeCCs at -1.4 V, indicating thatthe ceria layers markedly improved the pitting corrosion resistance of AA6060.

In order to investigate the effect of CeCC deposition voltage on the protective properties of the system CeCC/topepoxy coating, cerium-based coatings have been electrodeposited on AA6060 from 0.05 M $Ce(NO_3)_3$ aqueous solution at different deposition potentials of -0.95 V, -1.2 V and -1.4 V (Živković et al., 2015). A subsequent post-treatment of CeCCs in the 2.5 % Na_3PO_4, pH 4.5, at 85

°C formed a more uniform surface with lower roughness, as proven by AFM analysis (Table 3).

Table 1. Fitting results of EIS plots of CeCCs on AA6060 after 1h of exposure to 0.5 mol·dm^{-3} NaCl solution (Reprinted from (Živković et al., 2014) with permission from Elsevier, Copyright 2014).

t / min	$E_{dep.}$ = -1.1 V			$E_{dep.}$ = -1.4 V		
	R_p/ kΩ cm^2	$Y_o \cdot 10^6$/ $s^n\Omega^{-1}$ cm	n	R_p / kΩ cm^2	$Y_o \cdot 10^6$/ $s^n\Omega^{-1}$ cm	n
5	4.4	19.9	0.94	14.6	15.80	0.9
10	16.9	15.7	0.86	24.4	13.9	0.87
20	27.5	14.6	0.91	58.2	12.6	0.9

Table 2. Corrosion potentials and corrosion current densities of AA6060 and CeCCs, deposited at different potentials and times, in 0.5 M NaCl (Reprinted from (Živković et al., 2014) with permission from Elsevier, Copyright 2014).

Sample	E_{corr} / mV	j_{corr} / μm cm^{-2}	$\Delta E = E_{corr} - E_{pit}$ / mV
AA6060	- 775	4.31	0
CeCC, E_{dep} = - 1.1 V, 10 min	-854	0.39	79
CeCC, E_{dep} = - 1.4 V, 5 min	-1012	0.52	237
CeCC, E_{dep} = - 1.4 V, 10 min	-995	0.28	220
CeCC, E_{dep} = - 1.4 V, 20 min	-989	0.22	214

Table 3. Surface roughness of CeCCs deposited at different potentials without and with phosphate posttreatment (Reprinted from (Živković et al., 2015) with permission from Elsevier, Copyright 2015).

Deposition potential / V	RMS / nm	
	without post-treatment	with post-treatment
-0.95	120	80
-1.2	290	150
-1.4	363	282

The EIS data recorded over a longer time exposure in 3 wt% NaCl solution confirmed a strong influence of CeCCs post-treatment on the protective properties of the CeCC/epoxy coating protective system. The CeCCs without post-treatment exhibited better corrosion resistance than post-treated CeCCs, for all deposition potentials applied. The highest impedance value (Fig. 8) and the lowest corrosion current density (Fig. 9) were provided by the protective system epoxy coating/CeCC electrodeposited at -1.2 V and without post-treatment. This homogeneous and crack-free CeCC of intermediate surface roughness enabled an efficient bonding with epoxy top coating.

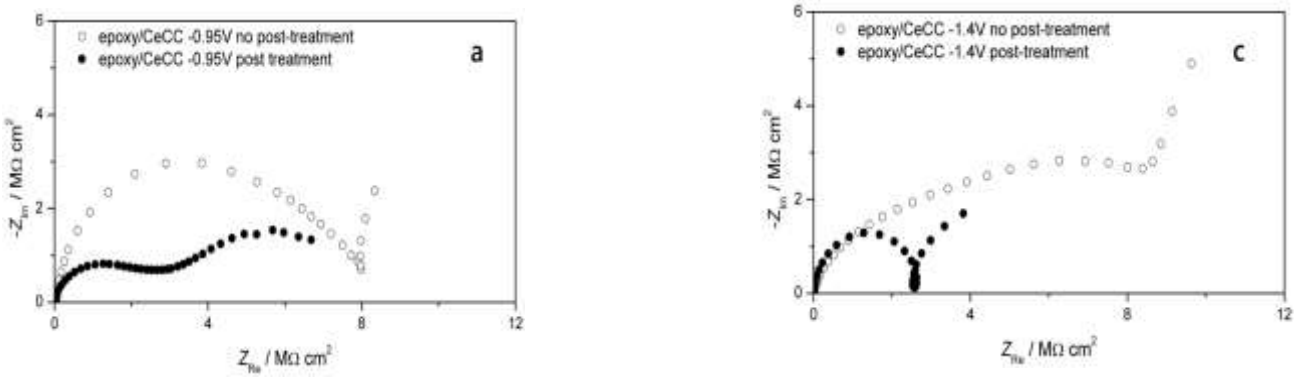

Figure 8. Nyquist plot for protective systems with epoxy coating/CeCCs

deposited at a) -0.95 V, b) -1.2 V and c) 1.4 V, without (o) and with (●) post-treatment, after 30 days of exposure to 3 wt.% NaCl solution (Reprinted from (Živković et al., 2015) with permission from Elsevier, Copyright 2015).

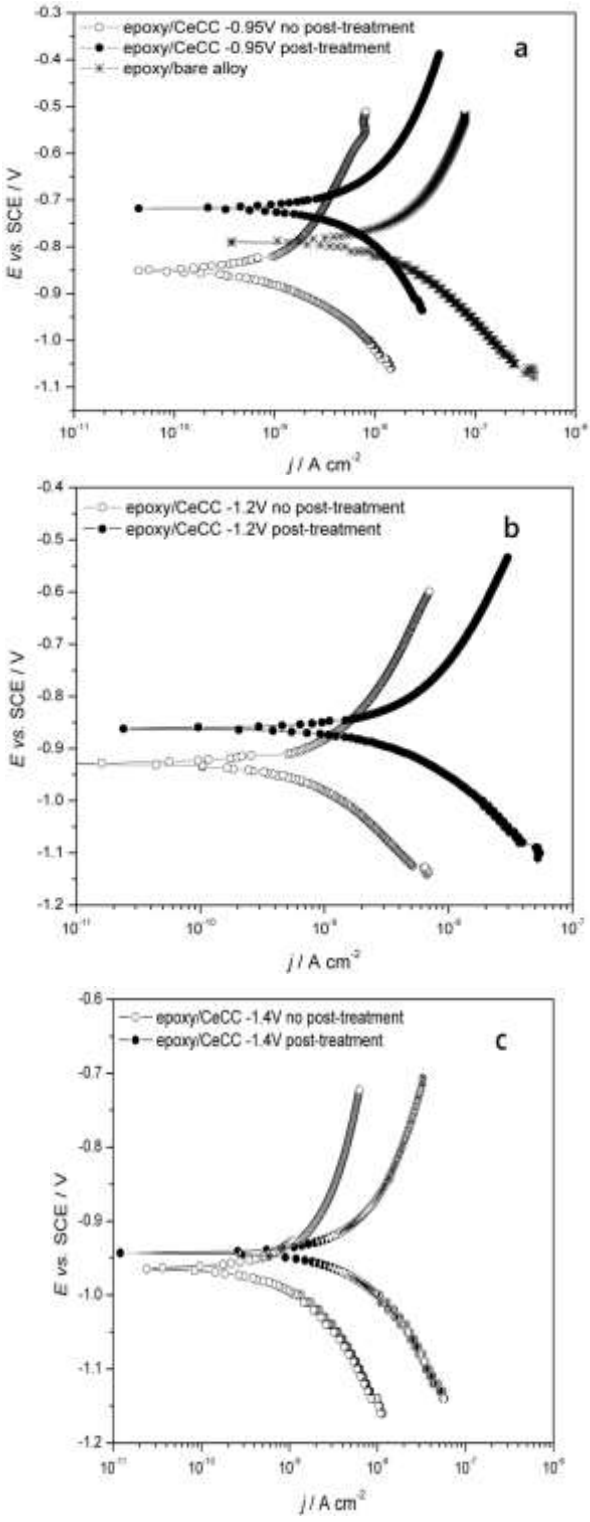

Figure 9. Polarization diagrams for protective systems epoxy coating/CeCCs deposited at (a) -0.95 V, (b) -1.2 V and (c) 1.4 V, without (o) and with (●) post-treatment, after 30 days exposure to 3 wt. NaCl solution (Reprinted from (Živković et al., 2015) with permission from Elsevier, Copyright 2015).

Figures 10-12 represent the images of microstructures of some electrodeposited CeCCs, while Table 4 summarizes the main findings of our study on CeCCs on aluminium, regarding the effect of deposition parameters on the characteristics of the deposited CeCCs alone and with top organic coating, with the aim to improve corrosion protection of aluminium substrate.

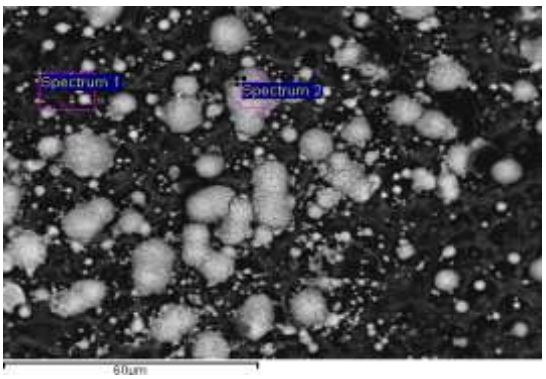

Figure 10. SEM microphotograph of CeCC electrodeposited at the potential E = -1.1 V for 10 min.

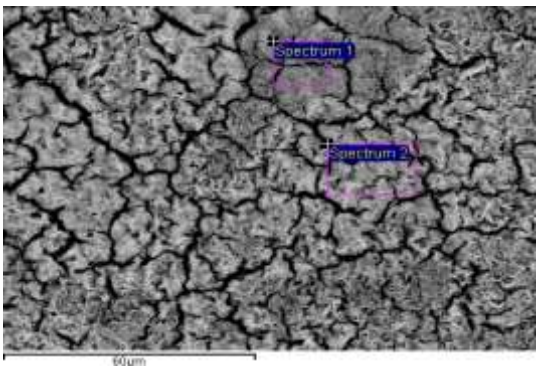

Figure 11. SEM microphotograph of CeCC electrodeposited at the potential E = -1.4 V for 10 min.

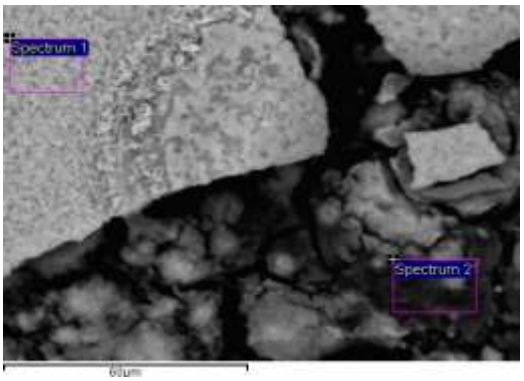

Figure 12. SEM microphotograph of CeCC electrodeposited at potential E = - 1.6 V for 10 min.

Table 4. Various pre-treatment and post-treatment techniques for depositing CeCCs on Al and Al alloy substrates, and the obtained results.

Substrate	Substrate pre-treatment	Coating process/bath composition	Post-treatment	Results/drawbacks	Ref.
Aluminium	Polishing, degreasing in alkaline solution and rinsing with distilled water	Sol-gel/$Ce(NO_3)_4$ solution in 0.2 M HNO_3	Drying in air at 35 °C 30 min	Increased corrosion resistance of CeO_2-coated Al in comparison to bare Al at long exposure times. The Al beneath CeO_2 coating was subjected to intrinsic formation of a uniform protective coating/Al interphase, cross-linked by AlO(OH) fibre-like structures	(Gulicovski et al., 2016)
Al alloy AA6060	Polishing, degreasing in alkaline solution and rinsing with distilled water	Dip-immersion/0.05 M $CeCl_3$, acidified to pH 2 with the addition of 30 % H_2O_2	Post-treatment in phosphate solution (2.5 % Na_3PO_4, pH 4.5) at 85 °C, 5 min. The post-treated coatings were rinsed in deionized water and dried in air.	The CeCCs prepared at longer deposition times and post-treated showed better corrosion protection than those prepared at shorter deposition times. However, due to their small thickness, even CeCCs prepared at longer deposition times and post-treated provided short term protection in the aggressive environment	(Jegdić et al., 2013)
Al alloy AA6060	Polishing, degreasing in alkaline solution and rinsing with distilled water	Dip immersion/0.05 M $CeCl_3$ and 0.05 M $Ce(NO)_3$, the pH was adjusted to 2 by small additions of HCl or HNO_3, respectively.	Post-treatment in phosphate solution (2.5 % Na_3PO_4, pH 4.5) at 85 °C, 5 min. The post-treated samples were rinsed with distilled water and dried in air.	Better corrosion protection of post-treated chloride-based CeCC compared to crack-free thin nitrate-based CeCC.	(Živković et al., 2013)
Al alloy AA6060	Polishing, degreasing in alkaline solution and rinsing with distilled water	Electrodeposition/ 0.05 M $Ce(NO_3)_3$, deposition potentials -1.1, -1.4 and -1.6 V, deposition time 5-20 min	CeCCs were rinsed with distilled water	The highest Rp and the smallest CPE values exhibited CeCC deposited at −1.4 V for 20 min deposition time. This CeCC improved pitting corrosion resistance owing to homogeneous microstructure and sufficient thickness.	(Živković et al., 2014)
Al alloy AA6060	Polishing, degreasing in alkaline solution and rinsing with distilled water	Electrodeposition/ 0.05 M $Ce(NO_3)_3$, deposition potentials –0.95, -1.2 and -1.4 V, deposition time 10 min, top epoxy coating.	CeCCs were rinsed with distilled water and subjected to a post-treatment in phosphate solution (2.5% Na_3PO_4, pH 4.5) at 85 °C, 5 min	The greatest impedance and the lowest corrosion current density were provided by the protective system epoxy coating/CeCC deposited at −1.2 V and without post-treatment.	(Živković et al., 2015)

4. Conclusion

This review discussed the ability of cerium-based conversion coatings (CeCCs) as the alternative for the toxic chromate conversion coating (CCC) to protect the aluminium substrate during exposure to corrosive environments, alone or with top organic coating. These coatings overcame the health hazard regarding CCC and appear favourable under certain conditions, because they provide the similar protective properties as CCC in corrosive environments. Moreover, various parameters that influence the quality of CeCCs, like deposition techniques, solution composition, concentration, pH, temperature, pre-treatment and post-treatment, must be investigated carefully in order to fill out specific requirements. Furthermore, the most critical challenge for the long-term application is their impact on the environment and health.

Since the new alternatives based on phosphate, cerium, zirconium, titanium salts, titanium zirconium salt, cobalt salts, molybdate, etc. are recently developed, the effect of prolonging exposure time to such coatings are not apparent yet and can take decades to develop and be recognized. Therefore, since CCC is replaced due to its toxic and cariogenic effect, it is crucial to find an alternative material that does not impose the same threat on human health and environmental wellbeing.

Acknowledgements

The authors wish to thank all colleagues who contributed to the experimental results and analyses presented in this review. Their names can be seen in our mutual papers listed in the references.

Vesna Mišković-Stanković would like to thank University Union-Nikola Tesla, Belgrade, Serbia, for the support.

Conflict of interest

Authors declare that there is no conflict of interest.

References

Alba-Galvín, J. J., González-Rovira, L., Botana, F. J., Lekka, M., Andreatta, F., Fedrizzi, L., & Bethencourt, M. (2021). Application of Commercial Surface Pretreatments on the Formation of Cerium Conversion Coating (CeCC) over High-Strength Aluminum Alloys 2024-T3 and 7075-T6. *Metals*, *11*(6), 930.

Allachi, H., Chaouket, F., & Draoui, K. (2010). Protection against corrosion in marine environments of AA6060 aluminium alloy by cerium chlorides. *Journal of Alloys and Compounds*, *491*(1-2), 223-229.

Arurault, L., Monsang, P., Salley, J., & Bes, R. (2004). Electrochemical preparation of adherent ceria coatings on ferritic stainless steel. *Thin Solid Films*, *466*(1-2), 75-80.

Aziz, I., Zhang, Q., & Du, J. (2011). Cerium-based thermal conversion treatments on silicon carbide reinforced 2009 aluminum alloy composites. *Materials and Corrosion*, *62*(3), 258-263.

Bethencourt, M., Botana, F., Calvino, J., Marcos, M., & Rodriguez-Chacon, M. (1998). Lanthanide compounds as environmentally-friendly corrosion inhibitors of aluminium alloys: a review. *Corrosion Science*, *40*(11), 1803-1819.

Bethencourt, M., Botana, F., Cano, M., & Marcos, M. (2002). High protective, environmental friendly and short-time developed conversion coatings for aluminium alloys. *Applied Surface Science*, *189*(1-2), 162-173.

Bethencourt, M., Botana, F., Cano, M., & Marcos, M. (2004). Advanced generation of green conversion coatings for aluminium alloys. *Applied Surface Science*, *238*(1-4), 278-281.

Bethencourt, M., Botana, F., Cano, M., Marcos, M., Sánchez-Amaya, J., & González-Rovira, L. (2008). Using EIS to analyse samples of Al–Mg alloy AA5083 treated by thermal activation in cerium salt baths. *Corrosion Science*, *50*(5), 1376-1384.

Bethencourt, M., Botana, F. J., Calvino, J. J., Marcos, M., & Rodriguez-Chacon, M. A. (1998). Lanthanide compounds as environmentally-friendly corrosion inhibitors of aluminium alloys: A review. *Corrosion Science*, *40*(11), 1803-1819. https://doi.org/10.1016/s0010-938x(98)00077-8

Braga, A. V. C., do Lago, D. C. B., Pimenta, A. R., & de Senna, L. F. (2020). The influence of heat treatment of inorganic conversion coatings produced by sol-gel dip coating on the anticorrosive properties of alumina films deposited on steel substrate-Part II: silica/boehmite or boehmite/silica multilayered conversion coatings. *Surface and Coatings Technology*, *386*, 125500.

Campestrini, P., Terryn, H., Hovestad, A., & De Wit, J. (2004). Formation of a cerium-based conversion coating on AA2024: relationship with the microstructure. *Surface and Coatings Technology*, *176*(3), 365-381.

Chen, L.-A., Lu, Y.-S., Lin, Y.-T., & Lee, Y.-L. (2021). Preparation and characterization of cerium-based conversion coating on a Fe50Mn30Co10Cr10 dual-phase high-entropy alloy. *Applied Surface Science*, *562*, 150200.

Conde, A., Arenas, M., De Frutos, A., & De Damborenea, J. (2008). Effective corrosion protection of 8090 alloy by cerium conversion coatings. *Electrochimica Acta*, *53*(26), 7760-7768.

Creus, J., Brezault, F., Rebere, C., & Gadouleau, M. (2006). Synthesis and characterisation of thin cerium oxide coatings elaborated by cathodic electrolytic deposition on steel substrate. *Surface and Coatings Technology*, *200*(14-15), 4636-4645.

Dabala, M. (2001). , L. Armelao, A. Buchberger, and I. Calliari. *Appl. Surf. Sci*, *172*(3-4), 312-322.

Dabala, M., Armelao, L., Buchberger, A., & Calliari, I. (2001). Cerium-based conversion layers on aluminum alloys. *Applied Surface Science*, *172*(3-4), 312-322. https://doi.org/10.1016/s0169-4332(00)00873-4

Dabala, M., Ramous, E., & Magrini, M. (2004). Corrosion resistance of cerium-based chemical conversion coatings on AA5083 aluminium alloy. *Materials and Corrosion-Werkstoffe Und Korrosion*, *55*(5), 381-386. https://doi.org/10.1002/maco.200303744

De Frutos, A., Arenas, M., Liu, Y., Skeldon, P., Thompson, G., De Damborenea, J., & Conde, A. (2008). Influence of pre-treatments in cerium conversion treatment of AA2024-T3 and 7075-T6 alloys. *Surface and Coatings Technology*, *202*(16), 3797-3807.

Decroly, A., & Petitjean, J.-P. (2005). Study of the deposition of cerium oxide by conversion on to aluminium alloys. *Surface and Coatings Technology*, *194*(1), 1-9.

Deng, C., Xie, X., Han, J., Lu, B., Liang, S., & Zhou, J. (2021). Stabilization of Zn Metal Anode through Surface Reconstruction of a Cerium-Based Conversion Film. *Advanced Functional Materials*, *31*(51), 2103227.

Exbrayat, L., Steyer, P., Rebere, C., Berziou, C., Savall, C., Ayrault, P., . . . Creus, J. (2014). Electrodeposition of zinc-ceria nanocomposite coatings in alkaline bath. *Journal of Solid State Electrochemistry*, *18*(1), 223-233. https://doi.org/10.1007/s10008-013-2264-3

Fahrenholtz, W. G., O'Keefe, M. J., Zhou, H., & Grant, J. (2002). Characterization of cerium-based conversion coatings for corrosion protection of aluminum alloys. *Surface and Coatings Technology*, *155*(2-3), 208-213.

Fedel, M., Ahniyaz, A., Ecco, L. G., & Deflorian, F. (2014). Electrochemical investigation of the inhibition effect of CeO2 nanoparticles on the corrosion of mild steel. *Electrochimica Acta*, *131*, 71-78. https://doi.org/10.1016/j.electacta.2013.11.164

Gigandet, M., Faucheu, J., & Tachez, M. (1997). Formation of black chromate conversion coatings on pure and zinc alloy electrolytic deposits: role of the main constituents. *Surface and Coatings Technology*, *89*(3), 285-291.

Golden, T. D., & Wang, A. Q. (2003). Anodic electrodeposition of cerium oxide thin films: II. mechanism studies. *Journal of the Electrochemical Society*, *150*(9), C621.

Gulicovski, J., Bajat, J., Jokić, B., Panić, V., Mišković-Stanković, V., & Milonjić, S. (2016). Protective ability and impedance response of sol–gel reversely transformed ceria conversion coating on aluminium. *Journal of Solid State Electrochemistry*, *20*(1), 293-303.

Gulicovski, J. J., Bracko, I., & Milonjic, S. K. (2014). Morphology and the isoelectric point of nanosized aqueous ceria sols. *Materials Chemistry and Physics*, *148*(3), 868-873. https://doi.org/10.1016/j.matchemphys.2014.08.063

Gulicovski, J. J., Milonjic, S. K., & Szecsenyi, K. M. (2009). Synthesis and Characterization of Stable Aqueous Ceria Sols. *Materials and Manufacturing Processes*, *24*(10-11), 1080-1085. https://doi.org/10.1080/10426910903032162

Hagans, P. L., & Haas, C. (1994). Chromate conversion coatings. *ASM Handbook*, *5*, 405-411.

Hamdy, A. S. (2006). Advanced nano-particles anti-corrosion ceria based sol gel coatings for aluminum alloys. *Materials Letters*, *60*(21-22), 2633-2637. https://doi.org/10.1016/j.matlet.2006.01.049

Hamlaoui, Y., Pedraza, F., Remazeilles, C., Cohendoz, S., Rébéré, C., Tifouti, L., & Creus, J. (2009). Cathodic electrodeposition of cerium-based oxides on carbon steel from concentrated cerium nitrate solutions: Part I. Electrochemical and analytical characterisation. *Materials chemistry and physics*, *113*(2-3), 650-657.

Heller, D. K., Fahrenholtz, W. G., & O'Keefe, M. J. (2009). Effect of phosphate source on post-treatment of cerium-based conversion coatings on Al 2024-T3. *Journal of the Electrochemical Society*, *156*(11), C400.

Heller, D. K., Fahrenholtz, W. G., & O'Keefe, M. J. (2010). The effect of post-treatment time and temperature on cerium-based conversion coatings on Al 2024-T3. *Corrosion Science*, *52*(2), 360-368.

Hill, J.-A., Markley, T., Forsyth, M., Howlett, P. C., & Hinton, B. R. (2011). Corrosion inhibition of 7000 series aluminium alloys with cerium diphenyl phosphate. *Journal of Alloys and Compounds*, *509*(5), 1683-1690.

Hoang, N., Khoa, T. A., Phuong, P. M., Hang, T. T. X., Van Chi, N., & Nguyen, T.-D. (2022). Corrosion protection of carbon steel using a combination of Zr conversion coating and subsequent zinc-rich silicate coating with a flake ZnAl alloy. *Arabian Journal of Chemistry*, 103815.

Hollamby, M. J., Borisova, D., Moehwald, H., & Shchukin, D. (2012). Porous 'Ouzo-effect' silica-ceria composite colloids and their application to aluminium corrosion protection. *Chemical Communications*, *48*(1), 115-117. https://doi.org/10.1039/c1cc15992e

Hughes, A., Scholes, F., Glenn, A., Lau, D., Muster, T., & Hardin, S. (2009). Factors influencing the deposition of Ce-based conversion coatings, part I: The role of Al3+ ions. *Surface and Coatings Technology*, *203*(19), 2927-2936.

Hughes, A. E., Taylor, R. J., Hinton, B. R. W., & Wilson, L. (1995). XPS and SEM characterization of hydrated cerium oxide conversion coatings. *Surface and Interface Analysis*, *23*(7-8), 11.

Ilevbare, G., & Scully, J. (2001). Oxygen reduction reaction kinetics on chromate conversion coated Al-Cu, Al-Cu-Mg, and Al-Cu-Mn-Fe intermetallic compounds. *Journal of the Electrochemical Society*, *148*(5), B196.

Jegdić, B. V., Živković, L. S., Popić, J. P., Bajat, J. B., & Mišković-Stanković, V. B. (2013). Electrochemical methods for corrosion testing of Ce-based coating prepared on AA6060 alloy by dip immersion method. *Journal of the Serbian Chemical Society*, *78*(7), 997-1011.

Johansen, H. D., Brett, C. M. A., & Motheo, A. J. (2012). Corrosion protection of aluminium alloy by cerium conversion and conducting polymer duplex coatings. *Corrosion Science*, *63*, 342-350. https://doi.org/10.1016/j.corsci.2012.06.020

Johnson, B. Y., Edington, J., Williams, A., & O'Keefe, M. (2005). Microstructural characteristics of cerium oxide conversion coatings obtained by various aqueous deposition methods. *Materials Characterization*, *54*(1), 41-48.

Joshi, S., Fahrenholtz, W. G., & O'Keefe, M. J. (2011). Effect of alkaline cleaning and activation on aluminum alloy 7075-T6. *Applied Surface Science*, *257*(6), 1859-1863.

Kamde, M. A., Mahton, Y., Ohodnicki, J., Roy, M., & Saha, P. (2021). Effect of cerium-based conversion coating on corrosion behavior of squeeze cast Mg-4 wt% Y alloy in 0.1 M NaCl solution. *Surface and Coatings Technology*, *421*, 127451.

Khast, F., Saybani, M., & Dariani, A. A. S. (2021). Effects of copper and manganese cations on cerium-based conversion coating on galvanized

steel: Corrosion resistance and microstructure characterizations. *Journal of Rare Earths*.

Kolesnikova, A., Abrashov, A., & Grigoryan, N. A high-performance Ti-Zr BASED conversion coating on 5556 aluminum alloy.

Kulp, E. A., Limmer, S. J., Bohannan, E. W., & Switzer, J. A. (2007). Electrodeposition of nanometer-thick ceria films by oxidation of cerium (III)–acetate. *Solid State Ionics*, *178*(11-12), 749-757.

Liu, H., Tong, Z., Yang, Y., Zhou, W., Chen, J., Pan, X., & Ren, X. (2021). Preparation of phosphate conversion coating on laser surface textured surface to improve corrosion performance of magnesium alloy. *Journal of Alloys and Compounds*, *865*, 158701.

Liu, X., Vonk, D., Kisslinger, K., Tong, X., Halada, G., Petrash, S., . . . Chen-Wiegart, Y.-c. K. (2021). Unraveling the Formation Mechanism of a Hybrid Zr-Based Chemical Conversion Coating with Organic and Copper Compounds for Corrosion Inhibition. *ACS Applied Materials & Interfaces*, *13*(4), 5518-5528.

Lu, C., Mu, S., Du, J., Zhang, K., Guo, M., & Chen, L. (2020). Investigation on the composition and corrosion resistance of cerium-based conversion treatment by alkaline methods on aluminum alloy 6063. *RSC Advances*, *10*(60), 36654-36666.

Lunder, O., Walmsley, J., Mack, P., & Nisancioglu, K. (2005). Formation and characterisation of a chromate conversion coating on AA6060 aluminium. *Corrosion Science*, *47*(7), 1604-1624.

Mansfeld, F., Wang, V., & Shih, H. (1991). Development of "Stainless Aluminum". *Journal of the Electrochemical Society*, *138*(12), 2.

Mansfeld, F., Wang, Y., & Shih, H. (1992). The Ce-Mo process for the development of a stainless aluminum. *Electrochimica Acta*, *37*(12), 6.

Naghdi, S., Jaleh, B., & Ehsani, A. (2015). Electrophoretic deposition of graphene oxide on aluminum: characterization, low thermal annealing, surface and anticorrosive properties. *Bulletin of the Chemical Society of Japan*, *88*(5), 722-728.

Naghdi, S., Jaleh, B., & Shahbazi, N. (2016). Reversible wettability conversion of electrodeposited graphene oxide/titania nanocomposite coating: Investigation of surface structures. *Applied Surface Science*, *368*, 409-416.

Naghdi, S., Jevremović, I., Mišković-Stanković, V., & Rhee, K. Y. (2016). Chemical vapour deposition at atmospheric pressure of graphene on molybdenum foil: effect of annealing time on characteristics and corrosion stability of graphene coatings. *Corrosion Science*, *113*, 116-125.

Naghdi, S., & Miskovic-Stankovic, V. (2022). A Review of the Corrosion Behaviour of Graphene Coatings on Metal Surfaces Obtained by Chemical Vapour Deposition. *Journal of the Electrochemical Society*.

Naghdi, S., Nešović, K., Mišković-Stanković, V., & Rhee, K. Y. (2018). Comprehensive electrochemical study on corrosion performance of graphene coatings deposited by chemical vapour deposition at atmospheric pressure on platinum-coated molybdenum foil. *Corrosion Science*, *130*, 31-44.

Naghdi, S., Nešović, K., Sanchez-Arriaga, G., Song, H. Y., Kim, S. W., Rhee, K. Y., & Mišković-Stanković, V. (2020). The effect of cesium dopant on APCVD graphene coating on copper. *Journal of Materials Research and Technology*, *9*(5), 9798-9812.

Naghdi, S., Rhee, K. Y., & Park, S. J. (2017). Oxidation resistance of graphene-coated molybdenum: effects of pre-washing and hydrogen flow rate. *International Journal of Refractory Metals and Hard Materials*, *65*, 29-33.

Nemes, P. I., Zaharescu, M., & Muresan, L. M. (2013). Initial corrosion behavior of composite coatings obtained by co-electrodeposition of zinc with nanoparticles of Ti and Ce oxides. *Journal of Solid State Electrochemistry*, *17*(2), 511-518. https://doi.org/10.1007/s10008-012-1901-6

Onofre-Bustamante, E., Dominguez-Crespo, M. A., Torres-Huerta, A. M., Olvera-Martinez, A., Genesca-Llongueras, J., & Rodriguez-Gomez, F. J. (2009). Characterization of cerium-based conversion coatings for corrosion protection of AISI-1010 commercial carbon steel. *Journal of Solid State Electrochemistry*, *13*(11), 1785-1799. https://doi.org/10.1007/s10008-009-0871-9

Pepe, A., Aparicio, M., Ceré, S., & Duran, A. (2004). Preparation and characterization of cerium doped silica sol–gel coatings on glass and aluminum substrates. *Journal of Non-Crystalline Solids*, *348*, 162-171.

Piao, N., Wang, L., Anwar, T., Feng, X., Tian, G., Wang, J., . . . He, X. (2019). Corrosion resistance mechanism of chromate conversion coated aluminium current collector in lithium-ion batteries. *Corrosion Science*, *158*, 108100.

Pinc, W., Geng, S., O'keefe, M., Fahrenholtz, W., & O'keefe, T. (2009). Effects of acid and alkaline based surface preparations on spray deposited cerium based conversion coatings on Al 2024-T3. *Applied Surface Science*, *255*(7), 4061-4065.

Qian, X., Zhan, W., Pan, J., Liu, Y., Huang, F., & Wang, B. (2021). Improving the corrosion resistance of LY12 aluminum alloy via a novel Mo–Zr–Ti composite conversion coating. *Materials Research Express*, *8*(3), 036403.

Rangel, C., Paiva, T., & Da Luz, P. (2008). Conversion coating growth on 2024-T3 Al alloy. The effect of pre-treatments. *Surface and Coatings Technology*, *202*(14), 3396-3402.

Roshan, S., & Sarabi, A. A. (2021). Improved performance of Ti-based conversion coating in the presence of Ce/Co ions: Surface characterization,

electrochemical and adhesion study. *Surface and Coatings Technology*, *410*, 126931.

Sainis, S., & Zanella, C. (2022). A localized study on the influence of surface preparation on the reactivity of cast Al-7Si-1Fe and Al-7Si-2Cu-1Fe alloys and their effect on cerium conversion coating deposition. *Applied Surface Science*, *585*, 152730.

Schem, M., Schmidt, T., Gerwann, J., Wittmar, M., Veith, M., Thompson, G., . . . Zheludkevich, M. (2009). CeO2-filled sol-gel coatings for corrosion protection of AA2024-T3 aluminium alloy [Article]. *Corrosion Science*, *51*(10), 2304-2315. https://doi.org/10.1016/j.corsci.2009.06.007

Shih, H., & Mansfeld, F. (1992). Passivation in Rare Earth Metal Chlorides - A New Conversion Coating Process for Aluminum Alloys. In V. S. Agarwala & G. M. Ugiansky (Eds.), *New Methods for Corrosion Testing of Aluminum Alloys, Issue 1124* (pp. 180-195). ASTM International.

Stoffer, J. O., O'Keefe, T. J., O'Keefe, M., Morris, E. L., Hayes, S. A., Yu, P., . . . Lin, X. (2006). Cerium-based spontaneous coating process for corrosion protection of aluminum alloys.

Stoychev, D. (2013). Corrosion protective ability of electrodeposited ceria layers. *Journal of Solid State Electrochemistry*, *17*(2), 497-509. https://doi.org/10.1007/s10008-012-1937-7

Sun, Z., Kong, G., Zhang, S., Wang, Y., & Che, C. (2021). Growth behaviour of cerium-based conversion coating on HF pre-treated Zn–5% Al alloy. *Surface Engineering*, *37*(4), 455-463.

Tang, J., Han, Z., Zuo, Y., & Tang, Y. (2011). A corrosion resistant cerium oxide based coating on aluminum alloy 2024 prepared by brush plating. *Applied Surface Science*, *257*(7), 2806-2812.

Wang, S., & Xu, S. (2021). Ti/Cr (III) conversion coating on aluminium foil for lithium-ion battery package. *Surface Engineering*, *37*(3), 365-372.

Yang, S., Li, S., Meng, Y., Yu, M., Liu, J., & Li, B. (2021). Corrosion inhibition of aluminum current collector with molybdate conversion coating in commercial LiPF6-esters electrolytes. *Corrosion Science*, *190*, 109632.

Yu, X. W., Cao, C. N., Yao, Z. M., Zhou, D. R., & Yin, Z. D. (2001). Study of double layer rare earth metal conversion coating on aluminum alloy LY12. *Corrosion Science*, *43*(7), 1283-1294.

Zand, R. Z., Verbeken, K., & Adriaens, A. (2013). Influence of the Cerium Concentration on the Corrosion Performance of Ce-doped Silica Hybrid Coatings on Hot Dip Galvanized Steel Substrates. *International Journal of Electrochemical Science*, *8*(1), 548-563.

Zhang, H., & Zuo, Y. (2008). The improvement of corrosion resistance of Ce conversion films on aluminum alloy by phosphate post-treatment. *Applied Surface Science*, *254*(16), 4930-4935.

Zhao, D.-W., Liu, C., Zuo, K.-Q., Su, P., Li, L.-B., Xiao, G.-Y., & Cheng, L. (2021). Strontium-zinc phosphate chemical conversion coating improves the osseointegration of titanium implants by regulating macrophage polarization. *Chemical Engineering Journal*, *408*, 127362.

Zhao, J., Xia, L., Sehgal, A., Lu, D., McCreery, R., & Frankel, G. S. (2001). Effects of chromate and chromate conversion coatings on corrosion of aluminum alloy 2024-T3. *Surface and Coatings Technology*, *140*(1), 51-57.

Zhitomirsky, I. (2002). Cathodic electrodeposition of ceramic and organoceramic materials. Fundamental aspects. *Advances in colloid and interface science*, *97*(1-3), 279-317.

Zhitomirsky, I., & Petric, A. (1999). Electrolytic and electrophoretic deposition of CeO2 films. *Materials Letters*, *40*(6), 263-268.

Zhitomirsky, I., & Petric, A. (2001). Electrochemical deposition of ceria and doped ceria films. *Ceramics International*, *27*(2), 149-155.

Zhou, P., Yang, L., Hou, Y., Duan, G., Yu, B., Li, X., . . . Wang, F. (2021). Grain refinement promotes the formation of phosphate conversion coating on Mg alloy AZ91D with high corrosion resistance and low electrical contact resistance. *Corrosion Communications*, *1*, 47-57.

Zhou, Y., & Switzer, J. A. (1996). Growth of cerium (IV) oxide films by the electrochemical generation of base method. *Journal of Alloys and Compounds*, *237*(1-2), 1-5.

Zuo, K., Wang, L., Wang, Z., Yin, Y., Du, C., Liu, B., . . . Lu, Y. (2022). Zinc-Doping Induces Evolution of Biocompatible Strontium–Calcium-Phosphate Conversion Coating on Titanium to Improve Antibacterial Property. *ACS Applied Materials & Interfaces*.

Zuo, M., Wu, T., Xu, K., Liu, S., Zhao, D., & Geng, H. (2015). Sol-gel route to ceria coatings on AA2024-T3 aluminum alloy. *Journal of Coatings Technology and Research*, *12*(1), 75-83. https://doi.org/10.1007/s11998-014-9621-8

Živković, L. S., Bajat, J. B., Popić, J. P., Jegdić, B. V., Stevanović, S., & Mišković-Stanković, V. B. (2015). Protective properties of cataphoretic epoxy coating on aluminium alloy AA6060 modified with electrodeposited Ce-based coatings: Effect of post-treatment. *Progress in Organic Coatings*, *79*, 43-52.

Živković, L. S., Jegdić, B. V., Popić, J. P., Bajat, J. B., & Mišković-Stanković, V. B. (2013). The influence of Ce-based coatings as pretreatments on corrosion stability of top powder polyester coating on AA6060. *Progress in Organic Coatings*, *76*(10), 1387-1395.

Živković, L. S., Popić, J. P., Jegdić, B. V., Dohčević-Mitrović, Z., Bajat, J. B., & Mišković-Stanković, V. (2014). Corrosion study of ceria coatings on AA6060 aluminum alloy obtained by cathodic electrodeposition: effect of deposition potential. *Surface and Coatings Technology*, *240*, 327-335.

Konverzione prevlake na bazi cerijuma na površinama aluminijuma

Samira Naghdi[1], Vesna Mišković Stanković[2,*]

[1] Physikalisch-Technische Bundesanstalt, Abbestr. 2-12, 10587 Berlin, Nemačka
[2] Fakultet za ekologiju i zaštitu životne sredine, Univerzitet Union-Nikola Tesla, Beograd, Srbija

*Autor za korespondenciju: vesna.miskovicstankovic@gmail.com

Abstrakt: Konverzione prevlake koje sadrže heksavalentni hrom (hromati) su decenijama masovno korišćene kao deo sistema za zaštitu legura aluminijuma od korozije. Ipak, hromati su zabranjeni zbog njihove toksičnosti i zato se moraju zameniti "zelenim" alternativnim ekološkim sistemima zaštite koji nisu štetni za životnu sredinu. Konverzione prevlake na bazi cerijuma (CeCCs) predstavljaju jednu od najperspektivnijih alternativa zato što pružaju efikasnu zaštitu od korozije, bezopasne su za životnu sredinu i ekonomične su jer imaju nisku cenu. Ovaj pregledni rad je fokusiran na zaštitna svojstva konverzionih prevlaka na bazi cerijuma (CeCCs) na aluminijumu i to kada se one koristi kao samostalne prevlake ili kao prevlaka u kombinaciji sa pokrivnom organskom prevalakom.

Ključne reči: cerijum, korozija, elektrodepozicija, EIS, polarizaciona merenja.

Global Sustainability Challenges
2023; Vol. 1(1): 23-32
https://gsc.unionnikolatesla.edu.rs/index.php/gsc/index
UDC: 616.71-018.4-092.9
615.466
615.33.032
ISSN: 2956-1051 (Online)

Antibiotics application in biomaterials for soft and hard tissue implants

Jadranka Odović [1, *], Vesna Mišković Stanković [2]

[1]Faculty of Pharmacy, University of Belgrade, Belgrade, Serbia
[2]Faculty of Ecology and Environmental Protection, University Union-Nikola Tesla, Belgrade, Serbia

[*]**Corresponding author:** jodovic@pharmacy.bg.ac.rs

To cite this article:
Odović, J. and Mišković-Stanković, V. (2023). Antibiotics application in biomaterials for soft and hard tissue implants. *Global sustainability challenges, 1*(1), pp. 23-32

Received: Oct 7, 2022;: **Revised:** Oct 20, 2022; **Accepted:** Oct 21, 2022

Abstract: One of the great challenges of modern medicine, pharmacy and chemistry as well is the treatment and replacement of damaged and injured soft and hard tissues, as well as bones and joints. Thus far variety of materials have been investigated and used in treating soft and hard tissues. On the other hand, application of soft or hard tissue implants brings high risk of infection by various microorganisms. Therefore, this paper presents the different possibilities of using soft and hard tissues implants particularly antibiotics-loaded implants with gradually releasing, with the aim to prevent bacterial infection, i.e. treat an infection that appeared as a result of the present microorganisms. The application of different antibiotics, gentamicin, ciprofloxacin, clindamycin, ampicillin, tetracycline, vancomycin for soft tissue implants as well as gentamicin and vancomycin as suitable antibiotics for hard tissue implants are reported.

Keywords: soft tissue implants, hard tissue implants, antibiotics.

1. Introduction

Simultaneously with the development of modern chemistry, pharmacy and medicine, significant increase in treating soft and hard tissues, as well as bones and joints diseases, injuries and wound, has been achieved. However, application of soft and hard tissue implants also brings the risk of infection by various microorganisms.

Traditionally, antibiotics have been used to treat bacterial infections. The most common route for their application is oral administration. In the case of severe infections, antibiotics are usually administered intramuscularly or more often intravenously. The choice of antibacterial agent is an important one, and different antibiotics are often used. However, prolonged systemic application of antibiotics may lead to increase of their side and toxic effects as well as developing resistance. Today, a large area of interest in nanomedicine is the application of antibiotics-loaded soft tissue implants, wound dressings or hard tissue implants. There are many advantages of their application since they can significantly reduce side and toxic effects of incorporated antibiotics or bacteria resistance in comparison to systemic application of antibiotics.

2. Bacterial infections in relation to soft tissue implants

Human skin as a physical barrier, serves as the first line of defence against microbial infection, by secreting sebaceous fluid and fatty acids to inhibit growth of pathogens and by possessing its own normal flora, thus deterring colonization by other pathogenic organisms. However, human skin is environment for many microbes. Infecting microorganisms may cause tissue damage and incite an inflammation processes. Also, different skin and tissue damages breaks this protective barrier and enable activity of pathogens. The organism's characteristic for the skin above the waist are usually Gram-positive species such as *Staphylococcus epidermidis*, *Corynebacterium species*, *Staphylococcus aureus* and *Streptococcus pyogenes* while both Gram-positive and Gram-negative species are microorganisms that inhabit at the skin below the waist. The infection agents

Enterobacteriaceae and *Enterococcus species* (enteric species) mainly colonize this area of the skin and they may originate from the colon and faeces (Eron et al., 2003).

Different factors i.e. chronic diseases, age or trauma and injuries of soft tissue represent specific risk factors that may increase progress of skin and soft tissue infections. Potential risk factors may be divided into two types. There are patient-related factors including critical illness, elderly age, immunocompromised state, liver and kidney disease, and vascular (especially lymphatic or venous) insufficiency. Certain risk factors (chronic renal or liver failure, immunocompromised state, vascular insufficiency or neuropathy) should be considered in the determination of disease severity. The second category is etiological risk factors. The mechanism of injury (trauma or others) or specific exposures to some infection agents can increases incidence of skin and soft tissue infections. The overlap between risk different factors in this grouping can be noticed (Ki & Rotstein, 2008) A list of different risk factors and their bacterial causes firstly proposed by Eron et al., 2003, were presented by in Table1.

Table 1. Risk elements for soft tissue infections(Ki & Rotstein, 2008)

Risk element	Pathogen
Diabetes mellitus	Staphylococcus aureus, anaerobes, Gram-negative bacilli
Cat or dog bite wounds	Pasteurellamultocida, C canimorsus
Rat bite wounds	Streptobacillusmoniliformis

Regardless of the risk of occurrence, skin and soft tissue infections (SSTIs) are infections with different clinical manifestations and degrees of severity. In Table 2 antibiotic election for different infection agents and degrees of infections are presented.

Table 2. Antimicrobial agents for skin and soft tissue infections (Ki & Rotstein, 2008)

Infection	Etiology	Antibiotic(s)
Mild infections (above waist)	Staphylococcus aureus Streptococcus pyogenes	Cloxacillin, cephalexin or clindamycin
Severe infections (above waist)	Staphylococcus aureus Streptococcus pyogenes	Cefazolin, cloxacillin, cephalexin
Mild infections (below waist)	Staphylococcus aureus Streptococcus pyogenes	Cloxacillin or cephalexin, clindamycin or metronidazole (anaerobes), second-generation cephalosporin or fluoroquinolone (if Gram-negative)
Severe infections (below waist)	Escherichia coli, Enterococcus species, Staphylococcus aureus Streptococcus pyogenes	Second-, Third- or fourth-generation cephalosporin, fluoroquinolones or piperacillin-tazobactam (in addition to above Gram-positive coverage)

*± Clindamycin

However, prolonged antibiotic or exposure hospitalization gets risk for infections with resistant organisms. At the first place it can be *Methicillin-resistant Staphylococcus aureus* (MRSA), but also *Pseudomonas aeruginosa, Enterococcus species, Streptococcus pyogenes* or *Clostridium species*. In such cases guidelines recommend second- or third-generation cephalosporin (mild to moderate), beta-lactam plus a fluoroquinolone or aminoglycoside with addition of vancomycin if MRSA suspected (Cohen & Kurzrock, 2004).

The infections caused by *Methicillin-resistant Staphylococcus aureus* (MRSA) bacteria are especially challenging since its resistance to number of usually used drugs. Antibiotics commonly recommended for treatment of MRSA infections are: mupirocin, clindamycin, trimethoprim-sulfamethoxazole, doxycycline, cephalexin, amoxicillin, vancomycin (Rajan, 2012).

In the case of infections caused with different bacteria the usual way of antibiotics administration is systemic: oral, intramuscular or intravenous application. On the other hand, systemic application of antibiotics especially for a long time may increase their side or toxic effects and led to developing of bacteria resistance.

Still, different drugs can be locally administered through the skin due its possibility to absorb by application of adhesive transdermal patch or wound dressings. Application of antibiotics loaded wound dressing can importantly improve soft tissue infections hilling and today takes large area of interest in nanomedicine. The local antibiotics application reduces side, toxic effects or bacteria resistance on applied antibiotics.

Many different polymers have been investigated as wound dressing materials. The applications require the use of biodegradable polymers in order to avoid the need of their removement by additional surgery. Until now, the most extensively used polymers are: polyvinyl alcohol (PVA) and dextran, poly(lactic acid) (PLA), poly(ε-caprolactone) (PCL) and the copolymer poly(lactic-co-glycolic acid) (PLGA), chitosan (Ch), nanofiber mesh (NFM), collagen conjugate, keratose hydrogels. These polyesters are sometimes blended with other synthetic or natural polymers, such as polyethylenoglycol (PEG) or gelatin, in order to regulate the biodegradability and hydrophilic nature of the fibers and to control the drug release kinetics of the encapsulated drug. Also, application of different antibiotics incorporated in wound dressing materials have been also studied, as will be presented in the next section.

3. Antibiotics for soft tissue implants

For soft tissue implants the most frequently used antibiotics according available literature are gentamicin,

ciprofloxacin, clindamycin, ampicillin, tetracycline, vancomycin.

3.1. Gentamicin-loaded wound dressing

Hwang et al., 2010 investigated application of gentamicin in wound dressing. For that purpose, polyvinyl alcohol (PVA) and dextran were used for preparation of cross-linked hydrogel films by application of freezing – thawing method. Two wound dressings with different composition were prepared. The first was composed of PVA (2.5%), dextran (1.13%) with gentamicin (0.1%) addition while no drug was added into the second wound dressings. I*n vitro* protein adsorption test, *in vivo* wound healing test, and histopathology were performed for prepared wound dressings. In aim to investigate *in vivo* wound healing, at the rat dorsum wound spot were made and then covered with hydrogels with gentamicin or without any drug. Each wound was observed for 15 days. Majority of wounds were completely healed after 9 days but for wounds covered with hydrogels with gentamicin reduction size was much greater in comparison to those without gentamicin. The gentamicin-loaded wound dressing enhanced reepithelialization rate, which was much higher for hydrogel with gentamicin (98±2%) then hydrogel without drug (91±2%). Also, hydrogels with gentamicin significantly decreased the possible granulation tissue area. Therefore, gentamicin-loaded wound dressing can be recommended as a potential wound dressing with improved healing effect in wound care (Hwang et al., 2010).

Another material with natural characteristics suitable for applications in wound dressing, chitosan (Ch) and nanofiber mesh (NFM) were proposes by (Monteiro et al., 2015). The gentamicin-loaded liposomes were immobilized at the surface of Ch/NFM. The total concentration of gentamicin was 140mM. The release profile of gentamicin-loaded liposomesimmobilized at the surface of electrospunsurface was investigated by application of dialysis method. Following *in vitro* susceptibility tests were performed to examine whether gentamicin released from the liposomes has activity against *Escherichia coli, Pseudomonas aeruginosa* and *Staphylococcus aureus*. The bactericidal activity was defined as reduction in bacterial number of the initial inoculum. For *Staphylococcus aureus, Escherichia coli and Pseudomonas aeruginosa* that reduction represent more than 99.9% for all strains. The bactericidal activity of released gentamicin and developed system has promising performance for wound dressing applications, avoiding infections caused by these common pathogens (Monteiro et al., 2015)..

The new hydrogels with gentamicin addition for infected wound treatment was proposed by (Păunică-Panea et al., 2015). Two proteins, fibrous, type I collagen and globular, albumin, were the main components of proposed hydrogels. The proposed hydrogels were prepared by continuous stirring of collagen 1% (at pH value 7.3), with 1M sodium hydroxide, gentamicin and albumin of different concentrations (10, 20 and 30%). The content of added gentamicin were 0.2% (w/v). Following, obtained gels were crosslinked with specific amount of glutaraldehyde (0.5% to collagen dry substance). The properties of the proposed hydrogels were investigated by rheological measurements and water up-take capacity. The hydrogels provided good properties for maximum of 20% albumin and 0.2% gentamicin indicating that proposed hydrogels may also provide good antimicrobial properties (Păunică-Panea et al., 2015).

(Nnamani, 2013) produced improved topical hydrogels using three polymeric agents with addition of gentamicin in aim to achieve predictable permeation of gentamicin in skin. The applied agents were: poloxamer407 and two polyacrylic acids (Cabopols ® 971P and 974P). The hydrogels were prepared with three concentrations of gentamicin which were varied (0.03, 0.06 and .09 w/w). For determination of total concentration of antibiotic in hydrogels antibiotic loaded hydrogel was dissolved in distilled water, centrifuged, filtered and after derivatization with o-phthaldialdehydeconcentration of gentamicin determined spectrophotometrically. The *in vitro* test for permeation of gentamicin in skin were done on male rats which were sacrificed with prolonged anesthesia and their abdominal skin was excised and prepared for experiments. The skin permeation studies were performed by using a Franz diffusion cell method. The prepared rat abdominal skin was mounted between the donor and receptor compartment of the diffusion cell and the gentamicin-loaded hydrogel was placed in the donor compartment containing 5 ml of PBS. The gentamicin-loaded hydrogels with higher percentage of drug offered better permeation and possible treatment of skin infections caused by gentamicin-susceptible bacteria (Nnamani, 2013).

(Lukáč et al., 2019) proposed a novel collagen wound dressing sponge prepared from freshwater fish (Cyprinus Carpio) skin collagen type I. Half of the sponges were cross-linked with carbodiimide. Both cross-linked and non-cross-linked collagen sponges were impregnated with gentamicin. Following, the impregnated sponges were frozen and lyophilized. The sponges were tested through a rat model for activity on *Pseudomonas aeruginosa* infected wound and compared with a reference commercial product. The examination of the rats on the first day after Pseudomonas aeruginosa inoculation showed that the rats in group treated with collagen sponge with gentamicin and group treated with intramuscularly administered gentamicin exhibited similar body temperature and hilling degree. However, rats in group treated with collagen sponge without gentamicin or no gentamicin intramuscularly showed importantly higher signs of generalized infection. The obtained results indicate that gentamicin released from the sponges, had good clinical properties and was active against investigated infective agents (Lukáč et al., 2019).

Recently,Coimbra et al., 2019 investigated the electrospunfiber mats composed of poly(lactic acid) (PLA), poly(ε-caprolactone) (PCL) and the copolymer poly(D,L,lactic-co-glycolide) (PLGA, L/G 50:50, ester terminated) as materials for immobilization of the antibiotic gentamicin sulfate (in concentration of 10% of the polymer weight). The four different formulations were prepared using the polymers PCL, PLA, PLGA and a mixture composed of 70% PLA and 30% PLGA (w/w): PCL, PLA, PLGA and by

a PLA/PLGA which were blend using an suspension (S) (S-PCL, S-PLGA, S-PLA, S-PLA/PGA) electrospinning and emulsion (E) (E-PCL, E-PLGA, E-PLA, E-PLA/PLGA) electrospinning method. The antibacterial activity of the gentamicin sulfate-loaded fiload was examined against Staphylococcus aureus, the most common strain of bacteria associated with bone infections, by a disc diffusion assay. The inhibitory effect was observed and evaluated by measuring the diameter of the inhibition zones (Fig 1). As can be seen all membranes produced inhibition zones (diameters between 2.4 and 3.6 cm), proving the antibacterial activity of the immobilized drug (Coimbra et al., 2019).

3.2. Ciprofloxacin-loaded wound dressing

Puoci et al., 2012proposed application of ciprofloxacin-collagen conjugate (CFX-T1C) for successful wound healing with reducing side effects usually recorded in systematic patient therapy. The antibacterial activities of CFX-T1C with addition of gentamicin in concentrations varied from 1,000 to 0.5 μg/mL, were determined through the testing against *Staphylococcus aureus* and *Escherichia coli*. The various concentrations of gentamicin were prepared with sterile, double-deionized water (autoclaved) in 96-well microtiter plates. The test organisms were added to each well. The microtiter plates were incubated at 37 °C for 24 h in a shaker. Following a small part of each mixture was spread on agar plates and incubated at 37 °C. The growth of bacterial cells was observed on agar plates after 48 h incubation. The antibacterial test was repeated at least four times in plates as negative and positive controls, respectively. The growth of the test bacterium was observed in all wells with positive controls while no growth was observed in the wells with theciprofloxacin-collagen conjugate (Puoci et al., 2012).

Sripriya et al., 2007 investigated the efficacy of bilayer dressing with drug ciprofloxacin in comparison with bilayer dressing without drug. The bilayer dressing was prepared from succinylated collagen and with incorporated ciprofloxacin-HCl in final concentration 0.2 mg/cm^2. Ciprofloxacin represents a class of quinolone antibiotics. Ciprofloxacin was used in presented experimental design because it has been proven as a very potent agent in eradicating *Pseudomonas aeruginosa* on biomedical device. Number of tests for collagen sponge and bilayer dressing with cipeofloxacin were performed. *In vitro* and *in vivo*tests of prepared bilayer dressings were made. *In vitro,*the release of ciprofloxacin from the bilayer dressing was investigated in Franz-type diffusion cells with HPLC determination of released antibiotic. Following, *in vitro* investigation of ciprofloxacin-incorporating dressings antimicrobial properties made on agar plates inoculated with a mixed culture of *Staphylococcus aureus* and *Pseudomonas aeruginosa* showed important zone of inhibition. *In vivo* investigations were performed on 90 intraperitonealy anaesthetized animals. The hair from the dorsal region was removed and wound (2 × 2 cm^2) was excised on the back of rats. The mixed culture of *Pseudomonas aeruginosa and Staphylococcus aureus* was injected. Following, wounds develop infection for 24 h. The release of drug gradually increased and 24.45 ± 3.2% of release was observed on day 1, which was continued on days 2 and 3 (31.45 ± 3.45% and 35.36 ± 3.54%, respectively). The bilayer dressing containing ciprofloxacin showed a clear zone of inhibition (33 ± 3 mm) against the mixed culture (*Staphylococcus aureus and Pseudomonas aeruginosa*) using the agar diffusion method and the zone was maintained for more than 3 days, but no zone was observed around the collagen dressing without drug. Also *in vivo* investigations of prepared ciprofloxacin-loaded wound dressing showed significant higher wound closure and confirmed possibility of its application in proper wound healing (Sripriya et al., 2007).

Roy et al., 2015investigated ciprofloxacin-loadedkeratose hydrogels using a porcine wound model, infected with *Pseudomonas aeruginosa*. Prepared hydrogels contained from 0 to 20mg/mL of ciprofloxacin. *In vitro* investigations were performed to determine if ciprofloxacin-loaded keratose hydrogels inhibit *Pseudomonas aeruginosa.* The keratose hydrogels loaded with 2 mg/mL ciprofloxacin completely inhibited bacteria growth for 9 days in vitro, while keratose hydrogels without ciprofloxacin do not exhibit any antimicrobial activity. Following, the examination of ciprofloxacin release was performed in period of nine days during which keratose hydrogels were placed in tubes overlaid with phosphate-buffered saline (PBS). The concentration of ciprofloxacin in the collected samples was quantified using the inherent fluorescence of ciprofloxacin. All keratose hydrogels released from 50% to 63% of their total ciprofloxacin amount within the first 5 days, independent of the initial ciprofloxacin concentration. Finally, ciprofloxacin-loaded keratose hydrogels were investigated *in vivo* in pigson skin wounds infected with *Pseudomonas aeruginosa* and treated on days 1 and 3 postinjury with keratose hydrogels with or without ciprofloxacin. Treatment with keratose hydrogels loaded with 5 mg/mL ciprofloxacin or 10 mg/mL ciprofloxacin significantly reduced the amount of *Pseudomonas aeruginosa* in the wound by > 99.9% compared to keratose hydrogel without ciprofloxacin which did not possess any antimicrobial activity against *Pseudomonas aeruginosa.* Ciprofloxacin-loaded keratose hydrogels displayed decreased wound contraction and reepithelialisation (Roy et al., 2015).

3.3. Clindamycin-loaded wound dressing

The polyvinyl alcohol and sodium alginate were used to develop clindamycin wound dressing. The hydrogel films were prepared using freeze-thawing method from solution which were including different proportions of polyvinyl alcohol and sodium alginate and 3%w/v clindamycin. The healing effect of prepared hydrogels were investigated on male rats. Male rats (from 250 to 300 g) were used to evaluate wound healing characteristics of hydrogels. The dorsal hair of rats was shaved and two full skin wounds of 1.5 cm x 1.5 cm area were prepared. Their wounds infected

with *Pseudomonas aeruginosa* were covered with PVA/SA wound dressings containing antibiotic clindamycin while control group of wounds were covered with dressings which contained no drug. It was found that application of hydrogels with clindamycin showed a significant effect on infected wound. For control group of animals after application of hydrogel without clindamycin more inflammatory cells were found in wounds and granulation tissue formation were also observed. On the other side application of hydrogel with clindamycin led to significant decrease of inflammation and inflammatory cells in wound. At fifteen day, the defect area was almost completely hilled. The obtained results could recommend application of clindamycin-loaded wound dressing for efficient hilling of wounds infected with *Pseudomonas aeruginosa* (Kim et al., 2008).

The polymeric nanofiber patch for topical disease treatment were prepared using several different concentrations of polyvinyl alcohol and tamarind seed gum. It was loaded with clindamycin (in concentration 1.0% to 2.5%) as antibacterial agent. The antimicrobial activity of the drug-loaded polyvinyl alcohol/gum polymeric nanofiber patch was evaluated and compared to that of a commercially available clindamycin gel for acne treatment. A disk-diffusion method was used to investigate drug-loaded wound dressing antibacterial activity against test strains (*Staphylococcus aureus or Propionibacterium*) on Müller–Hinton agar plates. To prepare the plates, 0.1 ml of Staphylococcus aureus or Propionibacterium acnes was transferred and then inoculated at 37 °C for 18–24 h. For comparison antibacterial efficiency of the polymeric nanofiber patch with commercial 1% clindamycin gel, beside clindamycin loaded polymeric nanofiber patch a standard paper disk was impregnated with 10 µl of 0.1% clindamycin solution. The zone of strain inhibition obtained with clindamycin loaded polymeric nanofiber patch was recorded and compared with inhibition obtained with commercial 1% clindamycin gel as well as with erythromycin disk and a blank disk which were used as the positive and negative controls, respectively after 16–18 h of incubation at 35 °C. The antibacterial activities of prepared wound dressing clindamycin showed excellent antibacterial activity which were in relation with clindamycin content. The antibacterial activities of the clindamycin-loaded wound dressing were significantly higher in comparison to commercial 1% clindamycin gel. However, the wound dressing prepared without drug did not exhibit any bactericidal activity indicating that the investigated clindamycin-loaded wound dressing has good antibacterial activity and can be applied as wound dressings in acne healing (Sangnim et al., 2018).

3.4. Ampicillin-loaded wound dressing

Ampicillin-loaded wound dressing were prepared from hydrophobic polyurethane and hydrophilic ampicillin which were mixed together in the same solvent and electrospun into a fibrous scaffold. The various ratios of ampicillin: polyurethane, were prepared (1:10 wt%, 1.5:10 wt%, 2:10 wt%). In vitro study of cytotoxicity of the examined nanofibrous scaffolds was performed with human keratinocyte showing that prepared scaffolds can be used as an appropriate biocompatible wound dressing material. The antibacterial property of prepared ampicillin loaded wound dressings were determined on Muller and Hinton Agar using disk diffusion method. Test pathogens, Staphylococcus aureus and Klebsiella pneumonia, were spread on Muller Hinton agar plates and antibacterial activity of polyurethane nanofiber with ampicillin were evaluated on the bases of zone of inhibition against Staphylococcus aureus and Klebsiella pneumonia. Ampicillin polyurethane fibers exhibited good zone of inhibition against Gram-positive *Staphylococcus aureus* and Gram-negative *Klebsiella pneumonia*. Also, increasing the ampicillin content in electrospun improve its antibacterial effect (Sabitha & Rajiv, 2015).

3.5. Tetracycline-loaded wound dressing

For preparation tetracycline-loaded wound dressing poly(vinyl alcohol) and chitosan were used with addition of Tetracycline hydrochloride to the polymer solution before the electrospinning process. The 5 mg/mL of tetracycline were mixed to the polymer solution, which correspond to 5% of the polymer weight in the nanofibers.

The antibacterial efficacy of prepared tetracycline-loaded wound dressing was evaluated and compared with wound dressings where tetracycline was not included. Their activity was investigated against the Gram-negative *Escherichia coli* as well as Gram-positive *Staphylococci epidermidis* and *Staphylococcus aureus*, using disc diffusion test (zone of inhibition). The bacterial suspension was seeded and then grown in Mueller Hinton broth at 37 °C for 24 h. Rectangular pieces of 20 mm × 10 mm were cut from the tetracycline-loaded and also unloaded wound dressing and they were placed on the agar plates. The wound dressing prepared without tetracycline were used as controls. After 24 h incubation at 37°C, the area of inhibition zones was measured. Examination showed no bacteria growth at the area of inhibition zones for the tetracycline-loaded wound dressing. Also, the results showed that the tetracycline loaded electrospun PVA and chitosan scaffolds are not deleterious for cell activity and may be safe for their use as wound dressing and soft tissue repair (Alavarse et al., 2017).

3.6. Vancomycin-loaded wound dressing

Kurczewska et al., 2015 used vancomycin as a model drug, very potent against gram-positive bacteria, for a new antibacterial wound dressing. Vancomycin-loaded wound dressing were prepared by application of alginate or gelatine/alginate hydrogel with addition of vancomycin in concentration which should remain 10mg per gram of the dried gel.

The *in vitro* release study of vancomycin from prepared wound dressing were performed. For this study samples of vancomycin-loaded wound dressing were immersed in phosphate-buffered saline solution and analysed using UV-vis Spectrophotometer. According obtained results after 24h about 95% of vancomycin was released from alginate and 75% from gelatine/alginate hydrogel.

The activity of vancomycin-loaded wound dressing was studied using disc diffusion method with Mueller-Hinton agar and zone of inhibition bacteria growth (various Staphylococcus and Streptococcus bacteria) were determined. The inhibition zone was determined by measurement of the appropriate diameter (mm). The discs used for the study had 9-11mm and 10-15mm diameter for vancomycin loaded alginate and gelatin/alginate hydrogels respectively. The strong antimicrobial activity against investigated bacteria were obtained. The inhibition zones obtained for vancomycin loaded alginate hydrogel were bigger (20-32nm depending on infection agent) in comparison to vancomycin loaded gelatine/alginate hydrogel (16-27nm). These differences can be consequence of differences in release rate of antibiotic from the hydrogel (Kurczewska et al., 2015).

4. Bacterial infections in relation to hard tissue implants

The application of bone cement dates from the mid-nineteenth century when it was introduced for total knee prosthesis fixation by Themistocles Gluck and reported in historic text, The Classic: Report on the positive results obtained by the modern surgical experiment regarding the suture and replacement of defects of superior tissue, as well as the utilization of re-absorbable and living tamponade in surgery (Gluck, 2011).

The firstly applied bone cement was consisted primarily of plaster and colophony. Almost whole century later, in 1960, Sir John Charnley introduced polymethylmethacrylate (PMMA) as a new modern type of bone cement in total hip replacement surgery and since this introduction, PMMA was for years used as golden standard in fixation of cemented total joint arthroplasty (Charnley, 1960).

Following, different materials were investigated and used as bone replacement. A number of biomaterials for hard tissue implants such as hips, knees, ankle, shoulder, elbow joints and their application as drugs delivery systems were investigate lately. During last 60 years, three different generations seem to be clearly marked: bioinert materials (first generation), bioactive and biodegradable materials (second generation), and materials designed to stimulate specific cellular responses at the molecular level (third generation). These applications require the use of biodegradable and/or bioerodible polymers in order to enable the permanent persistent of implanted drug carrier. The only requirement was for the first generation materials was their minimal toxic effect. To the first generation meterials belongs metallic stainless steel and cobalt–chrome-molibdene based, titanium based, nickel-titanium based), ceramic materials high alumina ceramics, bioglasses, biopex, glass–ceramics, calcium phosphate cements) and polimers (polymethacrylic acid (PMMA), polyethylene (PE), polydimethylsulphoxide (PDMS), polyglycolic acid (PGA), polylactic acid (PLA), polycaprolactone (PCL), polydioxanone (PDS)) (Ghalme et al., 2016; Navarro et al., 2008).

However, one of the most important problems in orthopaedic surgery are bacterial infections especially infections after total joints replacement. The infection after fracture fixation can be classified according time of appearance into three groups: infections with early appearance (less than two weeks), delayed (between two and ten weeks) and late (more than ten weeks) (Metsemakers et al., 2018).

Different bacteria may cause these infections such as Gram-negative species, *Escherichia coli, Pseudomonas* including *Enterobacteriaceae* or Gram-positive species such as *Staphylococcus aureus*, *Corynebacterium species and Streptococcus pyogene*s including *Methicillin-resistant Staphylococcus aureus* (MRSA).

MRSA infection is caused by a type of staph bacteria that's become resistant to many of the antibiotics used to treat ordinary staph infections. In many different studies, number of antibiotics (gentamicin, vancomycin, tobramicin, clindamicin, erythromycin, ciprofloxacin, cephalosporins, tetracycline and rifampicin) were investigated for application in antibiotic-loaded implants.

Antibiotics application are in relation not only with infective agents but also with implants consisting. Polymethylmethacrylate (PMMA) also referred as (acrylic) bone cement was tested for local delivery of number different antibiotics in orthopaedic treatment of bones or joints. The obtained results showed that gentamicin and vancomycin can cover broad spectrum of pathogens including MRSA (van Vugt et al., 2019).

5. Antibiotics for hard tissue implants

According available literature the most frequently used antibiotics for hard tissue implants are gentamicin and vancomycin what is in accordance with severity of bacterial infection that can occur during orthopaedic surgery for hips, knees, ankle replacement.

5.1. Gentamicin application

The chitosan, chitosan/bioglass and chitosan/bioglass/ gentamicin coatings were prepared to investigate antibacterial activity of incorporated antibiotic. Solutions of chitosan in acetic acid in water were prepared by magnetic stirring following with dispersion of bioglass particles and addition of gentamicin sulfate in suspension in concentration of 2 mg/mL.

The biological behavior of the prepared coatings and their in vitro bioactivity were studied using antibacterial tests. In order to quantify the amount of gentamicin incorporated in the coatings, coatings were scraped o ff the substrate and immersed in deionized water with borate buffer (pH 10.4) while in vitro release of gentamicin was studied by incubating coated samples in phosphate buffered saline. The amounts of loaded and released antibiotic were determined by HPLC UV method. It was found that during five days 40% of the loaded gentamicin in phosphate buffered saline were released. The antibacterial activity of released antibiotic were

investigated against the *Staphylococcus aureus*, using disc diffusion test (zone of inhibition). The bacterial suspension was seeded and then grown in Mueller Hinton broth at 37 °C for 24 h.

The antimicrobial disc susceptibility test indicated that the CS/BG/GS coatings subjected to immersion in PBS developed a zone of inhibition of about 13 mm up to 2 days while PBS control samples, and chitosan/bioglass coatings, did not develop any zone of inhibition against *Staphylococcus aureus* growth. The cellular metabolic activity was measured by alamar. Blue assay and the percentage of proliferated cell number was estimated. The proposed coatings exhibit significantly smaller number in comparison to previously prepared positive control (Pishbin et al., 2014).

The ceramic material containing of hydroxyapatite and calcium sulphate as bone substitute was developed with addition of gentamicin to prevent the occurrence of infection while enhancing the bone healing. The gentamicin concentration in synthetic bone substitute was 175mg per 10 mL. The gentamicin release examination was made by determination of its concentration in serum and in urine of number of patients for at least 30 days, to give evidence for local antibacterial activity and systemic toxicity. The gentamicin concentrations in the serum were always well below the maximum recommended level of 12 mg/L. For the week urine concentrations of gentamicin were approximately 100 times higher than in serum. The peak levels were around 100 mg/L while after one week it was around 1 mg/L, indicating high local gentamicin concentrations at the implantation sites. Following, the gentamicin concentration in the urine decreased below 1mg/L for the rest of the sampling time. At approximately28 days, all gentamicin was eluted from the implants reducing risk of developing bacterial resistance on gentamicin loaded to ceramic material (Stravinskas et al., 2018).

Composite coating on titanium substrate, containing natural polymer chitosan (CS) and hydroxyapatite (HAP) with addition of antibiotic gentamicin (Gent) (1mg/mL) was developed to avoid the incidence of postoperative infection in bone healing. Determination of gentamicin incorporated into coating was made by scrapping off coating surfaces and resuspending powder in distilled water. Gentamicin in the solution was determined by HPLC/UV method after its derivatization with o-phtalaldehyde. It was obtained that the average of gentamicin loaded on 1 cm^2 area of hydroxyapatite / chitosan /gentamicin coating was around 7.3μg. The antibacterial activity of gentamicin loaded coatings in comparison with coatings without gentamicin was tested by agar diffusion method against gram positive pathogenic bacterial strain *Staphylococcus aureus* and gram-negative *Escherichia coli*. The coating without antibiotic, hydroxyapatite / chitosan, did not exhibit antibacterial activity against applied bacterial species. However, hydroxyapatite / chitosan /gentamicin coating expressed strong bactericidal activity after inoculation, reducing initial count by 2 logarithmic units. The complete reduction of bacterial cells was achieved within 1h for *Staphylococcus aureus.* But, antibacterial activity of hydroxyapatite / chitosan /gentamicin coating against *Escherichia coli* was much less expressed, and noticeable reduction of bacterial cells was achieved within 24 h post incubation.

In vitro cytotoxicity of prepared coating was evaluated by standardized colorimetric MTT (3-(4,5-dimethylthiazol-2-yl)-2,5-diphenyl tetrazolium bromide) assay. The coatings of hydroxyapatite and chitosan with or without addition of antibacterial agent gentamicin developed on titanium substrate were compared by MTT tests. According obtained results no toxicity for HAP/CS sample was found. However, HAP/CS/gent-coated Titanium samples have shown slightly increased toxicity which can be considered as consequence of the gentamicin presence. However, prepared gentamicin loaded composite coating can be classified as noncytotoxic (Stevanović et al., 2018).

5.2. Vancomycin application

Cabrejos-Azama et al., 2016 developed new hard tissue implant, calcium phosphate cement with magnesium addition, loaded with antibiotic vancomycin in aim to obtain new vancomycin carrier system which will be active against *Staphylococcus aureus*, the most relevant pathogen related with bone infection in postoperative implant surgery.

Two methods to load the cements with vancomycin were applied, adsorption from a vancomycin solution (with concentration 5 g/mL) or incorporation of vancomycin (2g) into the solid phase (40g) during the cement production. Vancomycin release from the cement was investigated by immersion in phosphate-buffered saline (pH 7.4) at 37 ± 1 °C. The amount of drug released was measured using UV spectroscopy. The cumulative release profiles shown indicate fully release of drug from the cements during 6 days. However, cement prepared with 26.67% Mg presents faster release of vancomycin. The 50% of the antibiotic was released after 3 h and 98% after 72 h. The *in vitro* antimicrobial examination of vancomycin-loaded cement was performed in order to determine its antibacterial effect on pathogen *Staphylococcus aureus*. The antibiotic activity of released vancomycin was investigated by *in vitro* tests using pathogen *Staphylococcus aureus*. The antimicrobial assay consisted in the measuring inhibition zone of the antibiotic in a standard gel inoculated with the bacterium strain. The presence of clear zones of inhibition surrounding the cement tablets loaded with vancomycin confirms the inhibition of *Staphylococcus aureus* growth. However significantly bigger zone of inhibition was observed for cement prepared with 26.67% Mg what is in accordance with its faster release of vancomycin (Cabrejos-Azama et al., 2016).

Gentamicin and vancomycin are antibiotics that exhibits bactericidal activity against a broad spectrum of microorganisms, such as *Pseudomonas aeruginosa*, *Escherichia coli* and *Staphylococcus aureus* but also MRSA bacteria since bacterial resistance to gentamicin and Vancomycin are lower than to other group of antibiotics. The mixture of these antibiotics was prepared as bioabsorbable beads and used in operative revision of infected hip

replacement in dog. The vancomycin and gentamicin, were both put into the femoral canal before closure the implant. There has been no evidence of postoperative reinfection during next five years. Also, no additional antibacterial drugs were necessary during recovery period and demonstrating that antibiotic-impregnated bioabsorbable calcium sulphate beads can be very useful in veterinary orthopaedics (Guthrie & Fitzpatrick, 2019).

Acknowledgments

Vesna Mišković-Stanković wishes to thank University Union-Nikola Tesla, Belgrade, Serbia, for the support.

Conflicts of Interest

Authors declare that there is no conflict of interest.

References

Alavarse, A. C., de Oliveira Silva, F. W., Colque, J. T., da Silva, V. M., Prieto, T., Venancio, E. C., & Bonvent, J.-J. (2017). Tetracycline hydrochloride-loaded electrospun nanofibers mats based on PVA and chitosan for wound dressing. *Materials Science & Engineering. C, Materials for Biological Applications*, *77*, 271–281. https://doi.org/10.1016/j.msec.2017.03.199

Cabrejos-Azama, J., Alkhraisat, M. H., Rueda, C., Torres, J., Pintado, C., Blanco, L., & López-Cabarcos, E. (2016). Magnesium substitution in brushite cements: Efficacy of a new biomaterial loaded with vancomycin for the treatment of Staphylococcus aureus infections. *Materials Science and Engineering: C*, *61*, 72–78. https://doi.org/https://doi.org/10.1016/j.msec.2015.10.092

Charnley, J. (1960). Anchorage of the femoral head prosthesis to the shaft of the femur. *The Journal of Bone and Joint Surgery. British Volume*, *42-B*, 28–30. https://doi.org/10.1302/0301-620X.42B1.28

Cohen, P. R., & Kurzrock, R. (2004). Community-acquired methicillin-resistant staphylococcus aureus skin infection: an emerging clinical problem. *Journal of the American Academy of Dermatology*, *50*(2), 277–280. https://doi.org/https://doi.org/10.1016/j.jaad.2003.06.005

Coimbra, P., Freitas, J. P., Gonçalves, T., Gil, M. H., & Figueiredo, M. (2019). Preparation of gentamicin sulfate eluting fiber mats by emulsion and by suspension electrospinning. *Materials Science and Engineering: C*, *94*, 86–93. https://doi.org/https://doi.org/10.1016/j.msec.2018.09.019

Eron, L. J., Lipsky, B. A., Low, D. E., Nathwani, D., Tice, A. D., & Volturo, G. A. (2003). Managing skin and soft tissue infections: Expert panel recommendations on key decision points. *Journal of Antimicrobial Chemotherapy*, *52*(SUPPL. 1). https://doi.org/10.1093/jac/dkg466

Ghalme, S., Mankar, A., & Bhalerao, Y. (2016). Biomaterials in Hip Joint Replacement. *International Journal of Materials Science and Engineering*, *4*, 113–125. https://doi.org/10.17706/ijmse.2016.4.2.113-125

Gluck, T. (2011). The Classic: Report on the Positive Results Obtained by the Modern Surgical Experiment Regarding the Suture and Replacement of Defects of Superior Tissue, as well as the Utilization of Re-absorbable and Living Tamponade in Surgery. *Clinical Orthopaedics and Related Research®*, *469*(6), 1528–1535. https://doi.org/10.1007/s11999-011-1837-7

Guthrie, J., & Fitzpatrick, N. (2019). Single-Stage Revision of an Infected Total Hip Replacement Using Antibiotic-Impregnated Bioabsorbable Beads in a Canine Patient. *VCOT Open*, *02*(01), e5–e12. https://doi.org/10.1055/s-0038-1677523

Hwang, M.-R., Kim, J. O., Lee, J. H., Kim, Y. il, Kim, J. H., Chang, S. W., Jin, S. G., Kim, J. A., Lyoo, W. S., Han, S. S., Ku, S. K., Yong, C. S., & Choi, H.-G. (2010). Gentamicin-loaded wound dressing with polyvinyl alcohol/dextran hydrogel: gel characterization and in vivo healing evaluation. *AAPS PharmSciTech*, *11*(3), 1092–1103. https://doi.org/10.1208/s12249-010-9474-0

Ki, V., & Rotstein, C. (2008). Bacterial skin and soft tissue infections in adults: A review of their epidemiology, pathogenesis, diagnosis, treatment and site of care. *Canadian Journal of Infectious Diseases and Medical Microbiology*, *19*(2), 173–184. https://doi.org/10.1155/2008/846453

Kim, J. O., Choi, J. Y., Park, J. K., Kim, J. H., Jin, S. G., Chang, S. W., Li, D. X., Hwang, M.-R., Woo, J. S., Kim, J.-A., Lyoo, W. S., Yong, C. S., & Choi, H.-G. (2008). Development of clindamycin-loaded wound dressing with polyvinyl alcohol and sodium alginate. *Biological & Pharmaceutical Bulletin*, *31*(12), 2277–2282. https://doi.org/10.1248/bpb.31.2277

Kurczewska, J., Sawicka, P., Ratajczak, M., Gajęcka, M., & Schroeder, G. (2015). Will the use of double barrier result in sustained release of vancomycin? Optimization of parameters for preparation of a new antibacterial alginate-based modern dressing. *International Journal of Pharmaceutics*, *496*(2), 526–533. https://doi.org/10.1016/j.ijpharm.2015.10.075

Lukáč, P., Hartinger, J. M., Mlček, M., Popková, M., Suchý, T., Šupová, M., Závora, J., Adámková, V., Benáková, H., Slanař, O., Bartoš, M., Chlup, H., Lambert, L., & Grus, T. (2019). A novel gentamicin-releasing wound dressing prepared from freshwater fish Cyprinus carpio collagen cross-linked with carbodiimide. *Journal of Bioactive and Compatible Polymers*, *34*(3), 246–262. https://doi.org/10.1177/0883911519835143

Metsemakers, W. J., Kuehl, R., Moriarty, T. F., Richards, R. G., Verhofstad, M. H. J., Borens, O., Kates, S., & Morgenstern, M. (2018). Infection after fracture fixation: Current surgical and microbiological concepts. *Injury*, *49*(3), 511–522. https://doi.org/10.1016/j.injury.2016.09.019

Monteiro, N., Martins, M., Martins, A., Fonseca, N. A., Moreira, J. N., Reis, R. L., & Neves, N. M. (2015). Antibacterial activity of chitosan nanofiber meshes with

liposomes immobilized releasing gentamicin. *Acta Biomaterialia*, *18*, 196–205. https://doi.org/10.1016/j.actbio.2015.02.018

Navarro, M., Michiardi, A., Castaño, O., & Planell, J. A. (2008). Biomaterials in orthopaedics. *Journal of The Royal Society Interface*, *5*(27), 1137–1158. https://doi.org/10.1098/rsif.2008.0151

Nnamani, O. (2013). Characterization and controlled release of gentamicin from novel hydrogels based on Poloxamer 407 and polyacrylic acids. *African Journal of Pharmacy and Pharmacology*, *7*, 2540–2552. https://doi.org/10.5897/AJPP2013.3803

Păunică-Panea, G., Ghica, M. V., Marin, Ș., Ene, A. M., Marin, M. M., Dănilă, E., Nițipir, C., Albu, M. G., & Cristescu, I. (2015). Collagen-albumin-gentamicin hydrogels usable for infected wound healing. *Leather and Footwear Journal*, *15*(4), 249–256. https://doi.org/10.24264/lfj.15.4.4

Pishbin, F., Mouriño, V., Flor, S., Kreppel, S., Salih, V., Ryan, M. P., & Boccaccini, A. R. (2014). Electrophoretic Deposition of Gentamicin-Loaded Bioactive Glass/Chitosan Composite Coatings for Orthopaedic Implants. *ACS Applied Materials & Interfaces*, *6*(11), 8796–8806. https://doi.org/10.1021/am5014166

Puoci, F., Piangiolino, C., Givigliano, F., Parisi, O. I., Cassano, R., Trombino, S., Curcio, M., Iemma, F., Cirillo, G., Spizzirri, U. G., Restuccia, D., Muzzalupo, R., & Picci, N. (2012). Ciprofloxacin-collagen conjugate in the wound healing treatment. *Journal of Functional Biomaterials*, *3*(2), 361–371. https://doi.org/10.3390/jfb3020361

Rajan, S. (2012). Skin and soft-tissue infections: classifying and treating a spectrum. *Cleveland Clinic Journal of Medicine*, *79*(1), 57–66. https://doi.org/10.3949/ccjm.79a.11044

Roy, D. C., Tomblyn, S., Burmeister, D. M., Wrice, N. L., Becerra, S. C., Burnett, L. R., Saul, J. M., & Christy, R. J. (2015). Ciprofloxacin-Loaded Keratin Hydrogels Prevent Pseudomonas aeruginosa Infection and Support Healing in a Porcine Full-Thickness Excisional Wound. *Advances in Wound Care*, *4*(8), 457–468. https://doi.org/10.1089/wound.2014.0576

Sabitha, M., & Rajiv, S. (2015). Preparation and characterization of ampicillin-incorporated electrospun polyurethane scaffolds for wound healing and infection control. *Polymer Engineering & Science*, *55*(3), 541–548. https://doi.org/https://doi.org/10.1002/pen.23917

Sangnim, T., Limmatvapirat, S., Nunthanid, J., Sriamornsak, P., Sittikijyothin, W., Wannachaiyasit, S., & Huanbutta, K. (2018). Design and characterization of clindamycin-loaded nanofiber patches composed of polyvinyl alcohol and tamarind seed gum and fabricated by electrohydrodynamic atomization. *Asian Journal of Pharmaceutical Sciences*, *13*(5), 450–458. https://doi.org/https://doi.org/10.1016/j.ajps.2018.01.002

Sripriya, R., Kumar, M. S., Ahmed, M. R., & Sehgal, P. K. (2007). Collagen bilayer dressing with ciprofloxacin, an effective system for infected wound healing. *Journal of Biomaterials Science, Polymer Edition*, *18*(3), 335–351. https://doi.org/10.1163/156856207779996913

Stevanović, M., Đošić, M., Janković, A., Kojić, V., Vukašinović-Sekulić, M., Stojanović, J., Odović, J., Crevar Sakač, M., Rhee, K. Y., & Mišković-Stanković, V. (2018). Gentamicin-Loaded Bioactive Hydroxyapatite/Chitosan Composite Coating Electrodeposited on Titanium. *ACS Biomaterials Science & Engineering*, *4*(12), 3994–4007. https://doi.org/10.1021/acsbiomaterials.8b00859

Stravinskas, M., Nilsson, M., Horstmann, P., Petersen, M. M., Tarasevicius, S., & Lidgren, L. (2018). Antibiotic Containing Bone Substitute in Major Hip Surgery: A Long Term Gentamicin Elution Study. *Journal of Bone and Joint Infection*, *3*(2), 68–72. https://doi.org/10.7150/jbji.23901

van Vugt, T. A. G., Arts, J. J., & Geurts, J. A. P. (2019). Antibiotic-Loaded Polymethylmethacrylate Beads and Spacers in Treatment of Orthopedic Infections and the Role of Biofilm Formation. *Frontiers in Microbiology*, *10*, 1626. https://doi.org/10.3389/fmicb.2019.01626

Primena antibiotika u biomaterijalima za implantate mekih i tvrdih tkiva

Jadranka Odović [1, *], Vesna Mišković Stanković [2]

[1] Farmaceutski fakultet, Univerzitet u Beogradu, Beograd, Srbija

[2] Fakultet za ekologiju i zaštitu životne sredine, Univerzitet Union-Nikola Tesla, Beograd, Srbija

***Autor za korespondenciju:** jodovic@pharmacy.bg.ac.rs

Abstrakt: Jedan od velikih izazova savremene medicine, farmacije i hemije je lečenje i zamena oštećenih i povređenih mekih i tvrdih tkiva, kao i kostiju i zglobova. Do sada su istraženi različiti materijali koji se koriste u njihovom lečenju. Sa druge strane, primena implantata mekog ili tvrdog tkiva nosi visok rizik od infekcije različitim mikroorganizmima. Zbog toga su u ovom radu prikazane različite mogućnosti primene implantata mekih i tvrdih tkiva, posebno implantata sa antibiotikom sa postepenim otpuštanjem, u cilju prevencije bakterijske infekcije, odnosno lečenja infekcije koja je nastala kao posledica prisutnih mikroorganizama. Prikazana je primena različitih antibiotika, gentamicina, ciprofloksacina, klindamicina, ampicilina, tetraciklina, vankomicina za implantate mekog tkiva, kao i gentamicina i vankomicina kao odgovarajućih antibiotika za implantate tvrdog tkiva.

Ključne reči: implantati mekog tkiva, implantati tvrdih tkiva, antibiotici

Global Sustainability Challenges
2023; Vol. 1(1): 33-42
https://gsc.unionnikolatesla.edu.rs/index.php/gsc/index
UDC: 504.5:669.018.674(497.11)
ISSN: 2956-1051 (Online)

Contamination and health risk assessment of heavy metals in PM10 in central Serbia

Sanja Mrazovac Kurilić[1,*], Vladanka Presburger Ulniković[1], Ana Ćirišan[1]

[1]Faculty of Ecology and Environmental Protection, Union-Nikola Tesla University, Belgrade, Serbia

[*]**Corresponding author:** mrazovac@gmail.com

To cite this article:
Mrazovac-Kurilić, S., Presburger-Ulniković, V. and Ćirišan, A. (2023). Contamination and health risk assessment of heavy metals in PM10 in central Serbia. *Global sustainability challenges, 1*(1), pp. 33-42

Received: Nov 7, 2022;: **Revised:** Nov 20, 2022; **Accepted:** Dec 16, 2022

Abstract: The objective of study was to investigate concentration and spatial distribution of heavy metals (As, Cd, Pb and Ni) in PM10 in central Serbia. Human health risks for heavy metals were assessed. Results showed that air in central Serbia does not contain significant heavy metal elements concentrations except in mining area (Bor). The contamination evaluation indicated that As, Cd, Ni and Pb in the air originated from anthropogenic sources. The non-cancer health risk assessment showed that ingestion was the primary exposure route for all metals in the air and that Pb, and As were the main contributors to non-cancer risks. HI values were calculated for children (HI=6.3E-07), indicating that children will likely experience higher health risks compared with adults (HI=7.1E-08). The non-cancer risks posed by all studied heavy metal elements and the cancer risks posed by As, Cd, and Ni to children and adults fell within the acceptable range.

Keywords: air; heavy metal elements; contamination assessment; health risk assessment; particulate matters PM10

1. Introduction

The particulate matters (PM) not only influence the natural conditions and make climate change (L. Wang et al., 2014). They have critical effects on human health under the high levels due to their deposition in the respiratory system (Makkonen et al., 2010; Moreno et al., 2011). The trace elements within particulates are important components in the atmosphere. They are present in our surrounding and have a significant contribution to potential health on the lung under long-term environmental exposure owing to their high bioreactivity and toxicity (Betha et al., 2014; Han et al., 2015; Moreno et al., 2011; Pan et al., 2015) According to the International Agency for Research on Cancer (IARC) of WHO (World Health Organization), the carcinogenic compounds are classified into five groups: Group 1 (carcinogenic to humans), Group 2A (probably carcinogenic to humans), Group 2B (possibly carcinogenic to humans), Group 3 (not classifiable as to its carcinogenicity to humans), and Group 4 (probably not carcinogenic to humans). In that study, As, Cd and Ni belong to Group 1, and Pb is included in Group 2A (Han et al., 2015; Tian et al., 2015; Wei et al., 2018).These toxic elements associated with particulate matter have potential threat to human health through air pollutants inhalation, dermal contact and ingestion in the human bodies (Zhang et al., 2015) Especially for children heavy metal adsorptions from the digestion system and hemoglobin sensitivity to these metals are both much higher than those for adults due to children's body at early ages and lower body weight Click or tap here to enter text. Therefore, trace elements in particulates are a serious concern for human health.

Over the past decades, there has been increasing concern about exposure of people, adults and children, to air contaminants in order to assess the health impact and to reduce human health risks. Therefore, air quality is an increasing public health concern due to presence of chemical and biological contaminants that might pose health effects. Heavy metals exist in the environment naturally as trace elements in rocks and soils, however they also are released to the environment as a result of human activities. Heavy metals may originate from various sources in urbanized areas, including emissions from vehicles, discharges from industrial facilities and other activities (Thornton, 1991).

As pollutant metals are generally non-biodegradable and no known homeostasis mechanisms of them, it is very likely

that any high levels of heavy metals will pose serious effects on biological life. Accumulation in fatty tissues and circulatory system, negative effects on central nervous system and functioning of internal organs as well as acting as cofactors in other diseases and cancer can be listed as their negative effects on human (Dockery & Pope, 1996; Nriagu, 1988). Due to the maximal brain growth and differentiation of children at early ages, infants and toddlers are particularly vulnerable to heavy metal exposure and poisoning. Moreover, heavy metal adsorptions from the digestion system and hemoglobin sensitivity to these metals are much higher in children compared to adults (Bellinger, 1995).

Young children might be exposed to dust bounded contaminants, including heavy metals, at elevated levels due to their behaviors increasing indirect ingestion by way of hand-to-mouth activities, touching and mouthing of various dust-contaminated objects. Moreover, lower body-weight of children would result ingestion of greater amounts of dust compared to adults (Beamer et al., 2008). Health risk is especially high for children since their tolerance to toxins is lower (Acosta et al., 2009). A number of studies reported exposure of children to contaminated soils, dust and air particulates by ingestion a significant amount of toxic elements through the hand-mouth pathway as well as other routes of exposure (Chirenje et al., 2006; Inyang & Bae, 2006; Mielke et al., 1999; Raghunath et al., 1999).

Heavy metal elements in air (in PM10) are known to easily enter the human body through ingestion, inhalation, and dermal contact (Cook et al., 2005). The adverse effects on human health from exposure to heavy metal elements have been well-documented (Sun et al., 2010; Valko et al., 2006; Zheng et al., 2006).

Epidemiological studies have consistently shown an association between PM pollution and the number of deaths from cancer and cardiovascular and respiratory diseases (Pope et al., 2002). There is also evidence linking particulate air pollution and increases in hospital admissions for respiratory (Burnett et al., 1995; Pope, 1991; Roemer et al., 1993) and cardiovascular diseases (Burnett et al., 1995; Schwartz & Morris, 1995). In response to these adverse effects of air pollution, the EU Commission defined limit values for PM10 concentrations in ambient air (EU Directive 1999/30/EC).

Mining activities are notorious for their adverse impacts on the environment (Wang et al., 2008). Large quantities of dust laden with high levels of heavy metals can be released into the air as a result of mining operations including crushing, grinding, excavating, smelting, and refining (Csavina et al., 2012) Despite that, small regions affected by mining activities have received relatively limited attention. Thus, in comparison with mega-cities or capital cities, the environmental and human health risks in mining regions requires further investigation.

In this study, the attemption was made to evaluate the above mentioned issues by analyzing available PM10 data from 15 places in Serbia during 2017.

2. Materials and Methods

2.1. Site description

Central Serbia also referred to as Serbia proper, is the part of Serbia lying outside the provinces of Vojvodina to the north and the territory of Kosovo to the south. Central Serbia takes up, roughly, the territory of Serbia between the natural borders consisting of the Danube and Sava (in the north), the Drina (in the west), and the "unnatural" border to the southwest with Montenegro, south with Kosovo and FYR Macedonia, and to the east with Bulgaria, with a small strip of the Danube with Romania in the northeast. The Danube and Sava divides central Serbia from the Serbian province of Vojvodina, while the Drina divides Serbia from Bosnia and Herzegovina. The Great Morava, a major river, goes through central Serbia. Extensions of three major mountain chains are located within Serbia proper: Dinaric Alps in the west and south, and the Carpathians and Balkan Mountains in the east.

Table 1 lists the 15 towns (sites) in central Serbia where heavy metals in PM10 measurements have been performed. Figure 1 shows the geographical position of towns in central Serbia where the sites are placed.

Table 1. GPS coordinates of sites

Location	Sign	N (Latitude)	E (Longitude)
Belgrade 1	1	44.817237	20.477730
Belgrade 2	2	44.809956	20.380088
Belgrade 3	3	44.799531	20.475025
Bor 1	4	44.075725	22.108439
Bor 2	5	44.069892	22.098509
Valjevo	6	44.268273	19.890655
Veliko Gradište	7	44.749536	21.505809
Kragujevac	8	44.012793	20.911423
Kraljevo	9	43.723848	20.687254
Niš	10	43.320902	21.895759
Pančevo	11	44.874000	20.647567
Čačak	12	43.891414	20.350165
Ćuprija	13	43.925249	21.373496
Užice 1	14	43.855402	19.842094
Užice 2	15	43.679864	19.884480

The measurements of concentrations of pollutants were carried out by monitoring the air quality in the national and local networks.

2.2. Sample collection and processing

The urban stations monitor the influence of urban and suburban settlements over air quality. Radius of monitoring area varies between 1 and 5 km. Measurements of PM10 were performed by gravimetric analysis and those of heavy metals (Pb, Cd, Ni), in PM10, by atomic absorption spectrometry. Obtained data represent the average values of PM particles for a given region.

Sampling of suspended PM10 particles is carried out by an ambient air sampler Model LVS 3 Sven Leckel and Model MVS 6 Sven Leckel, Germany.

Test methods for suspended particles are:

-SRPS EN 12341:2008 Air quality - Determination of PM10 fraction of suspended particle-reference method and

field test procedure to demonstrate the equivalency of measurement methods (gravimetric method);

-SRPS EN 12341:2015 Ambient air - Standard gravimetric measurement method for determining the mass concentration of PM10 suspended particles;

-SRPS EN 14902:2008 Ambient air quality - Standard method for the determination of Pb, Cd, As and Ni in the PM10 fraction of suspended particles (ICP-MS).

2.3. Health risk assessment model

2.3.1. Exposed doses

Figure 1. Map of the study area and sampling sites in Serbia

In this study, the risk assessment model developed by the Environmental Protection Agency of the United States (US EPA) was used to evaluate the health risks posed by heavy metals in road dust. Local residents were divided into adults and children and the following exposure categories were used: (1) adults and children through mouth and nose; 2) ingestion of dust particles through mouth; and 3) dermal contact with dust through exposed skin. According to the human health evaluation manual (Part A) and supplemental guidance for dermal risk assessment (Part E) (US EPA, 1989, 2004), the daily intake dose (D) of a pollutant through each pathway can be evaluated:

$$Ding = (C \times IngR \times EF \times ED \times CF) / (BW \times AT)$$

$$Dinh = (C \times InhR \times EF \times ED) / (BW \times AT \times PEF) \quad (1)$$

$$Ddermal = (C \times SA \times SL \times ABS \times EF \times ED \times CF) / (BW \times AT)$$

According to the classification list developed by the International Agency for Research on Cancer (IARC), three carcinogenic metals (As, Cd and Ni) were investigated for their carcinogenic risks (IARC, 2014). The life time average daily dose for these three metals was calculated by:

$$LADD = ((C \times EF) / (AT \times PEF)) \times ((InhRchild \times EDchild) / (BWchild) + (InhRadult \times EDadult) / (BWadult)) \quad (2)$$

where C is the upper limit of the 95% confidence interval for the mean (95% UCL), which is considered as a conservative estimate of the "reasonable maximum exposure" (US EPA, 1992). The 95% UCL in this study was calculated using previously described methods (Zheng et al., 2010a, 2010b) The other exposure factors for these models are shown in Table 2.

2.3.2 Risk characterization

For non-carcinogenic risks, Hazard quotient (HQ) was used to assess the non-carcinogenic risks posed by metals in road dust.

$$HQ = D / RfD \quad (3)$$

where RfD is the corresponding reference dose. An HQ<1 indicates no adverse health effects, while HQ>1 indicates that adverse health effects are likely to occur.

Table 2. Exposure factors

Factor	Definition	Adults value	Children value	Unit	Reference
BW	Average body weight	70	15	kg	EPA, 1989
IngR	Ingestion rate	100	200	mg/day	EPA, 1989
InhR	Inhalation rate	20	7.6	m^3/day	Zheng et al., 2010a
PEF	Particle emission factor	1.36×10^9	1.36×10^9	m^3/kg	EPA, 2001
SA	Sourface areas of the skin that contacts the airborne particulates	5700	2800	cm^{-2}	EPA, 2004
SL	Skin adherence factor	0.07	0.2	mg/m^3	EPA, 2004
EF	Exposure frequency	180	180	days/year	Zheng et al., 2010a
ED	Exposure duration	24	6	years	EPA, 2004
ET	Exposure time	24	24	hour/day	EPA, 2001
AT (non-carcinogenic risk)	Averaging time	ED×365	ED×365	days	EPA, 2001
AT (carcinogenic risk)	Averaging time	70×365	70×365	days	EPA, 2001
ABS	Dermal absorption factor	0.03(As); 0.001(others)	0.03(As); 0.001(others)	-	EPA, 2004
CF	Conversion factor	1×10^{-6}	1×10^{-6}	kg/mg	EPA, 2004

The hazard index (HI) is equal to the sum of HQs and is used to represent the total potential non-carcinogenic risks of different pollutants via three exposure routes described previously. An HI<1 indicates that there is no significant risk of non-carcinogenic effects. If HI>1, then a noncarcinogenic

effect is likely to exist (US EPA, 1989).

In the case of carcinogenic risks, the life time cancer risk can be estimated by:

$$R = LADD / SF \quad (4)$$

where SF is the corresponding slope factor. Any cancer risk in the range of 10–6–10–4 is considered acceptable by the US EPA (US 1989). The RfD and SF values of all investigated metals (Ferreira-Baptista & de Miguel, 2005; Zheng et al., 2010b) are presented in Table 3.

2.4. Statistical analysis

CUCL (exposure-point upper confident limit content, mg kg−1) is considered to yield an estimate of the "reasonable maximum exposure" (Hu et al., 2011; US EPA, 1989; Zheng et al., 2010a, 2010b), which is the upper limit of the 95% confidence interval for the mean. The 95% upper confidence limit (UCL) was calculated by employing an approach called "adjusted Central Limit Theorem (CLT)" (Singh et al., 1997; US EPA, 2002). Although the approach was developed for normally distributed large data sets, the theorem does not say how many samples are sufficient for normality to hold. However, when sample size is moderate or small, the means will not generally be normally distributed yet the non-normality is intensified by the skewness of the distribution. Therefore, it is suggested that it can be employed for non-normal distributed moderate or small size data (US EPA, 2002). The 95% UCL concentration (CUCL) has been calculated as

$$C_{UCL} = \bar{X} + \left[z_\alpha + \frac{\beta}{6\sqrt{n}}(1 + 2 \cdot z_\alpha^2)\right] \cdot \frac{S.D.}{\sqrt{n}} \quad (5)$$

$\bar{X}$ = arithmetic mean; S.D.= standard deviation; β= skewness; α is the probability of making Type I error (false positive) and its value is 0.05; Zα= (1 −α)th quantile of the standard normal distribution. For the 95% confidence level, Zα= 1.645; n= number of samples and its value is 15 for all elements.

All statistical analysis were done in Statistica software package.

Table 3. RfD and SF values

	Oral RfD	Inhal RfD	Dermal RfD	Inhal SF
Pb	3.50E-03	3.52E-03	5.25E-04	-
As	3.00E-04	3.01E-04	1.23E-04	1.51E+01
Cd	1.00E-03	1.00E-03	5.00E-05	6.30E+00
Ni	2.00E-02	2.06E-02	5.40E-03	8.40E-01

3. Results

3.1. Heavy metals contents in air

The content of heavy metals Pb, As, Cd and Ni in suspended PM10 particles was determined during 2017. Mean annual value measurement of heavy metals were used for analysis in 2017. The descriptive statistics related to heavy metal content in air in Serbia are listed in Table 4.

Table 4. Statistical parameters for 15 sites and 4 HM

Concentration	Max ($\times10^{-6}$ mg/kg)	Min ($\times10^{-6}$ mg/kg)	Mean ($\times10^{-6}$ mg/kg)	Geom. Mean ($\times10^{-6}$ mg/kg)	Median ($\times10^{-6}$ mg/kg)	S.D.	Skewnes (β)	$C_{95\%\ UCL}$ ($\times10^{-6}$ mg/kg)
Pb	122.58	1.61	22.93	9.94	6.86	35.51	2.28	43.78
As	58.06	0.24	8.84	2.10	1.61	19.05	2.40	20.19
Cd	3.55	0.08	0.98	0.46	0.32	1.10	1.13	1.54
Ni	9.68	1.61	4.73	3.97	4.03	2.79	0.64	6.04

The concentrations of 4 metals varied widely in this region and followed the order Pb>Ni>As>Cd.

In 2017, the mean annual value of arsenic in PM10 in Bor exceeded the limit values at stations Bor1 and Bor2. These are the only stations where the values for the arsenic exceeded limit values, while the average annual value of indicative measurements did not exceed the limit value at other stations. The value of cadmium is not exceeded limit value at any station. The highest mean annual concentrations of cadmium were measured in Bor: at the stations Bor1 and Bor2. The content of nickel in PM10 during 2017 was not exceeded limit values. The maximum daily value was in Bor on station Bor1.

In comparison with measurements in other countries, a significantly lower concentration of heavy metals in the air is observed in our observed territory (Botsou et al., 2020; Chen et al., 2022; Hou et al., 2019; Men et al., 2020; X. Wang et al., 2020; Yang et al., 2020).

Within the statistical analysis of data, the correlation between the elements was made, the analysis of the main components, considering the values of the correlation coefficients, and the cluster analysis.

The correlation coefficients with values that mostly exceed 0.5 show relatively high linear interdependence of elements. A high degree of correlation between the parameters indicates the common origin of the analyzed metals. The same was confirmed using factor analysis.

Table 5. Correlations

	Pb	As	Cd	Ni
Pb	1.00	0.93	0.82	0.65
As	0.93	1.00	0.75	0.48
Cd	0.82	0.75	1.00	0.68
Ni	0.65	0.48	0.68	1.00

Based on Figure 2, it can be concluded that Pb and Cd, as well as Ni and As make the primary clusters.

Table 6. PCA

	Factor1	Factor2	Factor3	Factor4
Pb	-0.963804	0.178534	0.121523	-0.156335
As	-0.898914	0.397479	0.133536	0.127010
Cd	-0.916590	-0.061108	-0.395017	0.009531
Ni	-0.773149	-0.612250	0.161556	0.035917

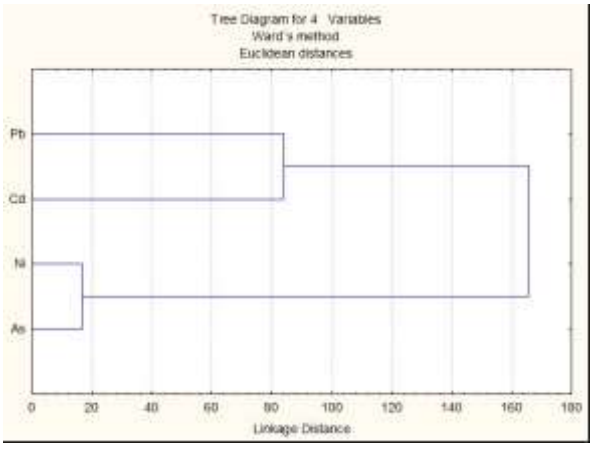

Figure 2. Clasters

Factor analysis showed the dominant influence of only one factor on the presence of analyzed 4 heavy metals in the air, and that is an anthropogenic factor-industry.

3.2. Spatial distributions of heavy metals in road dust

The spatial distribution pattern of 4 potentially toxic metals (As, Cd, Pb, and Ni) in PM10 in Serbia is presented in Figure 3. As, Cd, Pb, and Ni show spatial distribution patterns which coincide with the locations of industrial areas. The concentrations of those metals were higher near tailing pond and ore bodies (Bor). These results indicated that heavy metals likely originate from industrial sources in the study region.

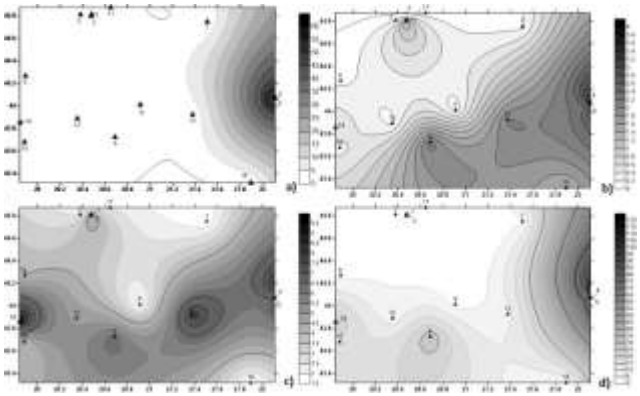

Figure 3. The spatial distribution of heavy metal elements (As, Cd, Ni and Pb) in air in Serbia (2017)

3.3. Health risk assessment results

3.3.1 Non-carcinogenic risk assessment

The HQ and HI for Ni, Pb, As and Cd in PM10 samples in Serbia were calculated (Table 7). The integrated HI values were 6.3E-07 for children and 7.1E-08 for adults living in Serbia, indicating children are likely to experience significantly higher non-cancer risks.

Among three different exposure pathways, the HQing values were the highest and contributed the most to HIs for both children and adults, indicating that ingestion of air appears to be the most threatening exposure way to human health in Serbia (Figure 4). The inhalation had the lowest contribution to health risks for children and the HQinh values were 3–4 orders of magnitude lower compared with the other two pathways for children, indicating that the non-cancer risks posed by the inhalation might be negligible compared with ingestion and dermal contact. Similar results were obtained by previous studies (Ferreira-Baptista & de Miguel, 2005; Zheng et al., 2010a).

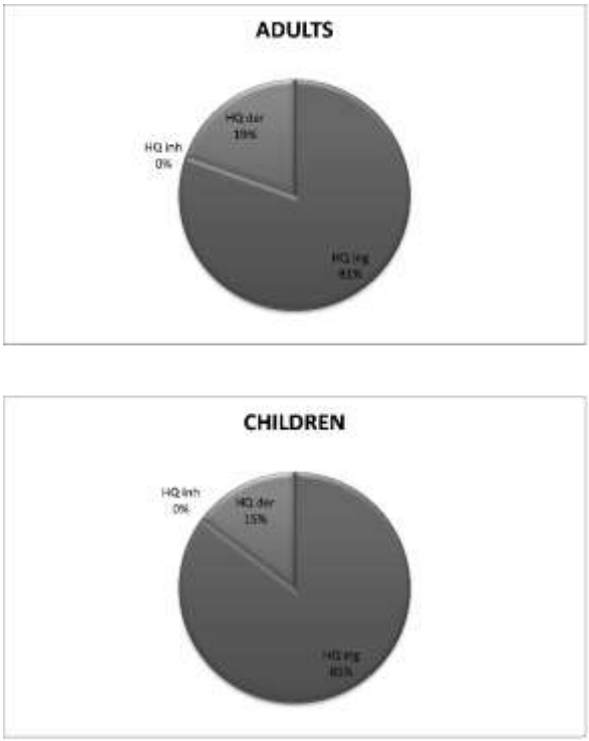

Figure 4. Non-carcinogenic risk distribution of different exposure ways for children and adults in Serbia (2017)

Additionally, children were found to experience higher health risks through ingestion compared with adults. The values of HQing for children were 9 times higher than those for adults and accounted for larger proportions (85% for children, 81% for adults) in integrated HI values. This result may be partially attributed to the special behavior patterns of children, particularly frequent hand-to-mouth contact (Figure 4).

The HIs for all studied metals were ranked in the order: As>Pb> Cd> Ni for adults, and for children (Table 7 and Figure 5). Pb and As were the main contributors to health risks posed by PM10 exposure for both children and adults,

and Ni had the smaller contribution.

The HI values for all metals tested in this study and the integrated HI values for children and adults, were within the safe level (<1), suggesting minimal non-carcinogenic risk to children and adults from exposure to PM10 metals.

3.3.2 Carcinogenic risk assessment

The cancer risks according to inhalation exposure to Cd, Ni and As are presented in Table 7. Results showed that the overall risk of cancer decreased in the order Ni>As> Cd. The leading heavy metal was Ni for which cancer risks were 1 order of magnitude higher than those for other metals. Overall, cancer risk values for all heavy metals in this study were within the acceptable range, implying negligible carcinogenic risk.

Table 7. HQ, HI and R values for each non-carcinogenic and carcinogenic heavy metal measured in air in Serbia (2017)

HM	HQ ingestion		HQ inhalation		HQ dermal		HI		R
	A	Ch	A	Ch	A	Ch	A	Ch	
Pb	8.81E-09	82.25E-09	1.29E-12	2.28E-12	0.023E-08	0.15E-08	9E-09	8.4E-08	-
As	4.74E-08	44.25E-08	0.69E-11	1.23E-11	1.38E-08	9.07E-08	6.1E-08	5.3E-07	0.69E-16
Cd	1.08E-09	10.13E-09	0.16E-12	0.28E-12	0.0008E-07	0.0056E-07	1.1E-09	1.1E-08	0.01E-15
Ni	2.13E-10	19.86E-10	0.31E-13	0.54E-13	0.003E-09	0.02E-09	2.2E-10	2E-09	0.04E-14
SUM	5.8E-08	5.4E-07	8.4E-12	1.5E-11	1.4E-08	9.3E-08	**7.1E-08**	**6.3E-07**	**4E-16**

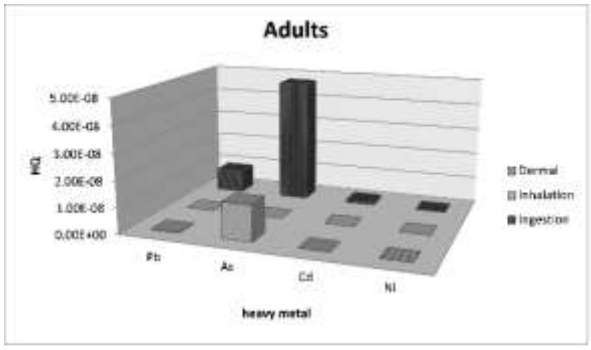

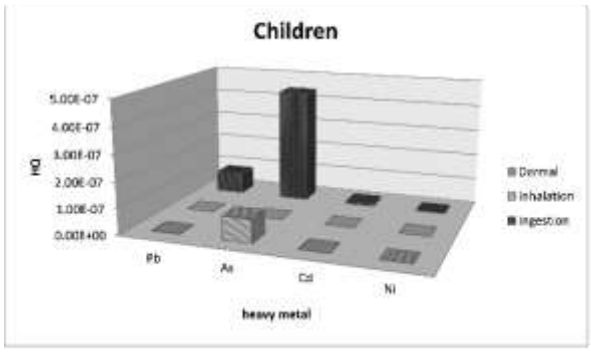

Figure 5 The HQs of each heavy metal in air in Serbia for adults (a) and children (b) (2017)

4. Conclusion

A total of 15 PM10 samples were collected from Serbia in 2017. The concentration and spatial distribution patterns of 4 potentially toxic heavy metal elements (As, Cd, Pb and Ni) in PM10 were analyzed. Human health risks for each heavy metal element were assessed using a human exposure model.

Results showed that concentrations of Cd, Pb, Ni and As, were not higher compared with limit values. The spatial distribution of Cd, Pb, Ni and As were all in accordance with the locations of industrial areas, indicating that these four heavy metals likely originated from industrial sources.

The health risks analysis showed that ingestion was the dominant exposure pathway for both children and adults. The HI value for As accounted for nearly 86% of the integrated HI value for adults and 84% for children, indicating that this heavy metal was the greatest contributors to non-cancer risks. Among the 3 carcinogenic metals, Ni was the leading contributor to cancer risks, followed by As and Cd. Although both non-carcinogenic and carcinogenic risk for each metal fell within acceptable values, children were more susceptible than adults and experienced higher non-carcinogenic risk from exposure to metals in air. The risks to children living in the central Serbia from exposure to heavy metal in air should receive greater attention.

Acknowledgments

Authors wish to thank University Union-Nikola Tesla, Belgrade, Serbia, for the support.

Conflicts of Interest

Authors declare that there is no conflict of interest.

References

Acosta, J. A., Cano, A. F., Arocena, J. M., Debela, F., & Martínez-Martínez, S. (2009). Distribution of metals in soil particle size fractions and its implication to risk assessment of playgrounds in Murcia City (Spain). *Geoderma*, *149*(1), 101–109. https://doi.org/https://doi.org/10.1016/j.geoderma.20

08.11.034

Beamer, P., Key, M. E., Ferguson, A. C., Canales, R. A., Auyeung, W., & Leckie, J. O. (2008). Quantified activity pattern data from 6 to 27-month-old farmworker children for use in exposure assessment. *Environmental Research*, *108*(2), 239–246. https://doi.org/10.1016/j.envres.2008.07.007

Bellinger, D. (1995). Neuropsychologic function in children exposed to environmental lead. In *Epidemiology (Cambridge, Mass.)* (Vol. 6, Issue 2, pp. 101–103).

Betha, R., Behera, S. N., & Balasubramanian, R. (2014). 2013 Southeast Asian Smoke Haze: Fractionation of Particulate-Bound Elements and Associated Health Risk. *Environmental Science & Technology*, *48*(8), 4327–4335. https://doi.org/10.1021/es405533d

Botsou, F., Moutafis, I., Dalaina, S., & Kelepertzis, E. (2020). Settled bus dust as a proxy of traffic-related emissions and health implications of exposures to potentially harmful elements. *Atmospheric Pollution Research*, *11*(10), 1776–1784. https://doi.org/https://doi.org/10.1016/j.apr.2020.07.010

Burnett, R. T., Dales, R., Krewski, D., Vincent, R., Dann, T., & Brook, J. R. (1995). Associations between ambient particulate sulfate and admissions to Ontario hospitals for cardiac and respiratory diseases. *American Journal of Epidemiology*, *142*(1), 15–22. https://doi.org/10.1093/oxfordjournals.aje.a117540

Chen, H., Zhan, C., Liu, S., Zhang, J., Liu, H., Liu, Z., Liu, T., Liu, X., & Xiao, W. (2022). Pollution Characteristics and Human Health Risk Assessment of Heavy Metals in Street Dust from a Typical Industrial Zone in Wuhan City, Central China. *International Journal of Environmental Research and Public Health*, *19*(17). https://doi.org/10.3390/ijerph191710970

Chirenje, T., Ma, L. Q., & Lu, L. (2006). Retention of Cd, Cu, Pb and Zn by Wood Ash, Lime and Fume Dust. *Water, Air, & Soil Pollution*, *171*(1), 301–314. https://doi.org/10.1007/s11270-005-9051-4

Cook, A. G., Weinstein, P., & Centeno, J. A. (2005). Health effects of natural dust. *Biological Trace Element Research*, *103*(1), 1–15. https://doi.org/10.1385/BTER:103:1:001

Csavina, J., Field, J., Taylor, M. P., Gao, S., Landázuri, A., Betterton, E. A., & Sáez, A. E. (2012). A review on the importance of metals and metalloids in atmospheric dust and aerosol from mining operations. *The Science of the Total Environment*, *433*, 58–73. https://doi.org/10.1016/j.scitotenv.2012.06.013

Dockery, D, and Pope, A. (1996). *Epidemiology of acute health effects: summary of time series studies* (S. Wilson, Ed.; Particles). Harvard University Press, Cambridge, MA (United States).

Ferreira-Baptista, L., & de Miguel, E. (2005). Geochemistry and risk assessment of street dust in Luanda, Angola: A tropical urban environment. *Atmospheric Environment*, *39*(25), 4501–4512. https://doi.org/https://doi.org/10.1016/j.atmosenv.2005.03.026

Han, Y.-J., Kim, H.-W., Cho, S.-H., Kim, P.-R., & Kim, W.-J. (2015). Metallic elements in PM2.5 in different functional areas of Korea: Concentrations and source identification. *Atmospheric Research*, *153*, 416–428. https://doi.org/https://doi.org/10.1016/j.atmosres.2014.10.002

Hou, S., Zheng, N., Tang, L., Ji, X., Li, Y., & Hua, X. (2019). Pollution characteristics, sources, and health risk assessment of human exposure to Cu, Zn, Cd and Pb pollution in urban street dust across China between 2009 and 2018. *Environment International*, *128*, 430–437. https://doi.org/10.1016/j.envint.2019.04.046

Hu, X., Zhang, Y., Luo, J., Wang, T., Lian, H., & Ding, Z. (2011). Bioaccessibility and health risk of arsenic, mercury and other metals in urban street dusts from a mega-city, Nanjing, China. *Environmental Pollution*, *159*(5), 1215–1221. https://doi.org/https://doi.org/10.1016/j.envpol.2011.01.037

IARC. (2014). *(International Agency for Research on Cancer)*.

Inyang, H. I., & Bae, S. (2006). Impacts of dust on environmental systems and human health. In *Journal of hazardous materials* (Vol. 132, Issue 1, pp. v–vi). https://doi.org/10.1016/j.jhazmat.2005.11.082

Kurt-Karakus, P. B. (2012). Determination of heavy metals in indoor dust from Istanbul, Turkey: Estimation of the health risk. *Environment International*, *50*, 47–55. https://doi.org/https://doi.org/10.1016/j.envint.2012.09.011

Makkonen, U., Hellén, H., Anttila, P., & Ferm, M. (2010). Size distribution and chemical composition of airborne particles in south-eastern Finland during different seasons and wildfire episodes in 2006. *The Science of the Total Environment*, *408*(3), 644–651. https://doi.org/10.1016/j.scitotenv.2009.10.050

Men, C., Liu, R., Xu, L., Wang, Q., Guo, L., Miao, Y., & Shen, Z. (2020). Source-specific ecological risk analysis and critical source identification of heavy metals in road dust in Beijing, China. *Journal of Hazardous Materials*, *388*, 121763. https://doi.org/https://doi.org/10.1016/j.jhazmat.2019.121763

Mielke, H. W., Gonzales, C. R., Smith, M. K., & Mielke, P. W. (1999). The Urban Environment and Children's Health: Soils as an Integrator of Lead, Zinc, and Cadmium in New Orleans, Louisiana, U.S.A. *Environmental Research*, *81*(2), 117–129. https://doi.org/https://doi.org/10.1006/enrs.1999.3966

Moreno, T., Querol, X., Alastuey, A., Reche, C., Cusack, M., Amato, F., Pandolfi, M., Pey, J., Richard, A., Prévôt, A. S. H., Furger, M., & Gibbons, W. (2011). Variations in time and space of trace metal aerosol concentrations in urban areas and their surroundings. *Atmospheric Chemistry and Physics*, *11*(17), 9415–9430. https://doi.org/10.5194/acp-11-9415-2011

Nriagu, J. O. (1988). A silent epidemic of environmental metal poisoning? *Environmental Pollution (Barking, Essex : 1987)*, *50*(1–2), 139–161. https://doi.org/10.1016/0269-7491(88)90189-3

Pan, Y., Tian, S., Li, X., Sun, Y., Li, Y., Wentworth, G. R.,

& Wang, Y. (2015). Trace elements in particulate matter from metropolitan regions of Northern China: Sources, concentrations and size distributions. *The Science of the Total Environment*, *537*, 9–22. https://doi.org/10.1016/j.scitotenv.2015.07.060

Pope, C. A. 3rd. (1991). Respiratory hospital admissions associated with PM10 pollution in Utah, Salt Lake, and Cache Valleys. *Archives of Environmental Health*, *46*(2), 90–97. https://doi.org/10.1080/00039896.1991.9937434

Pope, C. A. 3rd, Burnett, R. T., Thun, M. J., Calle, E. E., Krewski, D., Ito, K., & Thurston, G. D. (2002). Lung cancer, cardiopulmonary mortality, and long-term exposure to fine particulate air pollution. *JAMA*, *287*(9), 1132–1141. https://doi.org/10.1001/jama.287.9.1132

Raghunath, R., Tripathi, R. M., Kumar, A. v, Sathe, A. P., Khandekar, R. N., & Nambi, K. S. (1999). Assessment of Pb, Cd, Cu, and Zn exposures of 6- to 10-year-old children in Mumbai. *Environmental Research*, *80*(3), 215–221. https://doi.org/10.1006/enrs.1998.3919

Roemer, W., Hoek, G., & Brunekreef, B. (1993). Effect of ambient winter air pollution on respiratory health of children with chronic respiratory symptoms. *The American Review of Respiratory Disease*, *147*(1), 118–124. https://doi.org/10.1164/ajrccm/147.1.118

Schwartz, J., & Morris, R. (1995). Air pollution and hospital admissions for cardiovascular disease in Detroit, Michigan. *American Journal of Epidemiology*, *142*(1), 23–35. https://doi.org/10.1093/oxfordjournals.aje.a117541

Singh, A. K., Singh, A., & ME, E. (1997). *The Lognormal Distribution in Environmental Applications*.

Sun, C., Bi, C., Chen, Z., Wang, D., Zhang, C., Sun, Y., Yu, Z., & Zhou, D. (2010). Assessment on environmental quality of heavy metals in agricultural soils of Chongming Island, Shanghai City. *Journal of Geographical Sciences*, *20*(1), 135–147. https://doi.org/10.1007/s11442-010-0135-8

Thornton, I. (1991). Metal Contamination of Soils in Urban Areas. In *Soils in the Urban Environment* (pp. 47–75). https://doi.org/https://doi.org/10.1002/9781444310603.ch4

Tian, H. Z., Zhu, C. Y., Gao, J. J., Cheng, K., Hao, J. M., Wang, K., Hua, S. B., Wang, Y., & Zhou, J. R. (2015). Quantitative assessment of atmospheric emissions of toxic heavy metals from anthropogenic sources in China: historical trend, spatial distribution, uncertainties, and control policies. *Atmospheric Chemistry and Physics*, *15*(17), 10127–10147. https://doi.org/10.5194/acp-15-10127-2015

US EPA. (1989). *Risk Assessment Guidance for Superfund. Volume I Human Health Evaluation Manual (Part A)*. *I*(December), 289. https://doi.org/EPA/540/1-89/002

US EPA. (1992). *Supplemental Guidance to RAGS: Calculating the Concentration Term*. PB92-963373.

US EPA. (2002). *US-EPA, 2002. Calculating upper confidence limits for exposure point concentrations at hazardous waste sites. Office of Emergency and Remedial Response. OSWER 9285.6-10. December*.

US EPA. (2004). Risk assessment guidance for superfund (RAGS). Volume I. Human health evaluation manual (HHEM). Part E. Supplemental guidance for dermal risk assessment. *Us Epa*, *1*(540/R/99/005). https://doi.org/EPA/540/1-89/002

Valko, M., Rhodes, C. J., Moncol, J., Izakovic, M., & Mazur, M. (2006). Free radicals, metals and antioxidants in oxidative stress-induced cancer. *Chemico-Biological Interactions*, *160*(1), 1–40. https://doi.org/10.1016/j.cbi.2005.12.009

Wang, L., Guo, Z., Xiao, X., Chen, T., Liao, X., Song, J., & Wu, B. (2008). Heavy metal pollution of soils and vegetables in the midstream and downstream of the Xiangjiang River, Hunan Province. *Journal of Geographical Sciences*, *18*(3), 353–362. https://doi.org/10.1007/s11442-008-0353-5

Wang, L., Liang, T., Zhang, Q., & Li, K. (2014). Rare earth element components in atmospheric particulates in the Bayan Obo mine region. *Environmental Research*, *131*,64–70. https://doi.org/https://doi.org/10.1016/j.envres.2014.02.006

Wang, X., Liu, E., Lin, Q., Liu, L., Yuan, H., & Li, Z. (2020). Occurrence, sources and health risks of toxic metal(loid)s in road dust from a mega city (Nanjing) in China. *Environmental Pollution*, *263*, 114518. https://doi.org/https://doi.org/10.1016/j.envpol.2020.114518

Wei, Q. Z., Li, S., Jia, Q., Luo, B., Su, L. M., Liu, Q., Yuan, X. R., Wang, Y. H., Ruan, Y., & Niu, J. P. (2018). [Pollution characteristics and health risk assessment of heavy metals in PM(2.5) in Lanzhou]. *Zhonghua yu fang yi xue za zhi [Chinese journal of preventive medicine]*, *52*(6), 601–607. https://doi.org/10.3760/cma.j.issn.0253-9624.2018.06.008

Yang, S., Liu, J., Bi, X., Ning, Y., Qiao, S., Yu, Q., & Zhang, J. (2020). Risks related to heavy metal pollution in urban construction dust fall of fast-developing Chinese cities. *Ecotoxicology and Environmental Safety*, *197*, 110628. https://doi.org/https://doi.org/10.1016/j.ecoenv.2020.110628

Zhang, F., Wang, Z., Cheng, H., Lv, X., Gong, W., Wang, X., & Zhang, G. (2015). Seasonal variations and chemical characteristics of PM2.5 in Wuhan, central China. *Science of The Total Environment*, *518–519*, 97–105. https://doi.org/https://doi.org/10.1016/j.scitotenv.2015.02.054

Zheng, G., Yue, L., Li, Z., & Chen, C. (2006). Assessment on heavy metals pollution of agricultural soil in Guanzhong District. *Journal of Geographical Sciences*, *16*(1), 105–113. https://doi.org/10.1007/s11442-006-0111-5

Zheng, N., Liu, J., Wang, Q., & Liang, Z. (2010a). Heavy metals exposure of children from stairway and sidewalk dust in the smelting district, northeast of

China. *Atmospheric Environment*, *44*(27), 3239–3245. https://doi.org/https://doi.org/10.1016/j.atmosenv.2010.06.002

Zheng, N., Liu, J., Wang, Q., & Liang, Z. (2010b). Health risk assessment of heavy metal exposure to street dust in the zinc smelting district, Northeast of China. *The Science of the Total Environment*, *408*(4), 726–733. https://doi.org/10.1016/j.scitotenv.2009.10.075

Procena zagađenja i zdravstvenog rizika od teških metala u PM10 u centralnoj Srbiji

Sanja Mrazovac Kurilić[1,*], Vladanka Presburger Ulniković[1], Ana Ćirišan[1]

[1]Fakultet za ekologiju i zaštitu životne sredine, Univerzitet Union-Nikola Tesla, Beograd, Srbija

***Autor za korespondenciju**: mrazovac@gmail.com

Abstrakt: Cilj rada bio je da se ispita koncentracija i prostorna distribucija teških metala (As, Cd, Pb i Ni) u PM10 u centralnoj Srbiji. Procenjeni su rizici po ljudsko zdravlje od teških metala. Rezultati su pokazali da vazduh u centralnoj Srbiji ne sadrži značajne koncentracije teških metala osim u rudarskom području (Bor). Procena kontaminacije je pokazala da As, Cd, Pb i Ni u vazduhu potiču iz antropogenih izvora. Procena nekancerogenog zdravstvenog rizika je pokazala da je gutanje bio primarni put izlaganja svim metalima u vazduhu i da su Pb i As dali glavni doprinos nekarcinogenom riziku. HI vrednosti su izračunate za decu (HI=6,3E-07), što ukazuje da će deca verovatno imati veće zdravstvene rizike u poređenju sa odraslima (HI =7,1E-08). Nekancerogeni rizik koji predstavlja uticaj sva četiri proučavana teška metala i kancerogeni rizik koje predstavljaju As, Cd i Ni, u slučajevima za decu i odrasle bili su u prihvatljivom opsegu.

Ključne reči: vazduh; teški metalni elementi; procena kontaminacije; procena rizika po zdravlje; čestice PM10

Global Sustainability Challenges
2023; Vol. 1(1): 43-50
https://gsc.unionnikolatesla.edu.rs/index.php/gsc/index
UDC: 504.5:669.018.674
504.175:546.815
ISSN: 2956-1051 (Online)

Structural changes of fly ash-based geopolymers induced by a large amount of lead

Violeta Nikolić

Faculty of Ecology and Environmental Protection, University Union-Nikola Tesla, Belgrade, Serbia

[*]**Corresponding author:** violetanikolic22@unionnikolatesla.edu.rs, violeta.m.nikolic@gmail.com

To cite this article:
Nikolić, V. (2023). Structural changes of fly ash-based geopolymers induced by a large amount of lead. *Global sustainability challenges, 1*(1), pp. 43-50

Received: Dec 19, 2022; **Revised:** Dec 27, 2022; **Accepted:** Dec 30, 2022

Abstract: Geopolymers has emerged as possible techological and environmentally solution for the effective immobilization of heavy metals and other toxic materials. In this paper, structural changes of geopolymers induced by large amount of lead (up to 30%) were examined. Geopolymers were synthesized by alkali activation of fly ash using sodium silicate with modulus 1.5 as alkali activator. Lead was added in the form of water-soluble salt - lead-nitrate, during the synthesis of geopolymers. Structural changes of geopolymers due to Pb addition were assessed by means of XRD and ^{29}Si MAS NMR analysis. XRD analysis confirmed that the Pb addition led to the formation of new Pb-phases, which indicated that Pb formed chemical bonds with the geopolymers. ^{29}Si MAS NMR analysis showed the increase of less condensed Q^1 and Q^2 structural units of geopolymers with Pb addition.

Keywords: geopolymer, fly ash, immobilization, lead

1. Introduction

Geopolymers are the hotspot in research of new green cementitious materials. They are produced by alkaline activation of amorphous aluminosilicates, including industrial waste such as fly ash (FA) (Shi et al., 2011). Fly ash is a by-product produced from combustion of coal and collected by electrostatic separators from the fuel gasses of the thermal power plants (Komljenović et al., 2010). Accumulation quantities of fly ash are increasing yearly and estimated to be around 780 million tons annually (Toniolo & Boccaccini, 2017). There is a considerable interest in utilizing such by-product material in the synthesis and processing of high performance cementitious materials. These inorganic binder materials are very attractive environmentally for a number of reasons (Duxon et al., 2007). First, this type of binder represents a considerable benefit in terms of reducing global CO_2 emissions. High emission of CO_2 during Portland cement production (1 t of CO_2 per 1 t of Portland cement) is a reason enough to develop and use geopolymers. Further, the use of industrial by-product is consistent with the growing trend towards waste re-utilization (van Deventer et al., 2007). Geopolymers are also an alternative to Portland cement due to excellent mechanical properties, chemical resistance and durability in the long-term period (Provis & van Deventer, 2009). Some of these materials cross the boundaries defined by traditional cementitious materials (Fernandez-Jimenez & Palomo, 2003).

Geopolymers are the amorphous equivalent of certain synthetic zeolites, although the distinctive zeolite structure is absent (van Jaarsveld et al., 1997). The main product of fly ash geopolymerization is the three-dimensional hydrated sodium aluminosilicate gel "N-A-S-H", in which Si and Al atoms are bridged through oxygen atoms and tetrahedrally coordinated, while alkali metal ions play an important role in geopolymers structure, as they balance the negative charge of aluminum in tetrahedral coordination (Provis & van Deventer, 2009).

Geopolymer properties are influenced by numerous factors, such as the characteristics of the starting material (fly ash), the type and concentration of the alkali activator, as well as the synthesis and curing conditions of geopolymers (temperature, reaction time and the relative humidity) (Nikolić et al., 2015).

On the other hand, with the development of industry, there is an increasing amount of heavy metal wastes generated from metalwork industry, chemical industry, electrical equipment manufacturing and other fields, which brings great damage to

the environment (Wang et al., 2018). Unfortunately, landfilling is still the most widely used technic for processing of waste from the mining industry causing the environmental problems (van Jaarsveld et al., 1997). It is clear that a need exists for a technology that can handle large amount of fly ash, mine tailings, contaminated soil, municipal waste containing heavy metals (Shi & Fernández-Jiménez, 2006). Heavy metals pollution has become a very serious global environmental problem. In addition, heavy metals in soil, water and air may cause bioaccumulation of heavy metals in animals and humans. Lead (Pb) is one of the most common hazardous heavy metals due to the increasing human activity and industrial progress. Lead is a pollutant, which has long-term persistence in the environment and has detrimental effects on the human body, especially on the nervous, immune and reproductive system (Landrigan et al., 2000).

Geopolymers are a possible solution in the immobilization of heavy metals (Xu et al., 2006; Guo et al., 2017) for several reasons. Firstly, geopolymer has a three-dimensional network structure, and heavy metals can be "lock" in its structure. Secondly, the permeability of the geopolymers is very low, which can prevent leaching of heavy metals. Thirdly, Al (III) is a fourfold-coordinated atom, so $[AlO_4]^{5-}$ has ability to attract positive charge. In addition, geopolymers are durable and chemical resistant (van Jaarsveld et al., 1997).

The mechanism immobilization can be physical or chemical nature. Although it is well known that the geopolymers are suitable material for immobilization of lead (Guo et al., 2017), the mechanism of Pb immobilization is still unclear (Nikolić et al., 2014). Some authors (van Jaarsveld et al., 1998) indicated that Pb immobilization proceeds by a combination of physical encapsulation and chemical bonding, including adsorption, while other authors (Phair et. al., 2004) concluded that the Pb immobilization is a chemical process, rather than the sorption or physical encapsulation. Perera et al. (2005) suggested that Pb is encapsulated in the amorphous aluminosilicate structure of geopolymers while no new crystalline phases were observed. On the other hand, Palomo & Palacios (2003) reported that the addition of $Pb(NO_3)_2$ in the fly ash-based geopolymer led to the formation of vaguely identifiable insoluble crystalline compound Pb_3SiO_5. Zhang et al. (2008) tentatively supported the identification of Pb_3SiO_5. In addition, Lee et al. (2016) suggested that lead might contribute to the balancing charge of geopolymers network by replacing Na in the structure.

Regardless of the fact that there is no overall agreement regarding the mechanism of Pb immobilization, there is a general agreement that the process of Pb immobilization in geopolymers is successful (Nikolić et al., 2014; Palomo & Palacios, 2003). However, relatively low concentrations of Pb compound (up to 1% Pb in relation to the FA mass) in the Pb immobilization were mainly used (Nikolić et al., 2014; Perera et al., 2005), which made the mechanism of Pb immobilization still indefinable. In the previous studies, Nikolić et al. (2018) investigated the influence of curing conditions on the lead immobilization and confirmed that 4% of lead was successfully immobilized. Guo et al. (2017) were conducted research in order to immobilize higher concentration of Pb (up to 8%) in geopolymer matrix and to establish the immobilization mechanism of Pb. Obviously, higher concentrations of Pb are required to clarify the mechanism of Pb immobilization.

Structural changes of geopolymer induced by Pb addition were usually studied by XRD, FTIR, and SEM or TEM coupled with EDS analysis. However, these methods usually provide limited information, particularly XRD analysis, since the major product of alkali-activation - the aluminosilicate gel is amorphous. In order to obtain additional useful information regarding the mechanism of Pb immobilization, more appropriate method, such as ^{29}Si MAS NMR (Nikolić et al., 2018) was also used.

The aim of this paper is to determine how a large amount of lead (up to 30%) affects the structure of geopolymers, using XRD and ^{29}Si MAS NMR analysis and possibly clarify the mechanism of Pb immobilization.

2. Materials and Methods

2.1. Materials

In this study, FA Morava from thermal power plant "Morava" Svilajnac, Serbia was used. Chemical composition and classification according to ASTM C 618-03 of the initial FA sample are shown in Table 1.

Table 1. Chemical composition and classification according to ASTM C 618-03 of the initial FA sample.

Component	FA
SiO_2	55.23
Al_2O_3	21.43
Fe_2O_3	7.42
CaO	7.94
MgO	2.61
SO_3	0.81
Na_2O	0.64
K_2O	1.35
Loss on ignition at 1000 °C	1.66
Total	*99.09*
Classification according to the ASTM C 618-03 standard	class F

Sodium silicate solution ("Galenika–Magmasil", Serbia, 13.60% Na_2O, 26.25% SiO_2, 60.15% H_2O) was used as an alkaline activator. Starting sodium silicate modulus n (SiO_2/Na_2O mass ratio) was 1.93. This modulus was further adjusted by adding NaOH pellets (NaOH p.a. ASC reagent, (min. 98%), "Sigma Aldrich", Sweden). Lead nitrate $Pb(NO_3)_2$ was used as a heavy metal contained source ($Pb(NO_3)_2$ p.a., "Centrohem", Serbia).

2.2. Synthesis of geopolymers

The fly ash-based geopolymers was synthesized according to previously optimized procedure (Nikolić et al., 2014; 2018). Sodium silicate solution with modulus 1.5 was used as an alkali activator. The concentration of the activator was 10% Na_2O with respect to the FA mass.

Geopolymer paste samples were prepared by mixing FA with alkali activator and water. Water/binder ratio (water represents the total amount of water in the system including water from the activator, while binder represents the total FA

mass and solid part of the activator) was 0.41. Method preparation of geopolymers containing lead was similar to the method preparation geopolymers without lead. Pre-calculated amount of lead nitrate was dissolved in the amount of distilled water required to achieve appropriate consistency. The order of geopolymers preparing was as follows: the activator was added in the FA and then lead nitrate solution. The content of Pb accounting for the total mass of FA were 0%, 10% and 30%. Pastes were poured into plastic moulds on a vibrating table and then cured for 24 h at 55 °C, based on the previous research (Nikolić et al., 2018). After curing, pastes were demolded, crushed and pulverized in isopropyl alcohol for 1 h in order to stop further reaction, filtered, rinsed with acetone and dried at 50 °C for 2 h.

2.3. Methods of characterization

Mineralogical characterization of geopolymers was conducted by X-ray powder diffraction analysis (RIGAKU X-ray spectrometer KG-3). The diffraction patterns were recorded using Cu Kα radiation (λ = 1.54178 Å) within 10 – 50 ° 2Θ range, with a rate 1 °/min. For the identification of crystalline phases, the "PCPDFWIN" software (based on JCPDS-ICDD database) was used.

^{29}Si MAS NMR spectra of geopolymers were obtained at a Larmor frequency of 79.49 MHz using Bruker MSL 400 system, Apollo console upgraded (Tecmag). Chemical shifts δ(^{29}Si) were externally referenced to 2,2-dimethyl-2-silapentane-5-sulfonate (DSS) standard. Gaussian peak deconvolution of the obtained spectra was performed using DMFIT application (Massiot et al., 2002), by employing common routine for analyzing peak distribution. Prior to ^{29}Si MAS NMR analysis, iron content in the geopolymer samples was minimized by exposing the samples to a strong magnetic field (Nikolić et al., 2018).

3. Results and Discussion

3.1. XRD analysis of geopolymers

X-ray powder diffraction analysis of geopolymers with 0, 10 and 30% of Pb added is shown in Figure 1. XRD analysis of geopolymers samples indicated a wide and diffusive reflection in an interval from 25° to 35° 2Θ, so-called "geopolymer hump". In addition, XRD analysis confirmed the presence of crystalline phases typical for the initial FA: quartz (PDF#33-1161) as the most prominent, anhydrite (PDF#06-0226), feldspar (PDF#20-0528), hematite (PDF#24-0072), as well as secondary calcite (PDF#47-1743) formed due to geopolymer carbonation.

Apart from the mentioned phases, in the geopolymer samples with 10% and 30% Pb added, nitratine (sodium nitrate $NaNO_3$, PDF#07-0271) was detected. The nitrate formation was not surprising given that Pb was added in the form of highly soluble nitrate salt, while sodium came from the activator. In previous study (Nikolić et al., 2018), the presence of nitratine in the sample with 4% Pb added was also confirmed.

In the geopolymer samples containing lead, the appearance

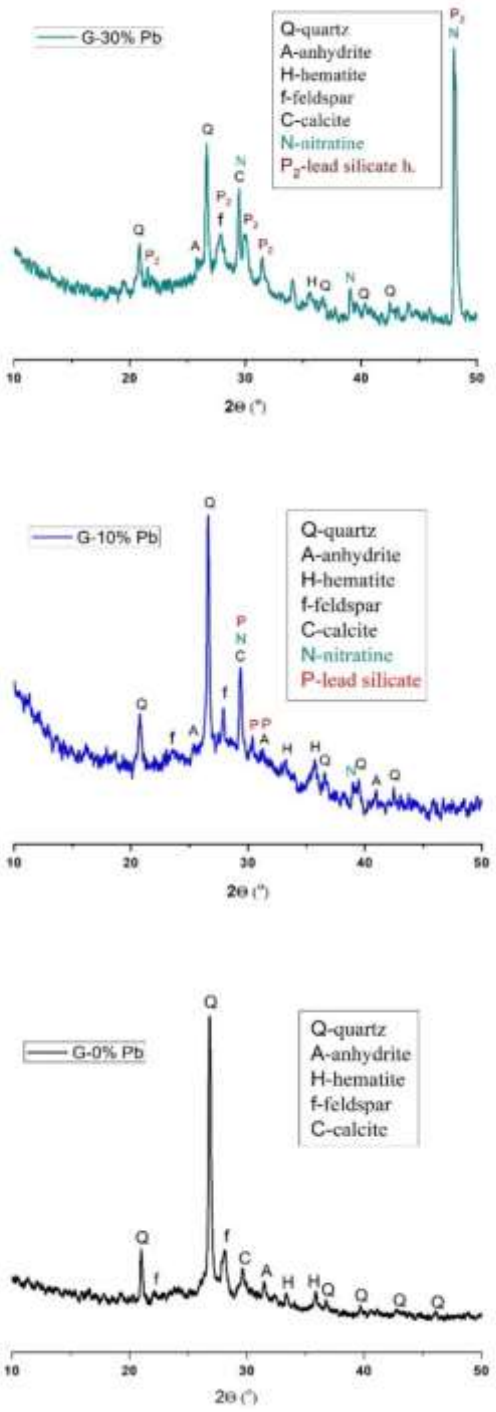

of new Pb-peaks was observed. In the sample with 10% Pb added, lead silicate Pb_5SiO_7 (PDF# 35-0274 marked with P) was noticed, although a main peak for this phase overlapped with the peaks for the calcite and nitratine. On the other hand, in the sample with 30% Pb added the presence of one more phase, probably lead silicate hydroxide (PDF# 44-0276 marked with P_2) was detected. However, because of the fact that some peaks of this phase overlap with the peaks of other phases it cannot be reliably verified. In addition, the possibility of the formation of other lead silicate phases should not be excluded. In the previous study (Nikolić et al., 2018), XRD analyses did not revealed formation of any new crystalline Pb

Figure 1. XRD analysis of geopolymers depending on concentration of Pb added

phase, although the formation of amorphous lead phases, either amorphous lead silicate or amorphous lead-incorporated aluminosilicate gel, was not excluded.

Palomo & Palacios (2003) have already indicated the occurrence of lead silicate in the Pb immobilization by fly ash-based geopolymers. The occurrence of new Pb-phases could indicate that Pb formed chemical bonds with the geopolymers. Furthermore, this points to the fact that the mechanism of Pb immobilization is the chemical nature.

3.2. NMR analysis of geopolymers

^{29}Si MAS NMR spectra of geopolymer samples characterized symmetric resonance lines, which were centered around - 93 ppm indicating poorly ordered aluminosilicate structures (Figure 2).

The spectra consist of overlapping resonances attributed to the silicon sites present in aluminosilicate gel, unreacted crystalline phases and unreacted glassy phase present in the initial FA (Nikolić et al., 2018). It is assumed that ^{29}Si MAS NMR spectrum of geopolymers consists of all five $Q^4(m\text{Al}, m = 4, 3, 2, 1 \text{ or } 0)$ silicon species, with Q^4(4Al), Q^4(3Al), Q^4(2Al), Q^4(1Al) and Q^4(0Al) resonating at approximately - 84, - 89, - 94, - 99 and - 107 ppm, respectively (Engelhardth & Michel, 1987; Duxon et al., 2005).

The deconvolution of broad ^{29}Si MAS NMR spectra of geopolymers consisting of individual $Q^n(m\text{Al})$ structural units of silicon, are shown in Table 2. In addition to $Q^4(m\text{Al})$ silicon peaks, small resonances at approximately - 73, - 79, - 107 (sharp peak) and - 112 ppm were observed in the spectra of all investigated geopolymer samples. Peaks at approximately – 73 and - 79 can be ascribed to the less condensed silicon species Q^1 and Q^2 (Criado et al., 2008; Ruiz-Santaquiteria et al., 2012). Sharp peak at approximately - 107 ppm indicated an ordered crystalline structure and can be attributed to quartz originating from the initial FA (Nikolić et al., 2018). Quartz content in geopolymer samples was almost constant, indicating its inertness during alkali activation. The resonance at - 112 ppm is usually attributed to different SiO_2 polymorphs (Fernández-Jiménez, 2006), i.e. unreacted fractions from the initial FA or Q^4(0Al) units in the products of alkali activation reaction (Ruiz-Santaquiteria et al., 2012).

By comparing the results of the spectra deconvolution of geopolymers with 0% and geopolymers with 10% and 30% Pb added, it could be concluded that the Pb addition led to an increase in the fraction of less condensed Q^1 and Q^2 structural units.

In addition to an increase in the fraction of less condensed Q^1 and Q^2 structural units, previous research of Nikolić et al. (2018) has shown that the Pb addition leads to changes in the structure of Q^4 geopolymer units. The authors pointed that addition of 4% Pb led to the reduction of the fraction of $Q^4(m\text{Al})$ structural units richer in aluminum (m = 3, 4) with respect to a fraction of the structural units richer in silicon (m = 0, 1, 2). This trend is also noticeable in the case of addition of a significantly higher amount of lead. However, more pronounce changes are the increase of less condensed Q^1 and Q^2 structural units (Figure 3), which means that Pb addition led to depolymerization of N-A-S-H gel.

The increase in the fraction of less condensed structural units, as well as reducing the fraction of higher condensed $Q^4(m\text{Al})$ structural units, with an addition of Pb has been also observed in lead silicate glasses (Fayon et al., 1998). This leads to the conclusion that geopolymers containing a considerable amount of Pb are similar to lead-silicate glasses.

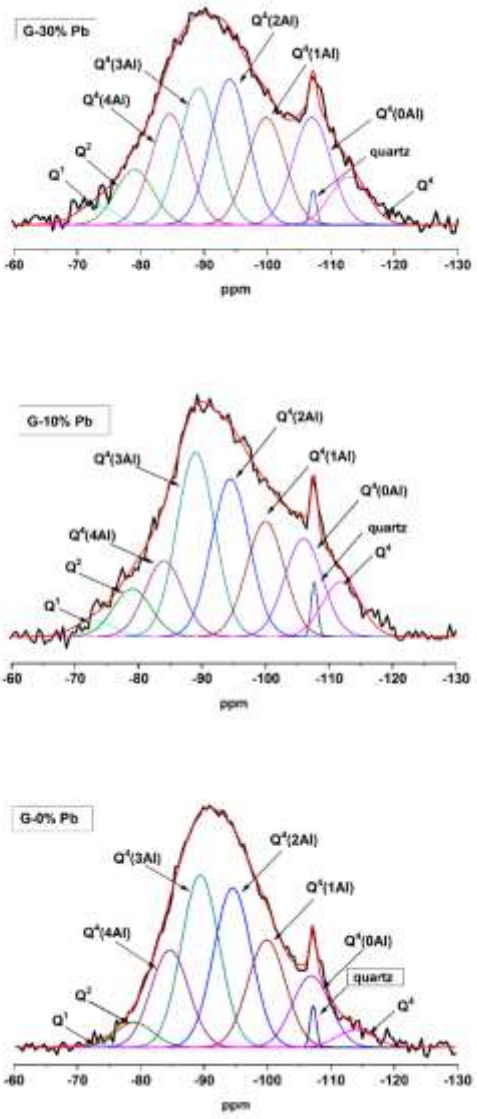

Figure 2. ^{29}Si MAS NMR spectra deconvolution of geopolymers depending on concentration of Pb added

4. Conclusion

In this paper, structural changes of fly ash-based geopoly-

mers induced by a large amount of lead (up to 30%) were examined by means of XRD and ^{29}Si MAS NMR analysis.

XRD analysis confirmed that crystalline phases, from the initial fly ash, as well as secondary calcite, were present in the fly-ash based geopolymers.

In the geopolymer samples containing lead, nitratine was detected. In addition, the appearance of new peaks, attributed to Pb-phases was observed. In the sample with 10% Pb added, lead silicate Pb_5SiO_7 was noticed, while in the sample with 30% Pb added the presence of one more phase, probably lead silicate hydroxide was observed. The occurrence of new phases indicated that Pb formed chemical bonds with the geopolymers. Furthermore, this points to the fact that the mechanism of Pb immobilization is the chemical nature.

Table 2. ^{29}Si MAS NMR spectra deconvolution of geopolymers depending on the concentration of Pb added (Figure 2)

Pb concentration		Q^{1*}	Q^{2*}	Q^4(4Al)	Q^4(3Al)	Q^4(2Al)	Q^4(1Al)	Q^4(0Al)	quartz**	Q^{4**}
0 %	δ (ppm)	-72.95	-79.00	-84.50	-89.40	-94.00	-99.30	-106.4	-107.0	-112.7
	w (ppm)	7	7	7	7	7	7	7	1.2	7
	area (%)	0.4	3.78	14.72	26.1	24.13	16.26	10.83	1.08	2.67
10 %	δ (ppm)	-72.90	-79.00	-84.58	-89.40	-94.50	-99.87	-106.9	-107.2	-113.9
	w (ppm)	7	7	7	7	7	7	7	1.2	7
	area (%)	2.12	6.3	9.97	24.27	20.78	15.14	12.88	1.24	7.28
30 %	δ (ppm)	-72.9	-79.00	-84.74	-89.98	-94.96	-99.97	-106.8	-107.2	-113.9
	w (ppm)	7	7	7	7	7	7	7	1.2	7
	area (%)	2.66	7.5	15.04	18.58	19.76	14.57	14.57	0.8	6.52

* Signals associated with less condensed silicon species, Q^1 and Q^2

** quartz and other Q^4 silicon unit

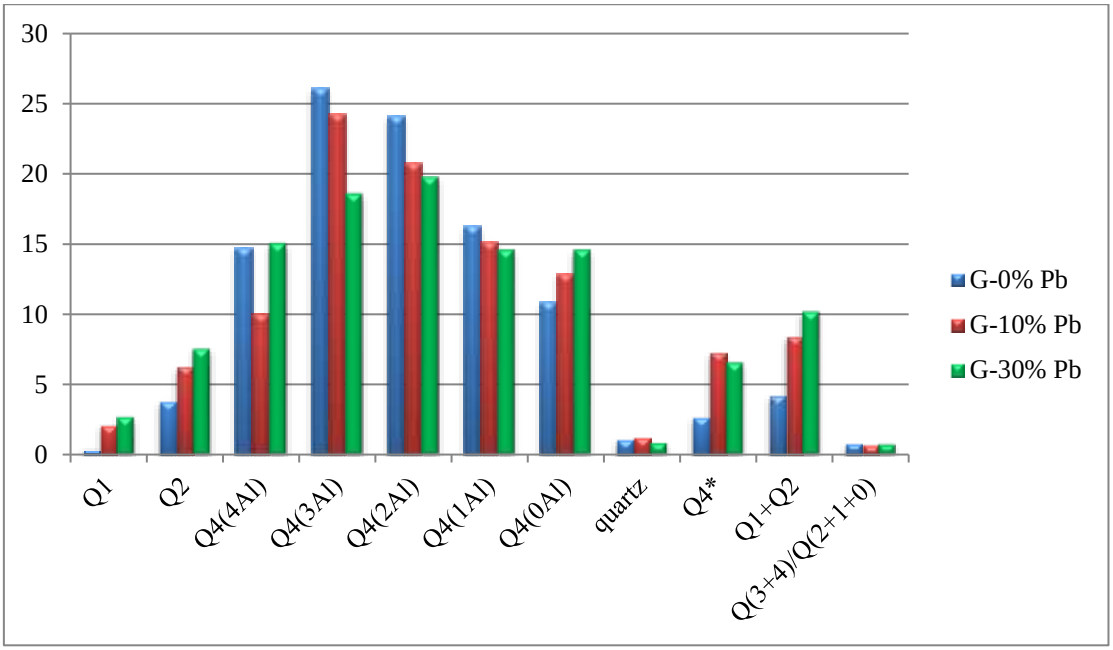

Figure 3. Q^n distribution of fly ash-based geopolymers depending on concentration of Pb added

The results of ^{29}Si MAS NMR spectra deconvolution of geopolymers with and without Pb added showed that the Pb addition led to an increase in the fraction of less condensed Q^1 and Q^2 structural units.

Acknowledgements

This research was financially supported by the Ministry of Education, Science and Technological Development, Republic of Serbia, within Project TR 34026.

References

Criado, M., Fernandez-Jimenez, A. Palomo, A., Sobrados, I., Sanz, J. (2008) Effect of the SiO_2/Na_2O ratio on the alkali activation of fly ash. Part II: ^{29}Si MAS-NMR Survey. *Microporous and Mesoporous Materials*, 109, 525–534 https://doi.org/10.1016/j.fuel.2005.03.030

Duxson, P., Provis, J.L., Lukey, G.C., Separovic, F., van Deventer, J.S.J. (2005).^{29}Si NMR Study of Structural Ordering in

Aluminosilicate Geopolymer Gels. *Langmuir*, 21, 3028–3036 https://doi.org/10.1021/LA047336X

Duxon, P., Fernandez-Jimenez, A. Provis, J.L., Luckey, G.C., Palomo, A. van Deventer, J.S.J. (2007). Geopolymer technology: the current state of the art. *Journal of Materials Science* 42, 2917–2933. http://dx.doi.org/10.1007/s10853-006-0637-z

Engelhardth, G. Michel, D. (1987). *High resolution solid state NMR of silicates and zeolites*, Wiley, New York.

Fayon, F., Bessada, C., Massiot, D., Farnan, I. Coutures, J.P. (1998) 29Si and 207Pb NMR study of local order in lead silicate glasses, *Journal of Non-Crystalline Solids*, 232-234, 403–408 https://doi.org/10.1016/S0022-3093%2898%2900470-0

Fernandez-Jimenez, A., Palomo, A. (2003). Characterization of fly ashes. Potential reactivity as alkaline cements. *Fuel*, 82, 2259–2265. https://doi.org/10.1016/S0016-2361(03)00194-7

Fernández-Jiménez, A., de la Torre, A.G., Palomo, A., Lopez-Olmo, G., Alonso, M.M., Aranda, M.A.G. (2006). Quantitative determination of phases in the alkali activation of fly ash. Part I. Potential ash reactivity. *Fuel*, 85, 625– 634 https://doi.org/10.1016/j.micromeso.2007.05.062

Guo, B., Pan, D., Liu, B., Volinsky, A.A., Fincan, M., Du, J., Zhang, S. (2017). Immobilization mechanism of Pb in fly ash-based geopolymer. *Construction and Building Materials*, 134, 123–130 https://doi.org/10.1016/j.conbuildmat.2016.12.139

Komljenović, M., Baščarević, Z., Bradić, V. (2010). Mechanical and microstructural properties of alkali-activated fly ash geopolymers. *Journal of Hazardous Materials*, 181, 35–42 https://doi.org/10.1016/j.jhazmat.2010.04.064

Landrigan, P.J. Boffetta, P. Apostoli, P. (2000). The reproductive toxicity and carcinogenicity of lead: a critical review. *American Journal of Industrial Medicine*, 38, 231–243 https://doi.org/10.1002/1097-0274(200009)38:3%3C231::AID-AJIM2%3E3.0.CO;2-O

Lee, S. van Riessen, A., Chon, C.M., Kang, N.H., Jou, H.T., Kim, Y.J. (2016). Impact of activator type on the immobilisation of lead in fly ash-based geopolymer. *Journal of Hazardous Materials* 305, 59–66 https://doi.org/10.1016/j.jhazmat.2015.11.023

Massiot, D., Fayon, F., Capron, M., King, I., Calve, S.L., Alonso, B., Durand, J.O., Bujoli, B., Gan, Z., Hoatson G. (2002). Modelling one- and two-dimensional solid-state NMR spectra. *Magnetic Resonance in Chemistry*, 40, 70–76 https://doi.org/10.1002/MRC.984

Nikolić, V., Komljenović, M. Marjanović, N., Baščarević, Z., Petrović, R. (2014). Lead immobilization by geopolymers based on mechanically activated fly ash. *Ceramics International*, 40, 8479–8488 http://dx.doi.org/10.1016/j.ceramint.2014.01.059

Nikolić, V., Komljenović, M., Baščarević, Z., Marjanović, N., Miladinović, Z., Petrović, R. (2015). The influence of fly ash characteristics and reaction conditions on strength and structure of geopolymers. *Construction and Building Materials*, 94, 361–370. http://dx.doi.org/10.1016/j.conbuildmat.2015.07.014

Nikolić, V. Komljenović, M. Džunuzović, N. Miladinović, Z. (2018). The influence of Pb addition on fly ash-based geopolymers. *Journal of Hazardous Materials*, 350, 98–107 https://doi.org/10.1016/j.jhazmat.2018.02.023

Palomo, A. Palacios, M. (2003) Alkali-activated cementitious materials: alternative matrices for the immobilisation of hazardous wastes part II. stabilisation of chromium and lead. *Cement and Concrete Research*, 33, 289–295 https://doi.org/10.1016/S0008-8846(02)00964-X

Perera, D.S., Aly, Z., Vance, E.R., Mizumo, M. (2005) Immobilization of Pb in a geopolymer matrix. Journal of *American Ceramics Society*, 88, 2586–2588. https://doi.org/10.1111/j.1551-2916.2005.00438.x

Phair, J.W., van Deventer, J.S.J., Smith, J.D. (2004). Effect of Al source and alkali activation on Pb and Cu immobilisation in fly-ash based geopolymers. *Applied Geochemistry*, 19, 423–434. https://ui.adsabs.harvard.edu/link_gateway/2004ApGC...19..423P/doi:10.1016/S0883-2927(03)00151-3

Provis, J.L., van Deventer, J.S.J. (2009). *Geopolymers, structure, processing, properties and industrial applications*. Wood-Head Publishing, Cambridge.

Ruiz-Santaquiteria, C., Skibsted, J., Fernandez-Jimenez, A. Palomo, A. (2012). Alkaline solution/binder ratio as a determining factor in the alkaline activation of aluminosilicates. *Cement and Concrete Research*, 42, 1242–1251 https://doi.org/10.1016/j.cemconres.2012.05.019

Shi, C. Fernández-Jiménez, A. (2006). Stabilization/solidification of hazardous and radioactive wastes with alkali-activated cements. *Journal of Hazardous Materials* B ,137, 1656–1663 https://doi.org/10.1016/j.jhazmat.2006.05.008

Shi, C., Fernández-Jiménez, A., Palomo, A. (2011). New cements for the 21st century: The pursuit of an alternative to Portland cement. *Cement and Concrete Research*, 41, 750–763 https://doi.org/10.1016/j.cemconres.2011.03.016

Toniolo, N., Boccaccini, A. R. (2017). Fly-ash based geopolymers containing added silicate waste. A review. *Ceramics International*. 43, 14545–14551 https://doi.org/10.1016/j.ceramint.2017.07.221

Van Deventer, J.S.J., Provis, J.L., Duxson, P., Lukey, G.C. (2007). Reaction mechanisms in the geopolymeric conversion of inorganic waste to useful products. *Journal of Hazardous Materials*, 139, 506–513. https://doi.org/10.1016/j.jhazmat.2006.02.044

Van Jaarsveld, J.G.S. Van Deventer, J.S.J., Lorenzen, L. (1997). The potential use of geopolymeric materials to immobilise toxic metals: Part I. Theory and applications. *Minerals Engineering*, 10 (7), 659–669. https://doi.org/10.1016/S0892-6875(97)00046-0

Van Jaarsveld, J.G.S. van Deventer, J.S.J., Lorenzen, L. (1998). Factors affecting the immobilization of metals in geopolymerized fly ash. *Metallurgical and Materials Transactions B*, 29B, 283–291. https://doi.org/10.1016/S0892-6875(97)00046-0

Wang, Y., Han, F., Mu., J. (2018). Solidification/stabilization mechanism of Pb(II), Cd(II), Mn(II) and Cr (III) in fly ash based geopolymers. *Construction and Building Materials*, 160, 818–827. https://doi.org/10.1016/j.conbuildmat.2017.12.006

Xu, J.Z., Zhou, Y.L., Chang, Q., Qu, H.Q. (2006). Study on the factors of affecting the immobilization of heavy metals in fly ash-based geopolymers. *Materials Letters*, 60, 820–822 https://doi.org/10.1016/j.matlet.2005.10.019

Zhang, J., Provis, J.L., Feng, D., van Deventer, J.S.J. (2008).

Geopolymers for immobilization of Cr6+, Cd2+ and Pb2+. *Journal of Hazardous Materials*, 157, 587–598 http://dx.doi.org/10.1016/j.jhazmat.2008.01.053

Strukturne promene geopolimera na bazi elektrofilterskog pepela izazvane velikom količinom olova

Violeta Nikolić*

Fakultet za ekologiju i zaštitu životne sredine, Univerzitet Union-Nikola Tesla, Beograd, Srbija

*Autor za korespondenciju: violetanikolic22@unionnikolatesla.edu.rs, violeta.m.nikolic@gmail.com

Apstrakt: Geopolimeri se smatraju mogućim tehnološkim i ekološkim rešenjem za efikasnu imobilizaciju teških metala i drugih toksičnih materijala. U ovom radu su ispitivane strukturne promene geopolimera izazvane velikom količinom olova (do 30%). Geopolimeri su sintetisani alkalnom aktivacijom elektrofilterskog pepela korišćenjem natrijum silikata modula 1,5 kao alkalnog aktivatora. Olovo je dodato u obliku soli rastvorljive u vodi – olovo-nitrata, tokom sinteze geopolimera. Promene strukture geopolimera usled dodavanja Pb određivane su XRD i ^{29}Si MAS NMR analizom. XRD analiza je potvrdila da je dodavanje Pb dovelo do formiranja novih Pb-faza, što je pokazalo da Pb formira hemijske veze sa geopolimerima. ^{29}Si MAS NMR analiza je pokazala porast slabije umreženih Q^1 and Q^2 strukturnih jedinica geopolimera sa dodatkom Pb.

Ključne reči: geopolimer, elektrofilterski pepeo, imobilizacija, olovo